AD

USAAML TECHNICAL REPORT 65-20

CURVED JET FLOWS

VOLUME I

May 1965

U.S. ARMY AVIATION MATERIEL LABORATORIES
FORT EUSTIS, VIRGINIA

CONTRACT DA 44-177-AMC-238(T)
PETER R. PAYNE, INC.

DDC Availability Notice

Qualified requesters may obtain copies of this report from DDC.

This report has been furnished to the Department of Commerce for sale to the public.

Disclaimer

The findings in this report are not to be construed as an official Department of the Army position, unless so designated by other authorized documents.

When Government drawings, specifications, or other data are used for any purpose other than in connection with a definitely related Government procurement operation, the United States Government thereby incurs no responsibility nor any obligation whatsoever; and the fact that the Government may have formulated, furnished, or in any way supplied the said drawings, specifications, or other data is not to be regarded by implication or otherwise as in any manner licensing the holder or any other person or corporation, or conveying any rights or permission, to manufacture, use or sell any patented invention that may in any way be related thereto.

Disposition Instructions

Destroy this report when it is no longer needed. Do not return it to the originator.

HEADQUARTERS
U S ARMY TRANSPORTATION RESEARCH COMMAND
FORT EUSTIS, VIRGINIA 23604

The present study was undertaken to describe more accurately viscous influences on the annular jet flow. The theory developed also correlated with inlet flow, Coanda flow, and jet-flap experimental data.

The report has been reviewed by the U.S. Army Transportation Research Command, and the data contained in it are considered to be valid. The report is published for the dissemination of information.

NOTE

On 1 March 1965, *after this report had been prepared,* the name of this command was changed from U.S. Army Transportation Research Command to:

U.S. ARMY AVIATION MATERIEL LABORATORIES

Task 1D121401A14203
Contract DA 44-177-AMC-238(T)
USAAML Technical Report 65-20
May 1965

CURVED JET FLOWS

Prepared by
Peter R. Payne, Inc.
12221 Parklawn Drive
Rockville, Maryland 20852

for

U. S. ARMY AVIATION MATERIEL LABORATORIES
FORT EUSTIS, VIRGINIA

ABSTRACT

A simple equation is derived to describe curvilinear flow, and this is then applied to various practical problems. In the case of annular jet flow, previous theories are shown to be approximate solutions to the general equation; the more exact solution of this report is shown to give better agreement with experiment.

The new theory is also applied to the flow of air in a curved duct, the flow into an intake, the jet flap, and Coanda flow. Comparison with experiment again gives good agreement.

Because curvilinear flow implies diffusion, the theory of diffusion is studied in some detail, and a general theory is developed for the total head lost in a rapid diffusion. When applied to the diffusion loss measured in the nozzle of an annular jet, and the analogous losses in a curved duct, the theory gives excellent agreement with experiment.

The various investigations cover fairly wide areas in subsonic aerodynamics. Thus, it has proved impossible to work out the applications of the theory completely for all the cases considered. The same is true of the experimental work reported, and further work in both areas is suggested.

PREFACE

The work herein reported was carried out at Peter R. Payne, Inc., Rockville, Maryland, in compliance with U. S. Army Transportation Research Command Contract DA 44-177-AMC-238(T).

The principal investigator was Mr. Peter R. Payne, and the Project Engineer was Mr. Alastair Anthony. In general, Mr. Payne was responsible for the theoretical work and the basic concepts introduced, and Mr. Anthony for the experimental work and the program management.

Mr. Anthony was ably assisted by Messrs. David Ullman and James Oxenham of the Payne, Inc. staff, and by Payne's associate consultant, Professor George Pick.

The technical administration representative of the U. S. Army Transportation Research Command was Mr. William E. Sickles, whose invaluable assistance is gratefully acknowledged.

CONTENTS

Page

ABSTRACT iii

PREFACE v

LIST OF ILLUSTRATIONS xvii

LIST OF SYMBOLS xxvii

CHAPTER ONE - SUMMARY AND DISCUSSION 1

THE FUNDAMENTAL PROBLEM 1

DIFFUSION LOSSES 5

ANNULAR JET THEORY 8

CHAPLIN'S SOLUTION (THIN-JET THEORY) 9

THE CROSS-STANTON-JONES SOLUTION (EXPONENTIAL THEORY) 11

PINNES' SOLUTION (FREE-VORTEX FLOW) 12

PAYNE'S CORRECTION FOR JET CURVATURE 14

THE ANNULAR JET SOLUTION OF THIS REPORT 14

MOMENTUM BALANCE OF THE ANNULAR JET 19

COANDA JET THEORY 20

INTAKE FLOW THEORY 24

MOMENTUM DRAG 26

THE JET FLAP 26

JET ISSUING NORMAL TO A FREE-STREAM FLOW 31

CHAPTER TWO - GENERAL DIFFUSION THEORY 35

THE FLOW OF A JET THROUGH A DISCONTINUITY IN STATIC PRESSURE 35

SOLUTION FOR CONSERVATION OF TOTAL HEAD. 35

THE GENERAL MOMENTUM SOLUTION 36

BORDA-CARNOT DIFFUSION IN TWO-DIMENSIONAL FLOW. . 41

VALUES OF THE SHAPE FACTORS λ AND ψ 48

THE LIMITING VELOCITY CHANGE 50

CHAPTER THREE - THE EQUATION FOR CURVILINEAR TWO-DIMENSIONAL FLOW 58

THE EQUATION OF MOTION 58

A LINEAR TRANSFORMATION TO JET ORDINATES 60

NONLINEAR TRANSFORMATIONS 61

CHAPTER FOUR - INVISCID FLOW ANNULAR JET THEORY FOR CONSTANT TOTAL HEAD 63

GENERAL MOMENTUM BALANCE CONSIDERATIONS. 63

A Thin Jet Solution (Pinnes' Geometry) 63

A Thick Jet Solution 67

The Variation of Curvature Across a Thick Jet 67

The Height Parameter. 69

Three-Dimensional Effects 70

SOME GENERAL RELATIONS FOR THE FLOW PARAMETERS OF AN ANNULAR JET 71

The Local Jet Velocity 72

The Jet Mass Flow. 72

The Nozzle Momentum Flux. 72

Total Nozzle Force. 72

Jet Power. 73

Total Lift 73

SOLUTION OF THE CURVED JET EQUATION FOR CONSTANT TOTAL PRESSURE. 73

Local Jet Velocity 74

Jet Mass Flow. 74

The Nozzle Momentum Flux. 74

Total Jet Force 74

The Jet Curvature Parameter. 75

Momentum Balance 76

Other Results 80

THE CUSHION PRESSURE PARAMETER 87

The General Expression for $\bar{\Delta\phi}_c$ 93

The Constant Total Head Solution 93

The Solution for Free-Vortex Flow (η = 1.0) 94

The Solution for Exponential Theory Flow (ν = 0) . . . 94

GENERAL SOLUTIONS FOR FREE-VORTEX FLOW WITH CONSTANT TOTAL PRESSURE 95

Calculation of Mass Flow. 95

Calculation to the Local Velocity. 95

The Nozzle Momentum Flux. 96

The Total Jet Force 96

The Jet Power. 96

Momentum Balance. 96

GENERAL SOLUTIONS FOR CONSTANT RADIUS FLOW (EXPONENTIAL THEORY) WITH CONSTANT TOTAL PRESSURE 97

The Local Jet Velocity 98

The Jet Mass Flow. 98

The Nozzle Momentum Flux. 98

The Total Jet Force 98

The Jet Power. 99

Momentum Balance. 99

SOME EXPERIMENTAL RESULTS AT CONSTANT TOTAL PRESSURE 100

The Annular Jet Test Rig 100

The Experiment. 100

Instrumentation 100

Flow at the Throat 103

Flow at the Nozzle 103

Flow Adjacent to the Annular Jet. 110

CHAPTER FIVE - THE EFFECT OF TOTAL PRESSURE VARIATION ACROSS AN ANNULAR JET 116

THE SPECIAL CASE OF CONSTANT JET VELOCITY. 116

Determination of the Jet Curvature Parameter η 118

Calculation of $\Delta\bar{p}_c$ For Free-Vortex Flow 118

Calculation of $\Delta\bar{p}_c$ for Constant Radius Flow. 119

Discussion of Results 119

THE INFLUENCE OF THE TOTAL PRESSURE DISTRIBUTION ON CUSHION PRESSURE IN TERMS OF MEAN TOTAL PRESSURE, FOR FREE-VORTEX FLOW. 122

The Jet Thickness Anomaly 126

Rectangular Total Head Distributions 127

A General Linear Variation 131

A General Power Law Variation 133

CUSHION PRESSURE AS A RATIO OF MEAN TOTAL PRESSURE WITH A LINEAR VARIATION IN TOTAL PRESSURE ACROSS THE JET (EXPONENTIAL THEORY) 134

THE EFFECT OF A LINEAR TOTAL HEAD VARIATION OF THE CUSHION PRESSURE PARAMETER $\Delta\bar{p}_c$ 137

Variation in Cushion Pressure Parameter According to Exponential Flow Theory With a Linear Gradient of Total Pressure Across the Jet 139

Variation in Cushion Pressure Parameter According to Free-Vortex Flow With a Linear Gradient of Total Pressure Across the Jet 141

Discussion of the Results. 144

CHAPTER SIX - VISCOUS MIXING EFFECTS IN THE ANNULAR JET . .147

THE "AIR FRICTION" CONCEPT 154

A GENERAL THEORY OF MIXING LOSS 162

THE STATIC PRESSURE IN THE PRIMARY VORTEX. 174

CHAPTER SEVEN - A SMALL PERTURBATION THEORY OF DIFFUSION LOSSES IN AN ANNULAR JET NOZZLE. 176

APPROXIMATE SOLUTION FOR A "STRAIGHT" NOZZLE 179

MEAN TOTAL PRESSURE LOSS. 180

TOTAL POWER LOSS DUE TO DIFFUSION. 182

CHAPTER EIGHT - COANDA JET FLOW. 185

SOLUTION FOR CONSTANT TOTAL HEAD. 186

APPROXIMATE SOLUTION FOR THE BOUNDARY LAYER EFFECT. 189

CHAPTER NINE - TWO-DIMENSIONAL FLOW IN A CURVED DUCT WITH CONSTANT TOTAL HEAD. 195

STATIC PRESSURE AND VELOCITY DISTRIBUTION 196

THE CONSTANT VELOCITY STREAMLINE 198

MASS FLOW DISTRIBUTION AROUND THE BEND. 200

TOTAL HEAD LOSS ON THE OUTSIDE OF THE CONSTANT VELOCITY STREAMLINE 200

TOTAL HEAD LOSS ON THE INSIDE OF THE CONSTANT VELOCITY STREAMLINE 203

MEAN TOTAL PRESSURE LOSS ACROSS THE DUCT 204

THE LOSS INCREMENT DUE TO SKIN FRICTION 204

COMPARISON WITH EXPERIMENT. 206

APTER TEN - FLOW INTO A TWO-DIMENSIONAL FLUSH INTAKE .208

MOMENTUM EQUATIONS 210

THE FLOW EQUATION FOR CONSTANT TOTAL HEAD 211

INTAKE MASS FLOW 212

THE FLOW CURVATURE PARAMETER η FOR CONSERVATION OF MOMENTUM 213

THE STATIC PRESSURE DISTRIBUTION Δp_s. 214

LIMIT SOLUTIONS FOR $\eta = 0$, Δp_s = CONSTANT 216

SOLUTIONS FOR $\eta = 1.0$, Δp_s = CONSTANT. 217

THE FLOW EQUATION WITH AN UPSTREAM BOUNDARY LAYER 219

SOLUTION FOR A THIN UPSTREAM BOUNDARY LAYER. 221

MOMENTUM DRAG 223

SOME EXPERIMENTAL MEASUREMENTS. 223

Intake Power Efficiency. 224

Experimental Measurement of Intake Power Efficiency. .225

Calibration of Yaw Probe, for Static Pressure Measurement. 226

Comparison With Theoretical Values 229

Comparison with Zero Tunnel Speed Case. 237

CHAPTER ELEVEN - SOME GENERAL PROBLEMS OF A JET DISCHARGING ACROSS A FREE-STREAM FLOW. 240

THRUST LOSS DUE TO MIXING 240

SOURCES OF APPARENT JET DRAG COMMON TO ALL JET CONFIGURATIONS 243

The Effect of Pressure Due to Free-Stream Flow. 244

The Effect of "Boundary Layer Pumping". 247

Jet-Induced Turbulence. 248

Nozzle Diffusion Losses 249

A SIMPLE HYPOTHESIS FOR JET PRESSURE IN A FREE-STREAM FLOW. 250

SOME EXPERIMENTAL OBSERVATIONS. 254

Flows in Square Feet Per Second 254

Velocities in Feet Per Second 254

RECOMMENDATIONS FOR FURTHER WORK 265

Annular Jet Theory 265

Intake [illegible] Theory 266

Curved Duct Flow Theory 266

Coanda Flow 267

Diffusion Theory 267

Jet Flap Theory. 267

BIBLIOGRAPHY. 268

DISTRIBUTION 271

APPENDIX I - SCALE EFFECT IN ANNULAR JET FLOW. 273

APPENDIX II - ESTIMATION OF DRAG FROM TOTAL HEAD SURVEYS 277

APPENDIX III - A NOTE ON THE THEORY OF A FREE VORTEX 278

APPENDIX IV - DIFFUSION LOSS MEASUREMENTS IN A PRE-CURVED NOZZLE 281

LIST OF ILLUSTRATIONS

Figure		Page
1	Curved Flow Fields Considered in This Report.	2
2	The "Thrust Hypothesis" for a Jet Flap in Inviscid Flow . .	3
3	Centrifugal Force on a Curved Jet Element.	5
4	Borda-Carnot Diffusion.	6
5	Chaplin's Curved Jet Geometry	10
6	Physical Interpretation of the Constant Radius of Curvature Jet	11
7	Pinnes' "Free Vortex" Assumption for Annular Jet Flo . .	13
8	Effect of Ground Clearance on Jet Radius of Curvature . .	15
9	Comparison of the New Inviscid Flow Theory With Previous Theories	17
10	Comparison of the New Inviscid Flow Theory With Some Experimental Data ($\theta = 0^{\circ}$)	18
11	Momentum Balance Geometry.	19
12	Equivalence of Annular Jet and Coanda Jet Flows	20
13	Variation of Augmentation Ratio ϕ With the Mixing Pressure Parameter $\Delta\phi_1$	21
14	Variation of Augmentation Ratio With Diffusion Efficiency, Assuming Optimum Mixing Pressure.	22
15	Variation of Entrainment Ratio With Jet Thickness for a Right-Angle Coanda Bend	23
16	A Coanda Profile Designed for Maximum Thrust Augmentation.	24

17	Leading Edge Separation With Intake Flow	25
18	Twenty-Percent Elliptical Aerofoil in the Smoke Tunnel. No Air Supply to Jet Flap	27
19	Streamlines Around the Elliptical Aerofoil When the Jet Flap is Operating	28
20	Jet Flap Experiment in the Two-Dimensional Wind Tunnel.	29
21	Results of Total Head Traverses 3.25 Chords Behind the Jet Flapped Aerofoil, With the Jet Flap On and Off	30
22	Observed Flow Patterns, With and Without Jet Flap Operating.	32
23	Assumed Geometry.	33
24	Geometry of Flow Through a Pressure Change.	35
25	Change in Momentum Flux Through a Static Pressure Change for One-Dimensional Flow	38
26	Constrained and Unconstrained Flow Through a Static Pressure Change.	39
27	The Integral $\int_{y_0}^{y_1} \Delta p \, dy$	40
28	Two Jet Flow Conditions	40
29	A Sudden Duct Expansion	41
30	Variables in a Sudden Diffusion	42
31	Power Lost in a Sudden Diffusion, for a Uniform Velocity Profile.	47
32	A Family of Radial Velocity Distributions in a Circular Duct	48

33 Variation of the Shape Integrals λ and ψ With the Shape Exponent m for the Power Law Family of Velocity Distributions 51

34 Power Lost in a Sudden Diffusion, as a Function of the Velocity Distribution Profile 52

35 Variation of Velocity Ratio $\hat{u}_e/\hat{u}_i$, With the Pressure Rise Parameter C_p, For Similar Profiles 53

36 Variation of Total Pressure Loss With Static Pressure Rise, For the Case of Uniform Velocity Distribution . . . 55

37 The Elemental Geometry of the Curved Flow Field . . . 58

38 A Flow Which Has Infinite Radius of Curvature at the Center Line 62

39 Potential Flow Solutions by Gabbay Applied to the Plenum Chamber Problem 64

40 "Thin Jet" Geometry in the Absence of Viscous Mixing . . 65

41 Geometry of a Thick Annular Jet With No Viscous Mixing . 68

42 Geometry of a Circular GEM 70

43 Cross-Plot of Equations (130) and (134) To Determine Values for the Jet Curvature Parameter η . (Solution for Conservation of Total Head) 77

44 Variation of Jet Curvature Parameter η With the Height Parameter h/R 78

45 Jet Thickness at Ambient Pressure, as a Function of the Height Parameter h/R . (Based on Continuity of Mass Flow) 79

46 Momentum Balance as a Function of the Height Parameter R/h 81

47	Variation of Cushion Pressure With the Height Parameter R/c	82
48	Discharge Coefficient C_D as a Function of the Height Parameter R/c	83
49	Comparison of Theoretical Discharge Coefficients for $\theta = 0.$	84
50	Comparison of Theoretical Discharge Coefficients for $\theta = 30^{\circ}$	85
51	Comparison of Theoretical Discharge Coefficients for $\theta = 60^{\circ}$	86
52	Total Nozzle Force, Measured Parallel to the Nozzle Axis, as a Function of the Height Parameter R/c	88
53	Comparison of Discharge Coefficient Ratio C_m/C for Two-Dimensional and Circular Planform GEMs ($\theta = 0^{\circ}$)	90
54	Effect of Planform on the Cushion Pressure Parameter $\Delta p_c/\Delta p_j$	91
55	The Annular Jet Test Rig With Side Panel Removed To Show Nozzle Configuration ($b/b_0 = 1.0$ $\theta = 30^{\circ}$)	101
56	Internal Dimensions of Annular Jet Test Rig	102
57	Velocity and Pressure Distribution in the Throat of the Annular Jet	104
58	Pressures and Velocity at Nozzle Exit $b/b_0 = 1.0$ $\theta = 30^{\circ}$ $b_0 = 2.0$ Inches	105
59	Redistribution of Power in Annular Jet	111
60	Static Pressure Variation Across a Jet - Comparison of Theoretical and Experimental Values	112
61	Pressures and Velocity in Annular Jet and Cushion. (Flat Cushion Board $b/b_0 = 1.0$ $\theta = 30^{\circ}$)	113

62 Pressures and Velocity in the Annular Jet and Cushion. (High Cushion Board $\kappa/h = 1.0$ $\theta = 30^{\circ}$) 114

63 Jet Total Head Distribution Needed to Give Constant Jet Velocity 120

64 The Cushion Pressure Parameter $\Delta\bar{p}_c$ as a Function of the Height Parameter R/κ 121

65 Comparative Effect of Constant Jet Velocity and Constant Total Head on Cushion Pressure Per Unit Air Power . . . 123

66 Symmetric and Asymmetric Jet Total Head Profiles . . . 125

67 Geometry for the Jet Thickness Anomaly 126

68 Two Rectangular Total Head Distributions 127

69 Solution Limits for the Rectangular Total Pressure Distribution 129

70 Effect of a Stopped Rectangular Jet Total Head Distribution Upon Cushion Pressure 130

71 General Linear Variation 131

72 Effect of a Linearly Varying Jet Total Head Distribution Upon Cushion Pressure. 132

73 General Power Law Distribution 133

74 Cushion Pressure as Affected by a Linear Distribution of Total Head Pressure in the Jet (Exponential Flow). . . . 136

75 Cushion Pressure as Affected by a Linear Distribution of Total Head Pressure in the Jet (Exponential Theory) . . . 138

76 Cushion Pressure Parameter With Linear Gradient of Total Pressure Across Jet - Free-Vortex and Exponential Flow 143

77 Pressure Distributions in Jets 146

78	Some Experimental Measurements on the Cushion Pressure Parameter at $\theta = 0^o$	149
79	Assumed Equivalent Linear Total Head Distribution Across the Kuhn and Carter Model Jet	150
80	Increment of the Cushion Pressure Ratio Due to Total Head Distortion in the Kuhn and Carter Model	151
81	Data of Figure 78 With the Kuhn and Carter Results Corrected to Two-Dimensional Flow With Uniform Total Head	152
82	Curved Jet Flow Field in Ground Proximity.	153
83	The "Air Friction" Theory of Viscous Losses in a Thick Jet Compared With Inviscid Flow Theory for $\theta = 0^o$	157
84	Effect of Nozzle Extensions on the Cushion Pressure Ratio ($\theta = 0^o$)	159
85	Effect of Exposing the Inner Surface of the Jet When Nozzle Extensions Are Used	160
86	Reduced Aeronautronic Data of Figure 85.	161
87	Mixing in the Annular Jet	162
88	Two Ways of Portraying the Overfed Jet.	164
89	Theoretical Loss in Cushion Pressure Caused by Viscous Mixing ($\theta = 0^o$)	172
90	Comparison of Viscous Mixing Theory With Experiment for $\theta = 0^o$	173
91	Primary Vortex Pressure as a Function of Hover Height ($\theta = 0^o$)	175
92	Basic Geometry of Nozzle Diffusion	176

93	Static Pressure Distribution on the Inside Nozzle Wall	177
94	Static Pressure Distribution on the Outside Nozzle Wall	178
95	Approximate Total Pressure Loss Due to Diffusion for $t/R = 1.0$, in a Straight Nozzle. (Based on the Exponential Theory Static Pressure Distribution).	181
96	Mean Total Pressure Loss as a Function of the Height Parameter R/t for a Straight Nozzle. (Based on Approximate Exponential Theory Static Pressure Distribution)	183
97	Basic Geometry	185
98	Separation of Coanda Flow	187
99	Variation of Wall Pressure With the Jet Thickness Parameter t/t_0	188
100	Variation of Local Diffusion Efficiency With Local Velocity Ratio	192
101	Flow Separation in a Curved Duct.	195
102	Cases Solvable Using the General Theory Developed in This Investigation	196
103	Assumed Geometry	196
104	Variation of Inner and Outer Bend Velocities With Duct Aspect Ratio	199
105	Position of the Constant Velocity Streamline	201
106	Ratio of Mass Flow on One Side of the Constant Velocity Streamline to the Total Mass Flow	202
107	Average Total Head Loss Around a Constant Duct Thickness Bend	205
108	Comparison Between Theory and Experiment for a Right-Angle Bend	207

109	Flow Into a Flush Intake	208
110	Flow Into a Flush Intake	209
111	Variation of η With $\bar{u}_1/u_\infty$, for Uniform Inflow (ΔP_3 = Constant)	215
112	Variation of Inlet Velocity With Intake Lip Radius. (Exponential Theory for $u_0/u_1 \to \infty$)	218
113	Variation of Inlet Velocity With Intake Lip Radius. (Free-Vortex Theory for $u_0/u_1 = 1.0$)	220
114	Arrangement of Intake in Floor of Wind Tunnel.	226
115	Location of Measuring Stations	227
116	Total and Static Pressures in Intake	230
117	Velocity Vector Profile at Mouth of Intake	231
118	Velocities at Mouth and at Throat of Intake	232
119	Theoretical Velocity Distributions for the Test Intake (Uniform Inflow)	233
120	Cross-Plot of Intake Velocity Ratio, as a Function of $\bar{u}_1/u_\infty$ for the Test Intake. (Conservation of Momentum Correlation Between η and $\bar{u}_1/u_\infty$)	234
121	Cross-Plot of Intake Velocity Ratio, as a Function of $\bar{u}_1/u_\infty$ for the Test Intake. (Conservation of Mass Flow Correlation Between η and $\bar{u}_1/u_\infty$)	235
122	Comparison of Experimental and Theoretical Velocity at Mouth	236
123	Resemblance Between (a) Velocity Profile in Upstream Boundary Layer and (b) Velocity Difference (Theoretical-Experimental) Near Upstream Wall of Intake Throat . . .	236
124	Total Pressure in Upstream Boundary Layer	238

125	Spanwise Distribution of Velocity at Mouth of Intake . . .	238
126	Velocity at Throat of Intake - Tunnel Speed Zero and 90 Feet/Second	239
127	Jet Drag Due to Entrainment in a 90-Degree Jet Flap . . .	242
128	Some Effects of Nozzle Shape on the Discharge Coefficient Under Static Conditions.	243
129	Jet Issuing From a Body in Inviscid Flow	244
130	Boundary Layer Entrainment in a Jet	247
131	Jet Influence on a Wake.	249
132	Nozzle Diffusion Losses	250
133	Jet Flap in Inviscid Flow	250
134	Smoke Tunnel Flow Observations of a Jet Flap.	251
135	Local Jet Geometry.	252
136	Pressure Integral on the Upstream Side of a Jet Exhausted Normal to a Free-Stream Flow	256
137	Arrangement of Jet Discharging Through Floor of Wind Tunnel	257
138	Velocity and Pressure Distribution Downstream Flow Jet. (Jet/Free-Stream Velocity Ratio 0.56)	258
139	(a) Velocity and Pressure Distribution at Mouth of Jet. (Jet/Free-Stream Velocity Ratio 0.56). (b) Velocity and Pressure Distribution in Jet Throat. (Jet/Free-Stream Velocity Ratio 0.56)	259
140	Velocity and Pressure Distribution Downstream From Jet. (Jet/Free-Stream Velocity Ratio 1.34).	260

141 (a) Velocity and Pressure Distribution at Mouth of Jet. (Jet/Free-Stream Velocity Ratio 1.34). (b) Velocity and Pressure Distribution in Jet Duct Throat (Jet/Free-Stream Velocity Ratio 1.34). 261

142 Velocity and Pressure Distribution Downstream From Jet. (Jet/Free-Stream Velocity Ratio 2.88) 262

143 (a) Velocity and Pressure Distribution at Jet Mouth. (Jet/Free-Stream Velocity Ratio 2.88). 263

(b) Velocity and Pressure Distribution at Jet Throat.(Jet/Free-Stream Velocity Ratio 2.88). 264

144 Apparent Effect of Reynolds Number on the Cushion Pressure Ratio 275

145 Effect of Nozzle Skin Friction Loss on Apparent Cushion Pressure Ratio 276

146 Geometry of a Two-Dimensional Vortex. 278

147 Total Pressure Loss at the Exit Plane of an Annular Jet Nozzle 282

SYMBOLS

The prefix Δ denotes an increment of the appropriate quantity. When it prefixes a pressure, it denotes that the pressure is "gauge"; that is, the pressure is measured relative to ambient static pressure p_a.

E.g., $\Delta P = P - p_a$

$\Delta p = p - p_a$

In general we employ the conventional x and y axes wherever possible. In different parts of the report the same symbol is sometimes used to denote different quantities. This is unavoidable because of the large number of different topics discussed, but the precise meaning is always made clear in the text when this duplication occurs.

Where special symbols are defined and used in only one place in the report, they do not appear in the following list.

A an area

A_c cushion area

C' periphery or length of a jet

C_D coefficient of discharge

or C_D a drag coefficient

C_f skin friction coefficient on a solid boundary

C_{fa} apparent skin friction coefficient at a fluid interface

C_p a pressure coefficient $= (p - p_i)/\frac{1}{2}\rho u_j^2$

C_τ coefficient of local skin friction stress

$= \tau_i/\frac{1}{2}\rho u_j^2$

D diameter of a circular planform GEM

	F	a force
	F_N	total nozzle thrust
	h	height of an annular jet nozzle above the ground plane
or	k	a dimension specified in Figure 23
	ΔH	a total pressure loss
	J	a momentum flux ($\int \rho u^2 dy$, for example)
	J_N	nozzle momentum flux
	K	a constant
	m	an exponent
	$\dot{m}$	a mass flow rate
	n	entrained air ratio
	p	a static pressure
	P	a total pressure ($p + \frac{1}{2}\rho u^2$, for example)
	$\mathcal{P}$	a power
	$\Delta\bar{p}_c$	a cushion pressure parameter defined in Equation (142)
	q	a dynamic pressure ($\frac{1}{2}\rho u^2$, for example)
	r	a radius, usually the local radius of a curved jet
	r_0	inner radius of a jet
	R	outer radius of a jet

t nozzle width or jet thickness

t_a thickness of a jet at ambient static pressure

u velocity parallel to the x axis

u_∞ free-stream velocity

$\hat{u}$ a mean velocity

v velocity parallel to the y axis

or v a resultant velocity

W width of a rectangular duct

x a height parameter $= \frac{t}{d}(1 + \sin\theta)$

or x distance along the x axis

X a height parameter $= \frac{t}{d}(1 + \sin\theta)/(1 - \frac{t}{d}\sin\theta)$

y distance along the y axis

z distance across a jet

δm an elemental mass

η a flow curvature parameter

$= \frac{t_a/t + \sin\theta}{1 + \sin\theta}$

or η an efficiency

θ angle at which a jet is inclined <u>inward</u> from the vertical

λ a velocity profile shape factor defined in Equation (48)

μ coefficient of fluid viscosity

ρ mass density of the fluid

τ local skin friction stress

ϕ an augmentation ratio (total thrust/primary thrust)

χ a velocity profile shape factor defined in Equation (53)

or ψ a parameter defined in Equation (258)

Chapter One

SUMMARY AND DISCUSSION

Although it is more usual to have a "Discussion of Results" near the end of a research report, the diffuse nature of the present program seems to render a different approach more appropriate. Accordingly we shall review the program in a fairly general way in this chapter, in order to place it in a proper perspective. Subsequent chapters will deal with the details of the various investigations.

THE FUNDAMENTAL PROBLEM

Underlying the whole of this program is the central phenomenon of a subsonic fluid flow field which is not rectilinear; that is to say, one which is constrained in some way to flow along a curved path. Some examples of practical problems which involve such flows are sketched in Figure 1,and it is evident that our study is not lacking in practical utility.

Until quite recently, practical aerodynamic theory was almost entirely based on the assumption that air was inviscid. Viscous effects were considered only to arise in the boundary layer, as first suggested by Prandtl, and simple methods were evolved for applying viscous effect "corrections" to the various inviscid flow theories. The reason for this was that the viscous shear stress in a fluid is proportional to the local velocity gradient; that is,

$$\text{stress} = \mu \frac{\partial u}{\partial y} \qquad (1)$$

so that, if $\partial u/\partial y$ is small, the viscous forces are negligible. Prandtl showed that the velocity gradient was negligibly small in practical flow fields, except for a very thin layer of fluid close to a solid boundary. Thus, by regarding this boundary layer as part of the body, we can use inviscid flow theory to determine the main flow field. The details of the boundary flow can then be treated as a separate problem; most usually, in fact, we do not need to study the boundary layer, but rather should represent its effect by an empirically determined "skin-friction" loss coefficient.

The foregoing might appear to relegate the boundary layer to a position of negligible importance in engineering aerodynamics. This is by no means so, of course, since it is responsible for most of the drag of streamline bodies and also is the controlling factor in separation of the flow ("stall") from the surface of a body. Until quite recently, however, and excluding some special cases, these problems have been dealt with on an entirely empirical basis.

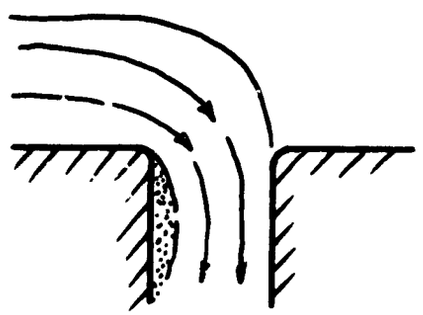

(a) Flow into a horizontal intake.

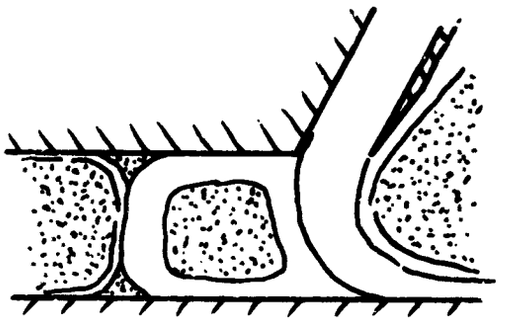

(b) Annular jet flow.

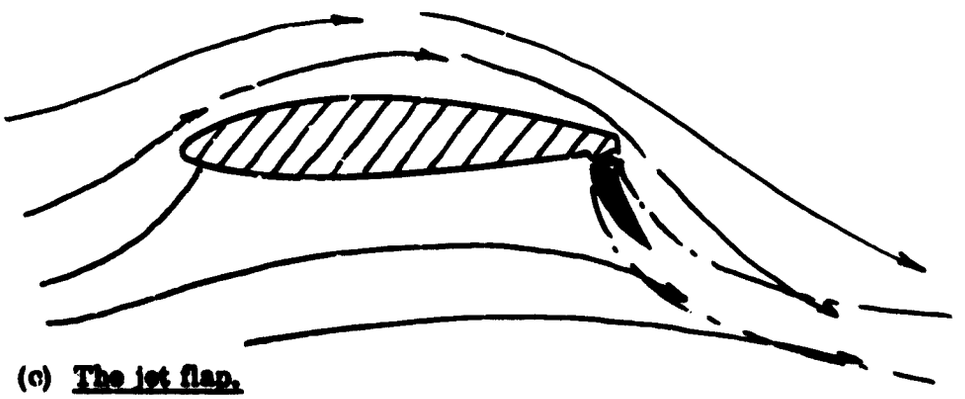

(c) The jet flap.

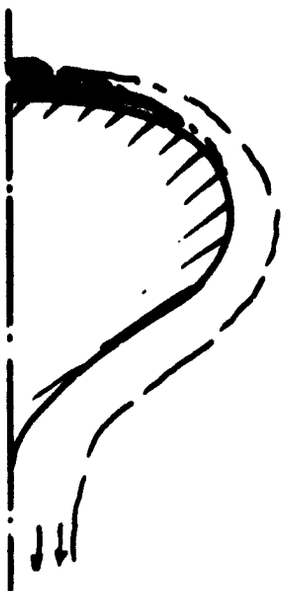

(d) Coanda jet flows.

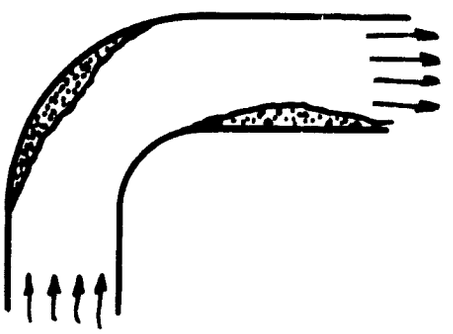

(e) Flow in a curved duct.

Figure 1 Curved Flow Fields Considered in This Report.

A jet is a stream of air which has a velocity markedly different from the main body of air being considered in a problem. A conventional jet is moving faster than the surrounding fluid, but it is no different, in principle, from the "negative jet flow" into an intake, Figure 1(a), or the wake behind a body. In all cases there exists a substantial velocity discontinuity at the surface of the jet so that, from Equation (1), viscous forces become important.

Jets did not play a significant role in aerodynamics until the advent of the gas turbine for propulsion; even then, it was the propulsive force obtained, rather than the finer details of the jet flow structure, that received most attention. The propulsive force depended on the flow condition at the engine exit nozzle, not on what happened downstream.

The advent of the jet flap, annular jet, and other similar concepts markedly changed this picture. For the first time, a jet was being used to influence the main flow field, and the characteristics of the jet after it left the nozzle were found to be the controlling parameters.

Early investigators tried to tackle these new problems with the well tried inviscid flow theory techniques, not only with limited success, but sometimes with nonsensical results. The famous "thrust hypothesis" for the jet flap is a good example of this.

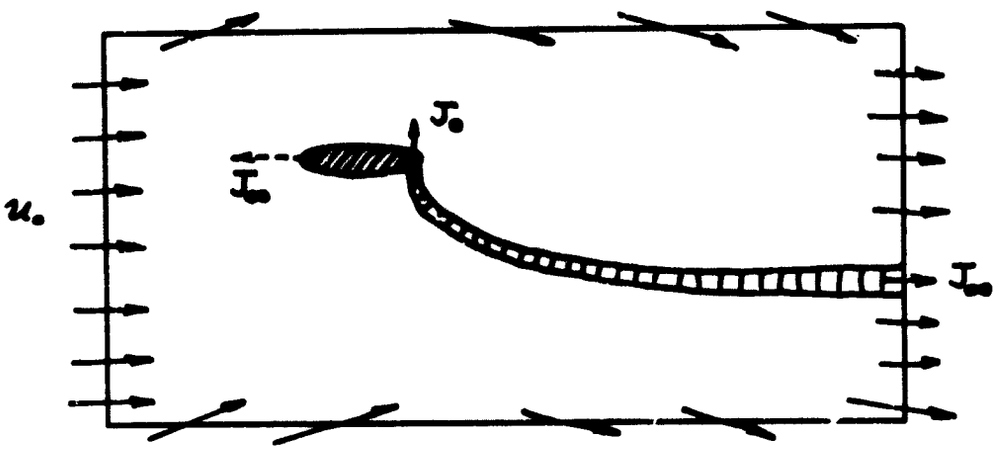

Figure 2. The "Thrust Hypothesis" for a Jet Flap in Inviscid Flow.

Davidson's original hypothesis[1] is illustrated in Figure 2. If the control boundaries are drawn far enough away from a jet-flapped wing, it can be shown that the horizontal momentum flux out of the box is greater than the flow in, by the amount J_{∞}. Thus, although J_0 is a vertical vector at the wing, we must expect a horizontal (propulsive) force J_{∞} to appear on the wing.

In inviscid flow, both Davidson and Stratford[2] assumed $J_{\infty} = J_0$, so that all the nozzle jet reaction should appear as a thrust force on the wing.

At the risk of being a little pedantic, perhaps, we should note that the total nozzle force (F_N) is greater than J_{∞}. The correct relationship for inviscid flow is

$$\frac{J_{\infty}}{F_N} = \frac{\sqrt{1 - \Delta p_N/\Delta P_N}}{1 - \frac{1}{2}\Delta p_N/\Delta P_N} \qquad (2)$$

where Δp_N = mean static pressure at the nozzle
= $f(u_0/u_j)$
ΔP_N = jet total head at the nozzle.

Equation (2) is always somewhat less than unity, so that the "thrust hypothesis" is only approximately correct, even in inviscid flow.

In a real fluid, free-stream air mixes with the jet. Payne[3] has shown that, when such mixing takes place at a pressure which is greater than ambient, the final momentum flux is always reduced. In other words, the loss of free-stream air momentum is greater than that gained by the jet. Calculations show that the reduction in J_{∞} caused by this effect adequately explains the measured "thrust loss" of a jet flap at high deflection angles, even though there are some small additional losses (such as nozzle diffusion loss) which will be identified in subsequent portions of this report.

We conclude, therefore, that jet flows cannot, in general, be explained by inviscid flow theory. Thus, a large part of the present program has been devoted to developing methods which allow viscous effects to be calculated.

Curved jet flows present the same general problems as rectilinear jets but with the added complication of centrifugal acceleration effects, as indicated in Figure 3.

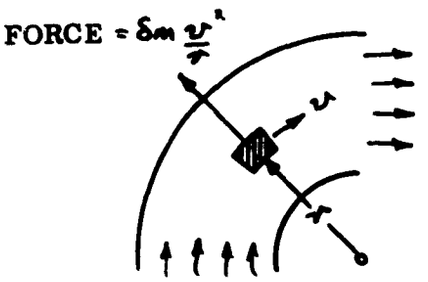

Figure 3. Centrifugal Force on a Curved Jet Element.

Since the centrifugal forces must be balanced by a static pressure gradient across the jet, even the inviscid flow field is fairly complicated in this case. Although many attempts have been made, we know of no completely satisfactory solution to this problem, so that development of an inviscid curved jet flow theory was the first task undertaken during this program. This was then used as the basis for corrections due to viscosity. Largely because of the terms of the initial work statement, this theory has been most fully developed and experimentally confirmed for the annular jet case. This has no particular significance, of course, and the general theory, with appropriate end-conditions, is equally applicable to any of the problems sketched in Figure 1. It is believed to be a powerful tool for the solution of a very large class of subsonic flow problems, and it was naturally impossible to develop its full potential in the present program.

DIFFUSION LOSSES

A viscous fluid can be accelerated without incurring important energy losses, so long as compressibility effects are not encountered. The process of slowing down a fluid -- diffusion -- always involves large energy losses, however. Thus,diffusion, and its associated phenomena of energy loss and flow separation, constitutes perhaps the most important problem in subsonic fluid dynamics. Paradoxically, it is a problem which has received relatively little attention, so that today the position is the same as it was decades ago, at least so far as minimizing diffusion losses are concerned.

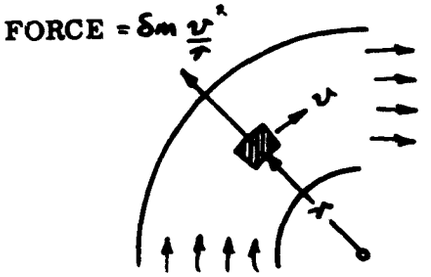

Figure 3. Centrifugal Force on a Curved Jet Element.

Since the centrifugal forces must be balanced by a static pressure gradient across the jet, even the inviscid flow field is fairly complicated in this case. Although many attempts have been made, we know of no completely satisfactory solution to this problem, so that development of an inviscid curved jet flow theory was the first task undertaken during this program. This was then used as the basis for corrections due to viscosity. Largely because of the terms of the initial work statement, this theory has been most fully developed and experimentally confirmed for the annular jet case. This has no particular significance, of course, and the general theory, with appropriate end-conditions, is equally applicable to any of the problems sketched in Figure 1. It is believed to be a powerful tool for the solution of a very large class of subsonic flow problems, and it was naturally impossible to develop its full potential in the present program.

DIFFUSION LOSSES

A viscous fluid can be accelerated without incurring important energy losses, so long as compressibility effects are not encountered. The process of slowing down a fluid -- diffusion -- always involves large energy losses, however. Thus,diffusion, and its associated phenomena of energy loss and flow separation, constitutes perhaps the most important problem in subsonic fluid dynamics. Paradoxically, it is a problem which has received relatively little attention, so that today the position is the same as it was decades ago, at least so far as minimizing diffusion losses are concerned.

Needless to say, the static pressure gradient generated in a curved jet flow means that diffusion must occur at some point. Hence, we were very concerned to find some way of analytically predicting the associated losses.

Even before the present program began, we noted two peculiarities. The first of these was the empirical observation (References 5, 6, and 7) that diffusion is possible only down to a velocity of about half the initial value, unless some means of renewing the boundary layer is used (multistage diffusion, boundary layer suction, etc.) The second point of interest was the fact that simple "Borda-Carnot" momentum theory for a rapid diffusion in a pipe gave very good agreement with measured losses.

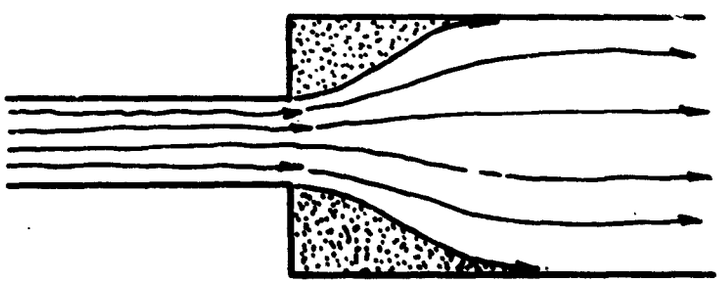

Figure 4 Borda-Carnot Diffusion.

The Borda-Carnot theory tended to be an isolated theoretical oddity, out of the main stream of fluid-dynamic theory, but we felt that it might offer important clues to more general cases.

In developing this theory in a more general form, we found that it tied in with the first (empirically observed) peculiarity in a very surprising way. If the velocity profiles before and after diffusion were mathematically similar, then the theory showed that the mean velocity ratio could not be less than 0.5. If the velocity profiles were dissimilar, then the maximum theoretically attainable diffusion varied in the same manner as indicated by boundary layer theory.

Obviously, it would have been desirable to follow up this clue, since we may well be on the threshold of a "unified theory" of diffusion. Unfortunately, the level of effort required was not possible under the present contract. However, it was possible to feel some confidence in the generalized (two-dimensional) diffusion theory produced during this part of the investigation, even though

its derivation, and certainly its application to some of the curved flow problems, could not be described as rigorous.

An interesting example of the application of the diffusion theory is the curved duct problem of Figure 1(e). The curved flow theory shows that, at the start of the bend, there is a sudden increase in static pressure on the outside wall and a reduction on the inner wall. At the end of the bend the situation is reversed, so that two diffusions occur: one on the outside wall at the beginning of the turn, and one on the inside wall at the end of the turn. By using the inviscid theory to calculate these pressure distributions, and then applying the new diffusion theory, we can calculate the total head lost in the turn. Not surprisingly, as shown in Chapter Nine, we find that, for two-dimensional flow,

$$\frac{\text{Total head lost}}{\text{initial dynamic head}} = \text{—} \left(\frac{\text{duct width}}{\text{radius of curvature}} \right)$$

Although no two-dimensional flow test data is available for this case, we find that extrapolation of the available three-dimensional data gives excellent agreement with the calculated theoretical loss. This obviously opens the way to significant improvements in the design of low-loss duct bends.

We have also applied this diffusion theory to the calculation of the total head lost in an annular jet nozzle. Once again, the agreement with experiment is good, both so far as total loss is concerned and for the loss distribution across the duct.

When applied to diffusion after a Coanda flow, the theory gives rather larger losses than for an equivalent pipe bend, but unfortunately, we know of no experimental data which can be used for comparative purposes in this case.

In summary, the new diffusion theory developed during the course of this program is apparently capable of dealing with relatively sudden pressure rises in two-dimensional flow and can (presumably) be extended to three-dimensional flow problems. A very limited comparison with experiment indicates good agreement, but substantially more work will have to be done before we can feel confident of it, because its basic derivation is not mathematically rigorous, at least for curvilinear applications.

In the following sections of this chapter we shall briefly summarize the basic work done on viscous mixing, curvilinear flow, and diffusion loss in the practical applications considered in this report.

ANNULAR JET THEORY

As for all of the problems considered, the basic differential equation for curvilinear flow applies to the annular jet problem. This equation is

$$\frac{dp}{dr} + \frac{\rho}{r} p_s = \frac{\rho}{r} P_s \qquad (3)$$

Here
- p_s is the local static pressure
- P_s is the local total pressure
- r is the local radius of curvature

In the following paragraphs we shall describe the solutions to this equation obtained by the investigators who pioneered annular jet theory. With the benefit of hindsight, we shall derive their solutions, from Equation (3), in one or two lines of analysis. This in no way detracts from their achievements, of course, because it is always easier to follow than to find a way. Also, it is doubtful that they realized that their problem was really the solution of Equation (3); rather, each appeared to formulate the physical description of the problem in a less fundamental way. Only in the present investigation has it been realized that Equation (3) is the starting point for all the formulations.

We shall also ignore, for the time being, the potential flow solution of Strand[14], since this is based upon an entirely different analysis. Strand's work was by far the most sophisticated attack on the annular jet problem, of course, and best agrees with the theory developed in this report over most of the operating height range. It suffers from a serious flaw, however, in that it deviates from known potential flow solutions as the nozzle approaches the ground plane, a defect which the present theory avoids. In the limit $h/t \to 0$, for example, the discharge coefficient approaches 0.5, instead of the known solution of approximately 0.62 for a slit.

The reason for this is not known. Strand himself, in verbal discussions with the senior author of this report, could only suggest a possible reason; thus an attempt to explain this anomaly is hardly likely to be fruitful.

In discussing inviscid flow solutions to the annular jet problem we shall not compare results with experiment. Many investigators have shown that real (viscous) annular jet flows generate relatively strong secondary flows, so that there is obviously a significant loss in cushion pressure, relative to the ideal inviscid fluid case. Also, as shown in the present report, there is a significant nozzle diffusion loss. Thus any appeal to experiment, as a means of judging an inviscid flow theory, is obviously likely to be unsatisfactory. Indeed, we might almost go so far as to say that an inviscid theory which agreed with experiment must be wrong, since the theory should not contain the viscous mixing and diffusion losses.*

CHAPLIN'S SOLUTION (THIN-JET THEORY)

The first important annular jet theory was Chaplin's[9], of course, where this Equation was expressed in finite, rather than infinitesimal, terms. By taking r as a constant ($r = R$ say), and assuming that the static pressure varies linearly across the jet, that is,

$$\frac{dp}{dr} = \frac{dp}{dz}\cdot\frac{dz}{dr} = \frac{dp}{dz} = \frac{\Delta p_c}{t} \qquad (4)$$

then Chaplin obtained, in effect,

$$\frac{\Delta p_c}{t} + \frac{2}{R}(z/t)\Delta p_c = \frac{2}{R}\Delta P_z.$$

In common with later investigators, he also assumed that the jet total pressure ΔP_z was constant (ΔP_j , say) across the jet.

Thus at the inner streamline ($z = t$),

$$\frac{\Delta p_c}{\Delta P_j} = \frac{2/R}{\frac{1}{t}+\frac{2}{R}} = \frac{2(t/R)}{1+2(t/R)}. \qquad (5)$$

He then calculated the radius of jet curvature (R),using the thin jet geometry shown in Figure 5.

---

*Since writing this report we have seen an excellent paper by Eames[27] in which this point is emphasized.

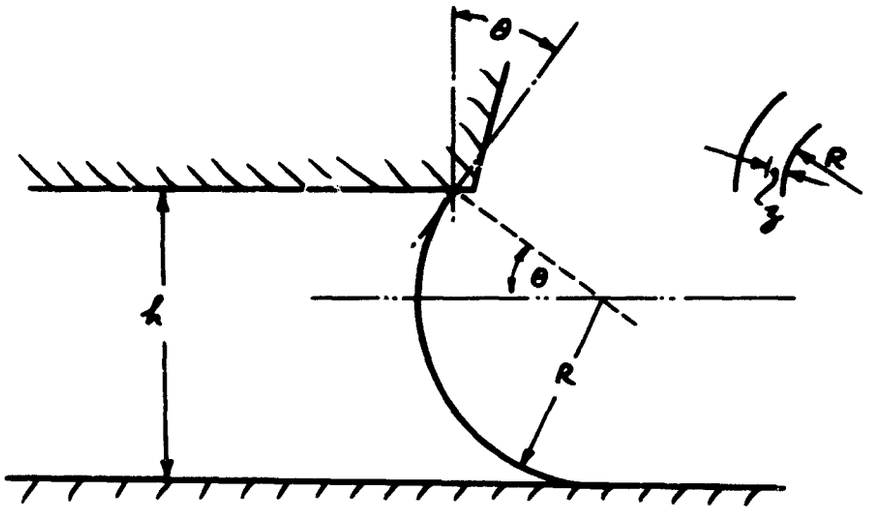

Figure 5 Chaplin's Curved Jet Geometry.

From this geometry, the clearance height (h) is evidently given by

$$h = R + R\sin\theta$$

$$\therefore R = \frac{h}{1+\sin\theta}$$

$$\therefore h/R = \frac{h}{h}(1+\sin\theta) = \varkappa \text{ (say).} \tag{6}$$

Thus Chaplin's relationship for the cushion pressure (Δp_c) becomes

$$\frac{\Delta p_c}{\Delta p_j} = \frac{2\varkappa}{1+2\varkappa} \tag{7}$$

It is found that this gives fair agreement with experiment for small values of $\varkappa$ (large hover heights) but becomes progressively less accurate as the height is reduced. When the vehicle is touching the ground ($h=0$), Equation (7) gives $\Delta p_c/\Delta p_j = 2.0$, whereas we know that the correct answer should be 1.0; that is, because no air is flowing, the total and static pressures are equal.

Chaplin recognized these limitations, of course, and specifically limited his theory to "thin jets" in which $\ell >> t$.

As mentioned above, Chaplin assumed that the jet radius of curvature was constant. To be more specific, he assumed it was constant along the jet because it divided two constant pressure areas: the "cushion" and the ambient air outside. He was able to show that the assumption of constant pressure boundaries of necessity required a constant curvature.

He also assumed that the curvature was constant across the jet. This is (mathematically) acceptable for thin jets, but gives rise to a rather meaningless physical picture, since the jet vanishes at the ground plane. This is illustrated in Figure 6, a thick jet being shown for clarity.

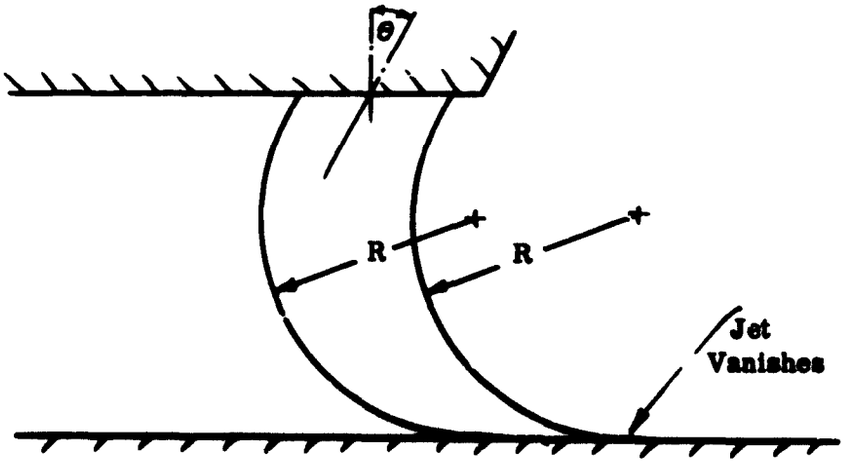

Figure 6 Physical Interpretation of the Constant Radius of Curvature Jet.

THE CROSS-STANTON-JONES SOLUTION (EXPONENTIAL THEORY)

Cross[10] and Stanton-Jones[11] (the precedence cannot be determined from the literature) extended Chaplin's theory to the case of "thick jets". Their only change was to reject the assumption of constant static pressure gradient across the jet, Equation (4). Since they retained Chaplin's constant radius assumption, their version of Equation (3) was

$$\frac{dp}{dr} + \frac{\rho}{R}\Delta p_z = \frac{2}{R}\Delta P_j . \qquad (8)$$

Or, since $dy = dr$

$$\frac{d\Delta p}{dy} + \frac{2}{R}\Delta p_y = \frac{2}{R}\Delta P_j \tag{9}$$

This is a simple first-order differential equation with constant coefficients, and the solution is well known. That is,

$$\Delta p_y = e^{-2y/R}\left[\frac{2}{R}\int e^{2y/R}\Delta P_j\, dy + K\right]. \tag{10}$$

When we insert the end condition $\Delta p_y = 0$ at $y = 0$ (jet static pressure the same as ambient at the outermost streamline) this equation simplifies to

$$\frac{\Delta p_y}{\Delta P_j} = 1 - e^{-2y/R}. \tag{11}$$

and the cushion pressure, which corresponds to the innermost streamline ($y = t$), is then

$$\frac{\Delta p_c}{\Delta P_j} = 1 - e^{-2t}. \tag{12}$$

This equation tends to unity as the ground clearance height (t) tends to zero, thus avoiding the most important limitation of Chaplin's solution. When compared with experimental results it gives quite good agreement. As a result, the general theory which follows from Equation (11) is widely used in the industry. Yet if this agreement is fortuitous, acceptance of exponential theory could prevent the obtaining of a better physical picture of annular jet flow, and hence prevent the discovery of more efficient ways of generating an annular jet.

PINNES' SOLUTION (FREE-VORTEX FLOW)

Exponential theory is based upon an impossible physical picture, as we have seen, since the jet cannot possibly vanish as it strikes the ground. Pinnes[12] chose to circumvent this by assuming that the jet thickness remained constant, as shown in Figure 7.

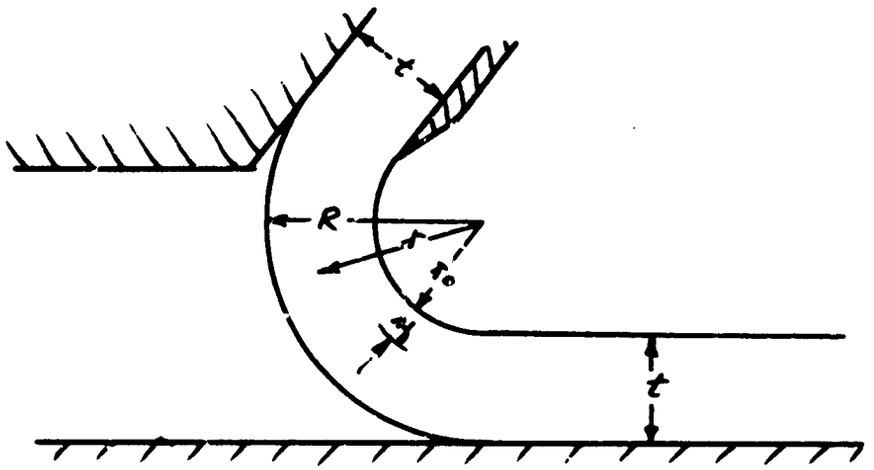

Figure 7 Pinnes' "Free Vortex" Assumption for Annular Jet Flow.

We can immediately see that this formulation must be to a "thin-jet" theory, since if $h < t$, the outer radius r_o will have to be negative, a physical impossibility.

While retaining the assumption that any jet streamline will have constant curvature along its length, the Pinnes formulation assumes that (r) will vary across the jet in a linear manner. That is,

$$\left.\begin{aligned} r &= r_o + z \\ R &= r_o + t \end{aligned}\right\} . \tag{13}$$

This is a significant improvement in rigor, relative to exponential theory. The basic differential equation now becomes

$$\frac{dp}{dz} + \frac{2}{(r_o+z)}\Delta p_z = \frac{2}{(r_o+z)}\Delta P_j . \tag{14}$$

The standard form solution then gives

$$\frac{\Delta p_z}{\Delta P_j} = \frac{2\int_0^z (r_o+z)\,dz}{(r_o+z)^2} \tag{15}$$

and the cushion pressure

$$\frac{\Delta p_c}{\Delta p_j} = \frac{\left(2\frac{r_0}{t}+1\right)}{\left(\frac{r_0}{t}+1\right)^2}$$

$$= 2x - x^2 \qquad (16)$$

In this case $\Delta p_c/\Delta p_j = 1.0$ when $x = 1.0$, a result which is obviously in error, due to the geometrical limitations noted above. Also, as $x \to 1.0$, the theoretical mass flow tends to zero. Thus,we have to conclude, rather paradoxically, that although the Pinnes formulation is more rigorous, it results in a less accurate description of annular jet flow. In the sense that it pointed the way to further developments, however, the Pinnes theory represented an important advance.

PAYNE'S CORRECTION FOR JET CURVATURE

All the previous theories used Chaplin's relationship (6) for jet curvature. Payne[13] pointed out that this was correct only for zero jet deflection angle, or when the jet was of negligible thickness. The correct relationship for a jet of finite thickness (t) is actually

$$R = \frac{h - t\sin\theta}{(1+\sin\theta)} \qquad (17)$$

so that

$$t/R = \frac{t/h\,(1+\sin\theta)}{(1-\quad\sin\theta)} = X \text{ (say)} \qquad (18)$$

in place of Chaplin's relationship given in Equation (6). In Reference 13, Payne showed that the available experimental data correlated better against this new parameter X .

THE ANNULAR JET SOLUTION OF THIS REPORT

Although Pinnes improved the physical representation of the annular jet at large heights, he stopped short of realising a perfectly general description. As indicated in Figure 8, his geometry is approximately correct at large ground clearances and the exponential theory (constant radius) geometry is approximately correct for very low clearances.

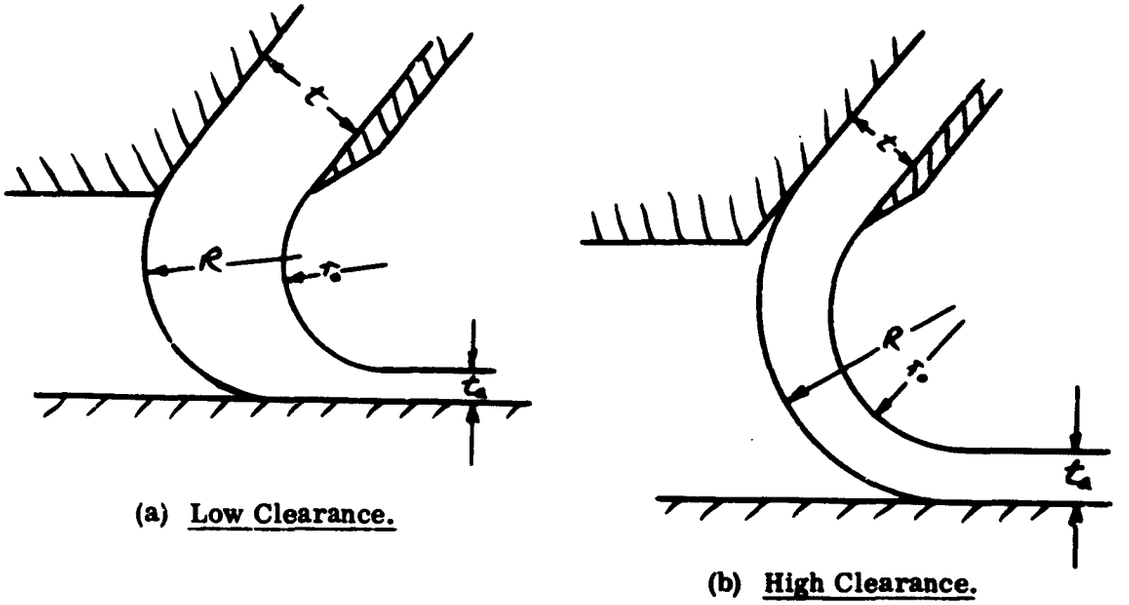

(a) Low Clearance.

(b) High Clearance.

Figure 8. Effect of Ground Clearance on Jet Radius of Curvature.

At low heights the static pressure in the jet is high and the mass flow is low. Thus, after the jet has expanded to ambient pressure along the ground plane, it is moving much faster, and its thickness (t_a) is much less than the nozzle thickness (t). Under these conditions, r_0 is only a little less than R, and exponential theory gives a good description of the flow.

At high heights, there is little difference between the cushion pressure and ambient, so that $t_a \to t$. Under these conditions there is little change in jet thickness and Pinnes solution gives a good description of the flow. Thus the two limits are

$$\left.\begin{aligned} R &\to r_0 \quad \text{as } h \to 0 \\ R &\to (r_0 + t) \quad \text{as } h \to \infty \end{aligned}\right\} . \tag{18}$$

We naturally wondered if it would be possible to interpolate these two limit cases with a more general variation.

$$R = r_0 + \eta z \tag{20}$$

where $\eta = f(\Delta P_z)$

When $\eta = 0$, we have exponential theory and when $\eta = 1.0$ we have free-vortex theory. In general, η will be between these two extreme values.

As will be shown later, it turns out that such an interpolation is possible, and we find

$$\eta = \frac{\epsilon/\ell + \sin\theta}{1 + \sin\theta} . \tag{21}$$

Thus the local radius in the jet is now given by

$$r = r_0 + \eta z . \tag{22}$$

Equation (3) then becomes

$$\frac{\partial \Delta p_z}{\partial z} + \frac{2}{(r_0 + \eta z)} \Delta p_z = \frac{2}{(r_0 + \eta z)} \Delta P_z . \tag{23}$$

and the general solution is therefore

$$\Delta p_z = (r_0 + \eta z)^{-2} \left\{ 2 \int_0^z (r_0 + \eta z)^{2-1} \Delta P_z \, dz \right\} . \tag{24}$$

Note that in this equation we have retained ΔP_z as an arbitrary function of (z), rather than assume it to be constant, as previous workers have done. We shall find that a variation in ΔP_z across the jet influences the cushion pressure generated and that this can be quite different from the result obtained by assuming a constant total pressure equal to the mean value.

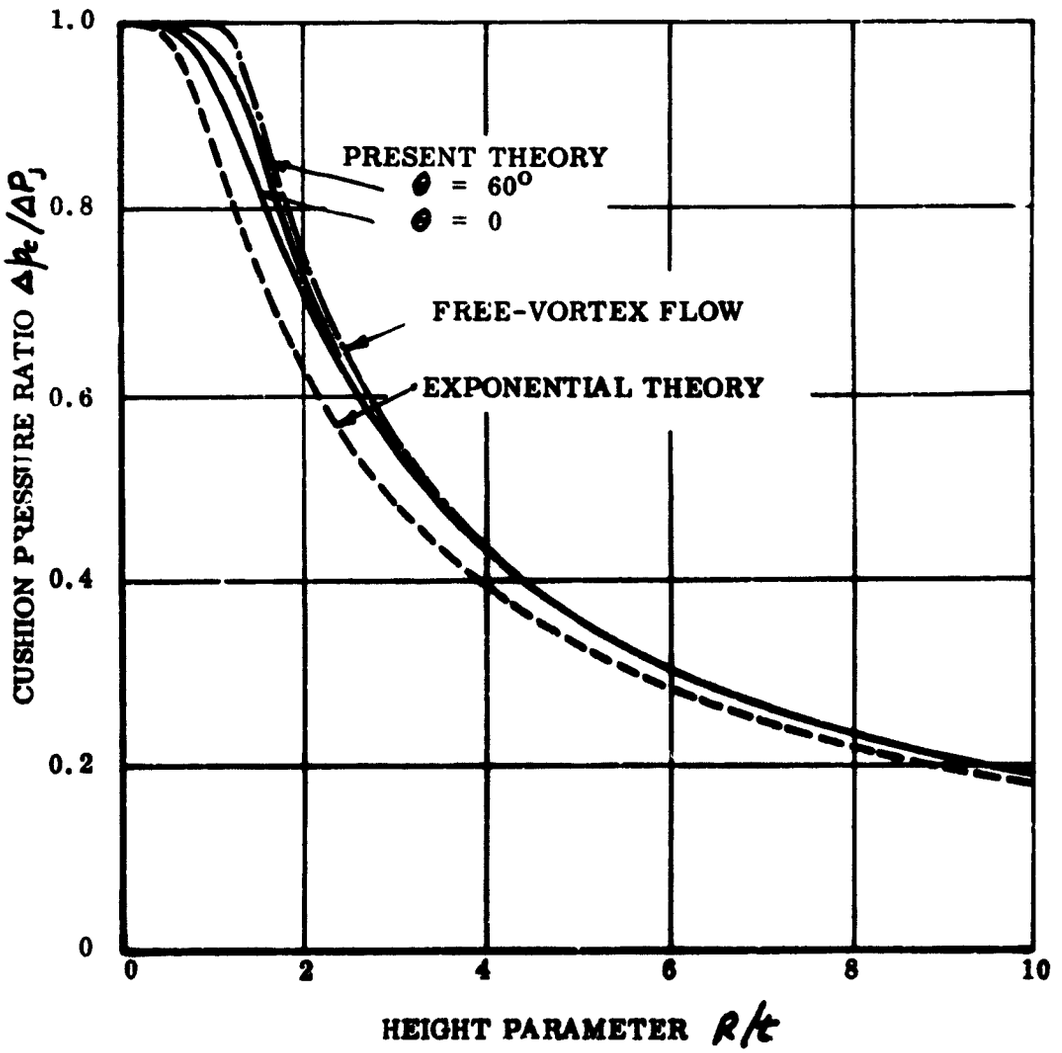

Figure 9. Comparison of the New Inviscid Flow Theory With Previous Theories.

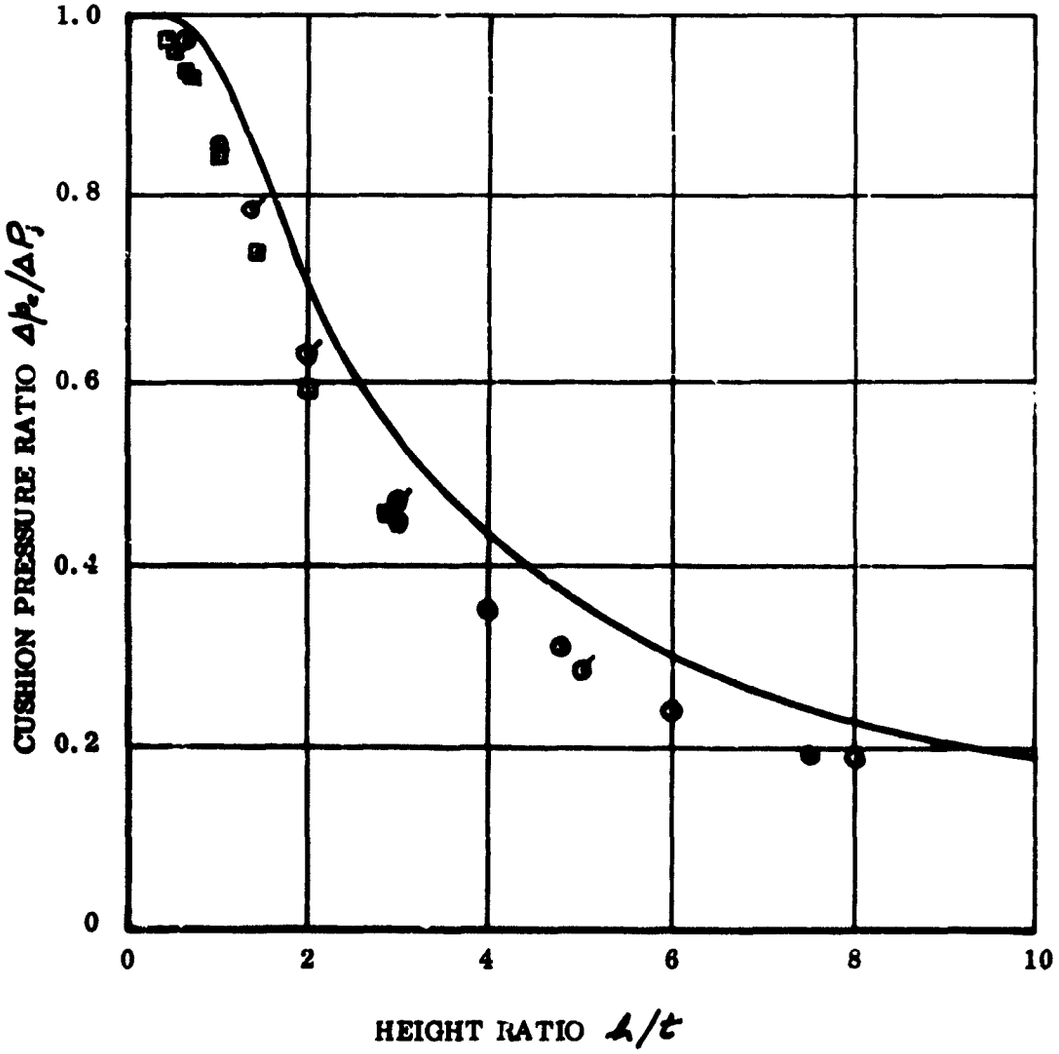

Figure 10. Comparison of the New Inviscid Flow Theory With Some Experimental Data (θ = 0°).

For the case of uniform jet total pressure, the new theory is compared with exponential and free-vortex theories in Figure 9. As we should expect, it falls between these two limits, tending to the Pinnes solution above $R/4 = 4.0$. In the intermediate range, it gives a cushion pressure which is quite significantly greater than that given by exponential theory.

Referring now to Figure 10, which shows some experimental data in comparison with the new theory, we may wonder whether the new theory was worth developing, since all the data points fall below it! The theory is for inviscid flow, however, and we shall see that when we correct it to allow for the effects of nozzle diffusion loss and viscous entrainment in the jet, good agreement with experiment is obtained. The older theories disregarded these effects and hence offered no rational methods of minimizing them.

MOMENTUM BALANCE OF THE ANNULAR JET

An important offshoot of the analysis presented in this report is the concept of momentum balance.

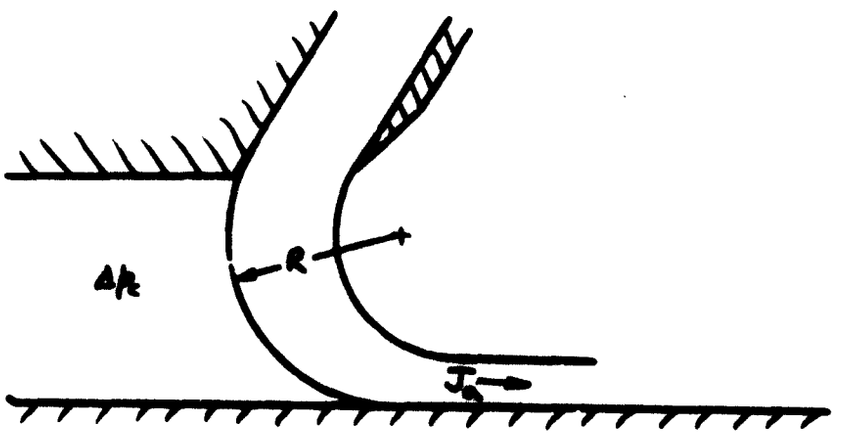

Figure 11. Momentum Balance Geometry.

Referring to Figure 11, it will be shown quite rigorously that, if R is a constant, then

$$\Delta p_c = \frac{J_a}{R C_e} \tag{25}$$

where J_a is the momentum flux to ambient and C_e is the effective jet periphery (jet length in the two-dimensional case).

This simple relationship is of considerable value, since it is quite fundamental.

COANDA JET THEORY

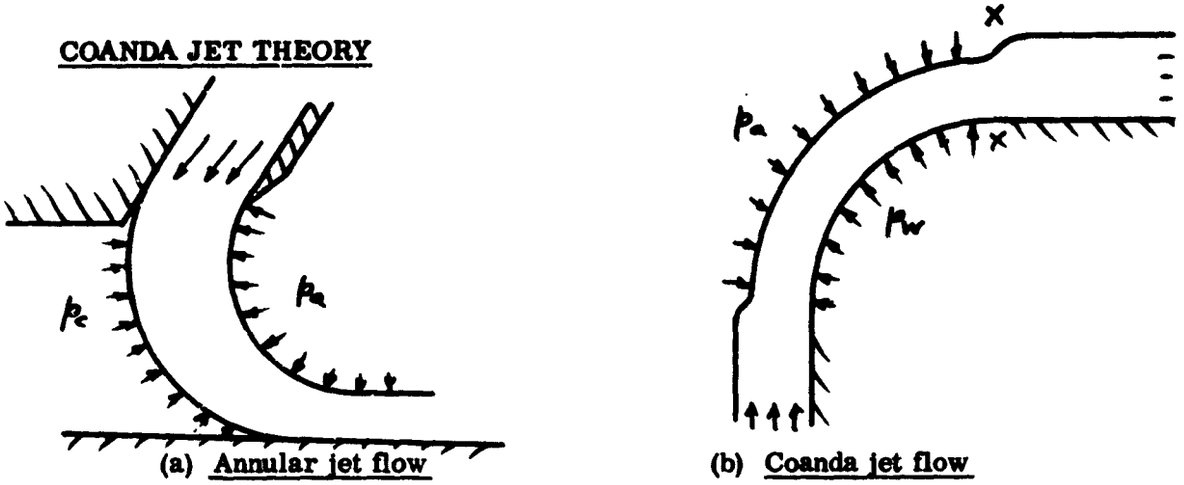

(a) Annular jet flow (b) Coanda jet flow

Figure 12. Equivalence of Annular Jet and Coanda Jet Flows.

As indicated in Figure 11, there is no difference, in principle, between the annular jet, which is curved outward by the cushion overpressure, and the Coanda jet flow, which is curved inward by wall "suction". Equation (3) is still applicable but the "end condition" of ambient static pressure is now transferred to the opposite side of the jet.

In the present investigation we have considered only the free-vortex solution ($r = r_0 + z$) although the more general case of ($r = r_0 + nz$) may be more applicable when the jet thickness is large.

One basic difference in the overall flow system is the diffusion which occurs at the end of the curved flow path (X-X in Figure 12b). If the curve intersects with a tangential straight wall, then the sudden disappearance of the centrifugal forces in the flow must result in a sudden static pressure rise at the intersection. This effect is amenable to the diffusion loss analysis mentioned earlier, and we find that quite large pressure losses are to be expected when the jet is thick. Coupled with the skin friction loss and the static pressure gradient across the jet, this diffusion loss explains why laboratory studies of the Coanda effect do not show any thrust augmentation effect, even though the jet entrains ambient air at a lower-than-ambient static pressure.

In Reference 3 (part of which was written under the present contract), it was shown that thrust augmentation occurs when a jet mixes with ambient air at a static pressure which is lower than ambient. As indicated in Figure 13, there is an optimum static pressure for maximum augmentation; mixing at pressures away from this optimum results in less than optimum augmentation.

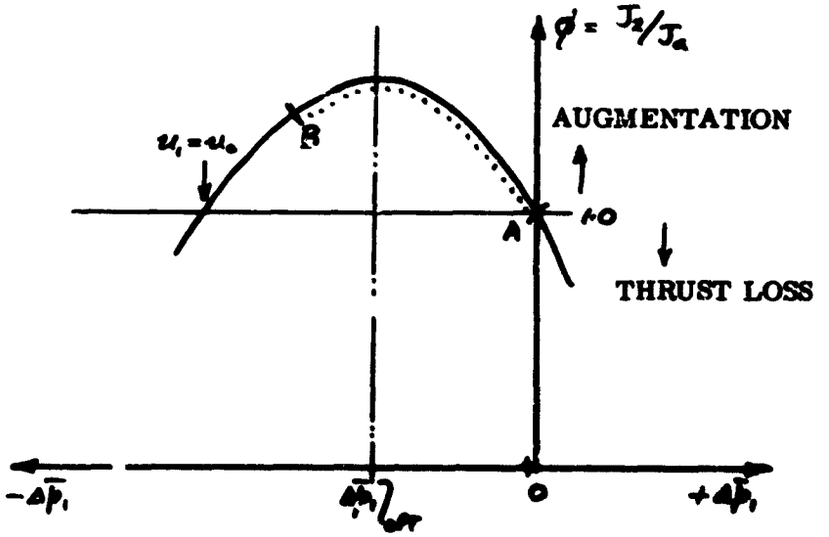

Figure 13. Variation of Augmentation Ratio ϕ With the Mixing Pressure Parameter $\Delta\bar{p}_1$.

Thrust augmentation is defined as

$$\phi = \frac{J_2}{J_a} = \frac{\text{Total thrust of the augmentor}}{\text{Thrust of primary exhausting to ambient}} .$$

The mixing pressure parameter is

$$\Delta\bar{p}_1 = \frac{\Delta p_1}{\frac{1}{2}\rho u_a^2} = \frac{\text{Static pressure at which mixing occurs}}{\text{Dynamic head of primary jet}} .$$

In Coanda flow, the mixing pressure varies from ambient ($\Delta\bar{p}_1 = 0$, point A in Figure 13) at the outside of the jet to

$$\Delta\bar{p}_1\Big|_{max} = \frac{-t/r_2\,(2 + t/r_2)}{(1 + t/r_2)^2} \qquad (26)$$

at the wall (point B in Figure 13). Thus,the mixing pressure can only be optimum at one streamline (ζ),and the overall augmentation will be less than optimum.

A second factor determining augmentation is the efficiency at which the flow is diffused back to ambient from the mixing pressure Δp_1 . A typical variation is sketched in Figure 14.

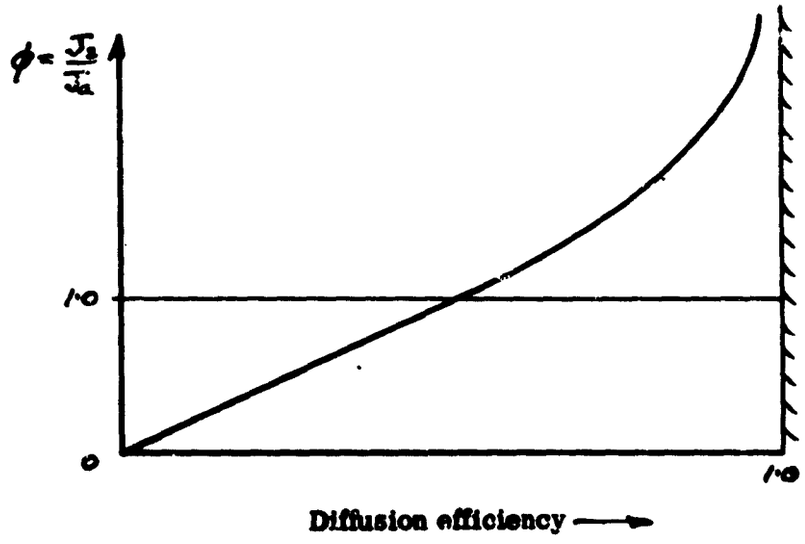

Figure 14. Variation of Augmentation Ratio With Diffusion Efficiency, Assuming Optimum Mixing Pressure.

It is obvious that worthwhile thrust increases can be obtained only when the diffuser efficiency is high -- 90% or greater, say. For relatively thick jets, the diffusion loss at the end of a Coanda curve can be quite large -- η_2 as low as 0.5 -- so that high augmentation ratios can be obtained only by keeping the jet thin. The losses due to skin friction then become important, however.

Another reason for using thin jets when augmentation is required is the amount of ambient fluid entrained in the jet. The attainable augmentation ratio naturally increases with the amount of fluid entrained and, as indicated in Figure 15, this becomes important only below t/r_2 = 0.1. Very high entrainment ratios require a jet thickness which is only a few percent of the radius of curvature; and in this case, boundary layer effects start to become important.

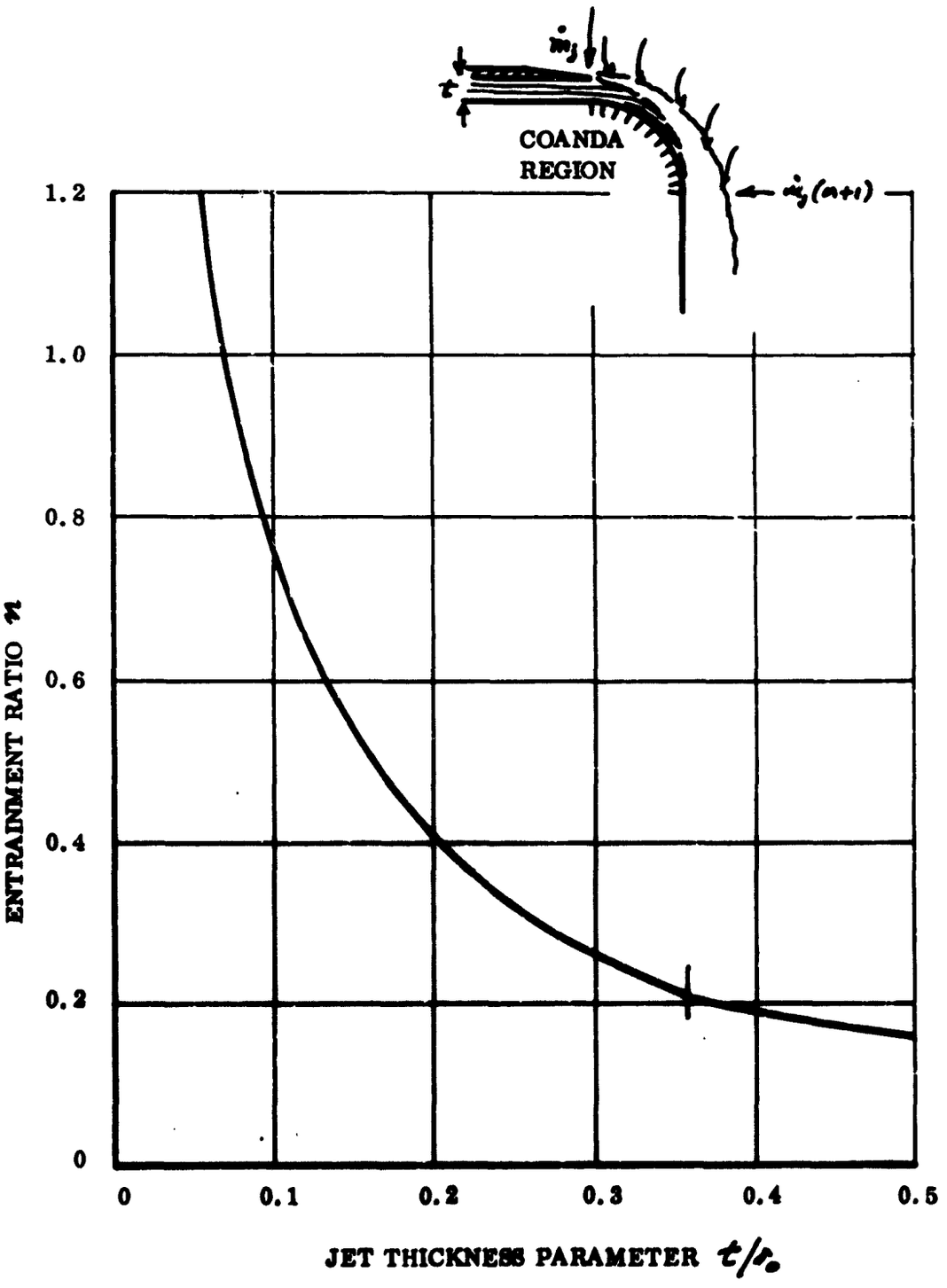

Figure 15. · Variation of Entrainment Ratio With Jet Thickness for a Right-Angle Coanda Bend.

Although nothing can be done about Coanda mixing at nonoptimum pressures, we can avoid the efficiency loss due to diffusion, as indicated in Figure 16.

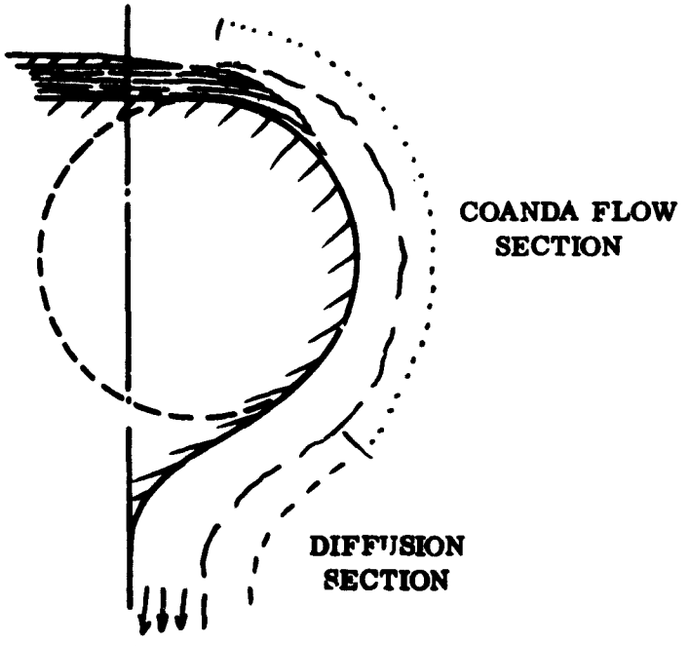

Figure 16. A Coanda Profile Designed for Maximum Thrust Augmentation.

In the present program we have tended to regard the Coanda effect as an interesting test of the theoretical methods as they were developed, so that the amount of coherently connected study of this phenomenon was rather slight. The basic techniques, however, would seem to satisfy all the requirements for an exhaustive study. We believe that such a study would be very fruitful and might lead the way to important future applications of this interesting phenomenon.

INTAKE FLOW THEORY

The intake flow field depicted in Figure 1(a) is becoming increasingly important in hardware applications, some examples being the XV-4A, XV-5A, and various GEM configurations.

Since it is a curvilinear flow problem, Equation (3) again applies; and in a subsequent chapter of this report, the appropriate end-conditions are defined, and solutions obtained for certain simple cases. Characteristically, the air

accelerates over the forward lip and then diffuses into the duct, so that separation of the flow can occur, as indicated in Figure 17.

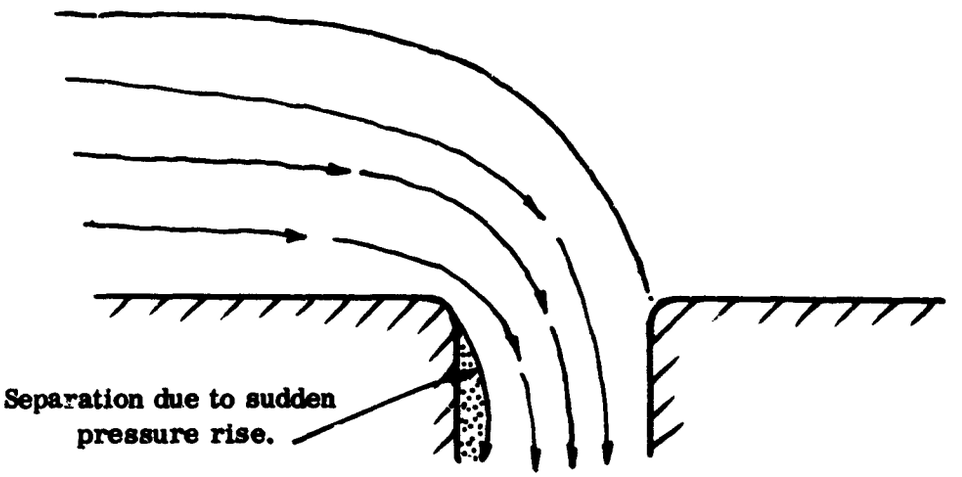

Figure 17. Leading Edge Separation With Intake Flow.

Even without separation, total pressure losses occur, and once again, these can be calculated with the diffusion theory developed during this program, although lack of time has prevented us from actually doing this. Thus, the theoretical concepts developed present us with the means of designing optimum intake geometries.

The classical approach to such problems is to use the method of singularities to calculate the inviscid flow field. This has drawbacks, of course, because a real fluid tends to separate in regions of high adverse pressure gradient. Moreover, the fact that a real flow is not at a constant energy level precludes such an approach from ever giving precise results unless the configuration under consideration is one in which constant energy is a viable assumption.

In a practical intake flow problem, it is usual for some boundary to exist upstream of the intake opening. It will be shown that even a very thin boundary layer can have a very marked effect on the intake flow distribution. More importantly, the separation or flow distortion which results from high drag areas upstream of the intake can have a large influence upon the intake flow distribution and on whether diffusion separation of the flow will occur.

These effects can be studied, using the techniques developed, but once again, lack of time has precluded such studies in the present program.

MOMENTUM DRAG

The momentum drag of an intake is usually defined as

$$\text{Drag} = (\text{mass flow}) \times (\text{free-stream velocity}) = \dot{m} U_\infty \quad . \tag{27}$$

Various investigators have reported anomalies, in that the difference between the measured profile drag (air off) of a vehicle -- particularly a GEM -- and the total drag is less than ($\dot{m} U_\infty$); sometimes there is no difference at all.

The present work on intake flow indicates that Equation (27) is not correct, since the intake is not swallowing undisturbed air in most cases. If there is a substantial skin surface upstream of the intake, for example, the boundary layer air has already been slowed down to a velocity less than U_∞ . If there is a high-drag element (such as a stalled wing leading edge, or a bluff body shape, upstream) then all the intake air may have an initial velocity which is substantially less than U_∞ . It is felt that this probably explains all the observed anomalies, although it has naturally proved impossible to undertake a detailed review of them.

THE JET FLAP

The "thrust hypothesis" of the jet flap was earlier referred to and illustrated in Figure 2. In an effort to obtain some first-hand experience, we built a 20% thick elliptical aerofoil for the Payne two-dimensional tunnel, and also ran a similar model in the smoke tunnel.

Typical smoke tunnel runs are illustrated in Figures 18 and 19. These are quite conventional results, except for the indication of turbulence in the wake of the wing. It is also very interesting to note that, below the wing, the free-stream air enters the jet, rather than being deflected by it, as would be expected in inviscid flow.

We then studied the forces generated in the two-dimensional tunnel; using the test setup indicated in Figure 20. As indicated in Figure 21, operation of the jet flap generated more drag, rather than a thrust force!

Figure 18. **Twenty Percent Elliptical Aerofoil in the Smoke Tunnel. No Air Supply to Jet Flap.**

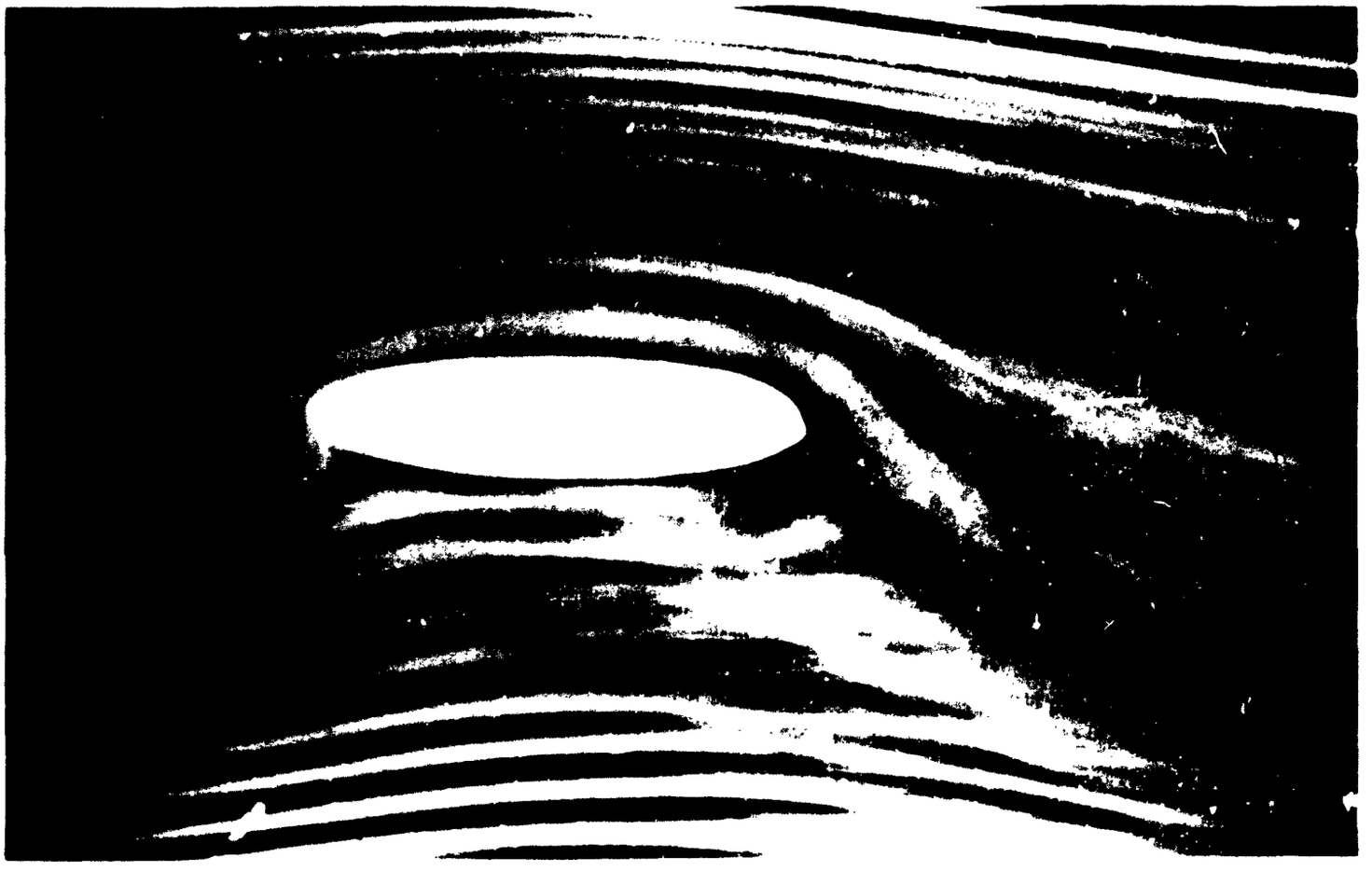

Figure 19. Streamlines Around the Elliptical Aerofoil When the Jet Flap is Operating.

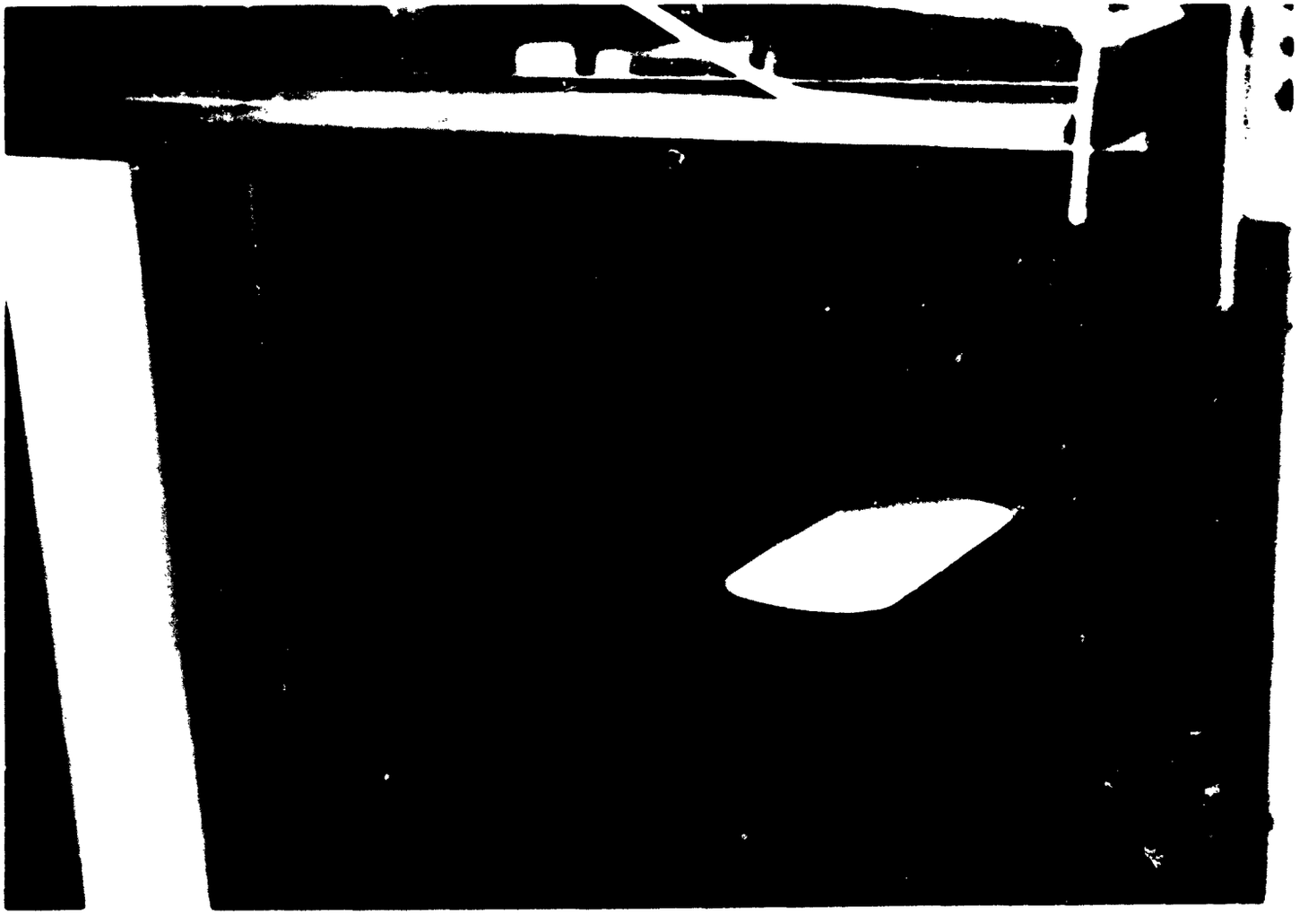

Figure 20. **Jet Flap Experiment in the Two-Dimensional Wind Tunnel. (Total Pressure Traverses Are Made With the Kiel Probe on the Left.)**

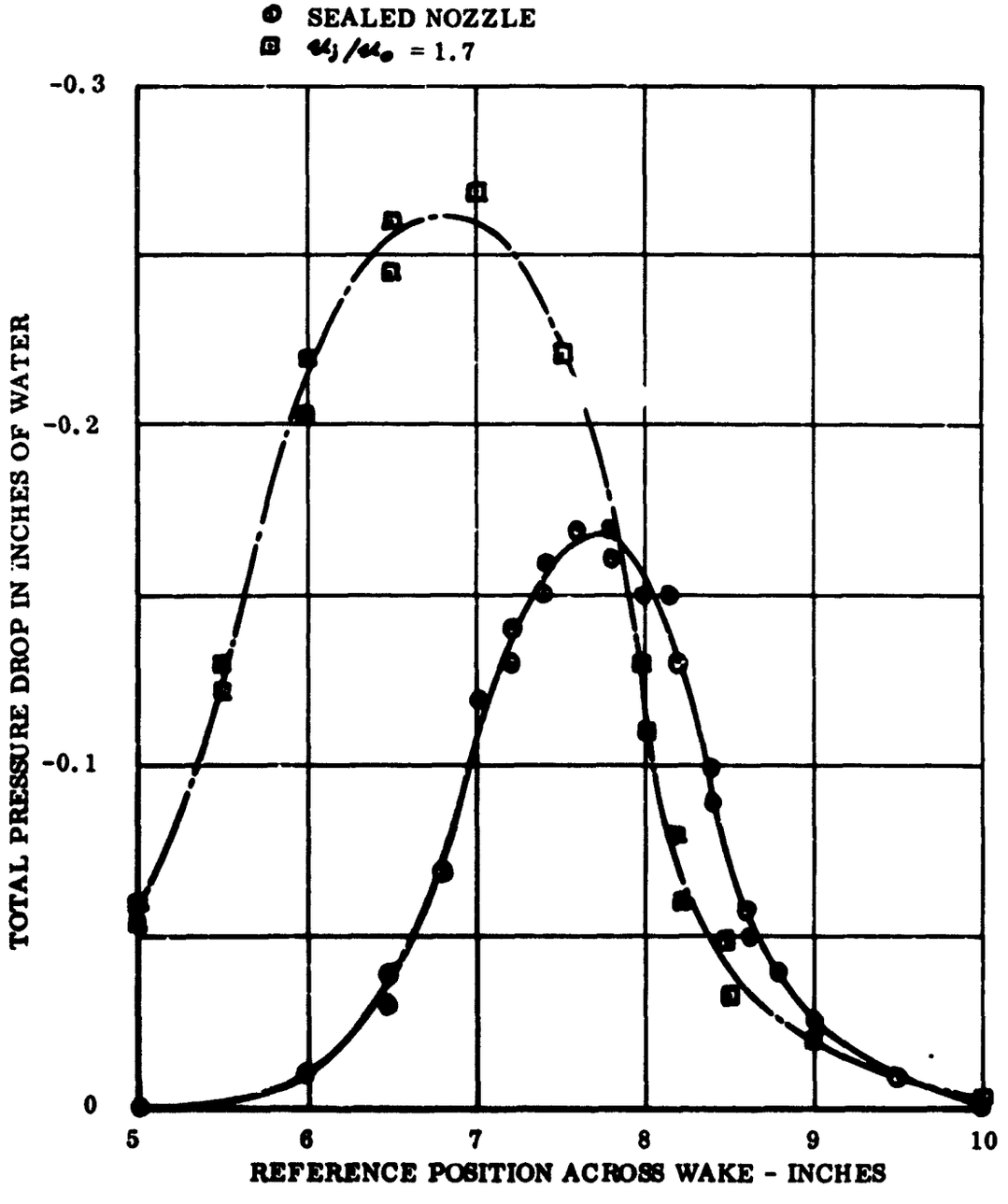

Figure 21. Results of Total Head Traverses 3.25 Chords Behind the Jet Flapped Aerofoil, With the Jet Flap On and Off.

The main reason for this is indicated in Figure 22. Because of the relatively low jet to free-stream velocity ratio, the jet entrainment is insufficient to avoid flow separation around the trailing edge of the wing. Thus, the jet sheet actually increases the depth of the wake.

Given a relatively slow-speed wake, the jet now loses more energy by mixing with it, and also by mixing with free-stream air in the region marked X—X in Figure 22.

The net result was that, instead of obtaining

$$\frac{J_\infty}{J_0} \simeq +1.0$$

as Figure 2 would indicate, we measured

$$\frac{J_\infty}{J_0} \simeq -0.32$$

Presumably J_∞/J_0 would have been positive if the jet had been energetic enough to prevent flow separation at the trailing edge. Mixing in the region X—X would still have occurred, however, and in Reference 3 it is shown that even this is enough to explain the low values of thrust recovery ($J_\infty/J_0 \simeq 0.2 - 0.4$) reported by other workers.

JET ISSUING NORMAL TO A FREE-STREAM FLOW

The jet-flap measurements indicated that the physical picture was extremely complicated. In an effort to isolate some of the variables we therefore designed an experiment in which a jet issued from the tunnel floor, as illustrated in Figure 23.

From Equation (25) we should expect the balance of momentum flux and the pressure forces to give

$$J_a \simeq \int \Delta p_s \, dy - \Delta p_s \, h. \qquad (28)$$

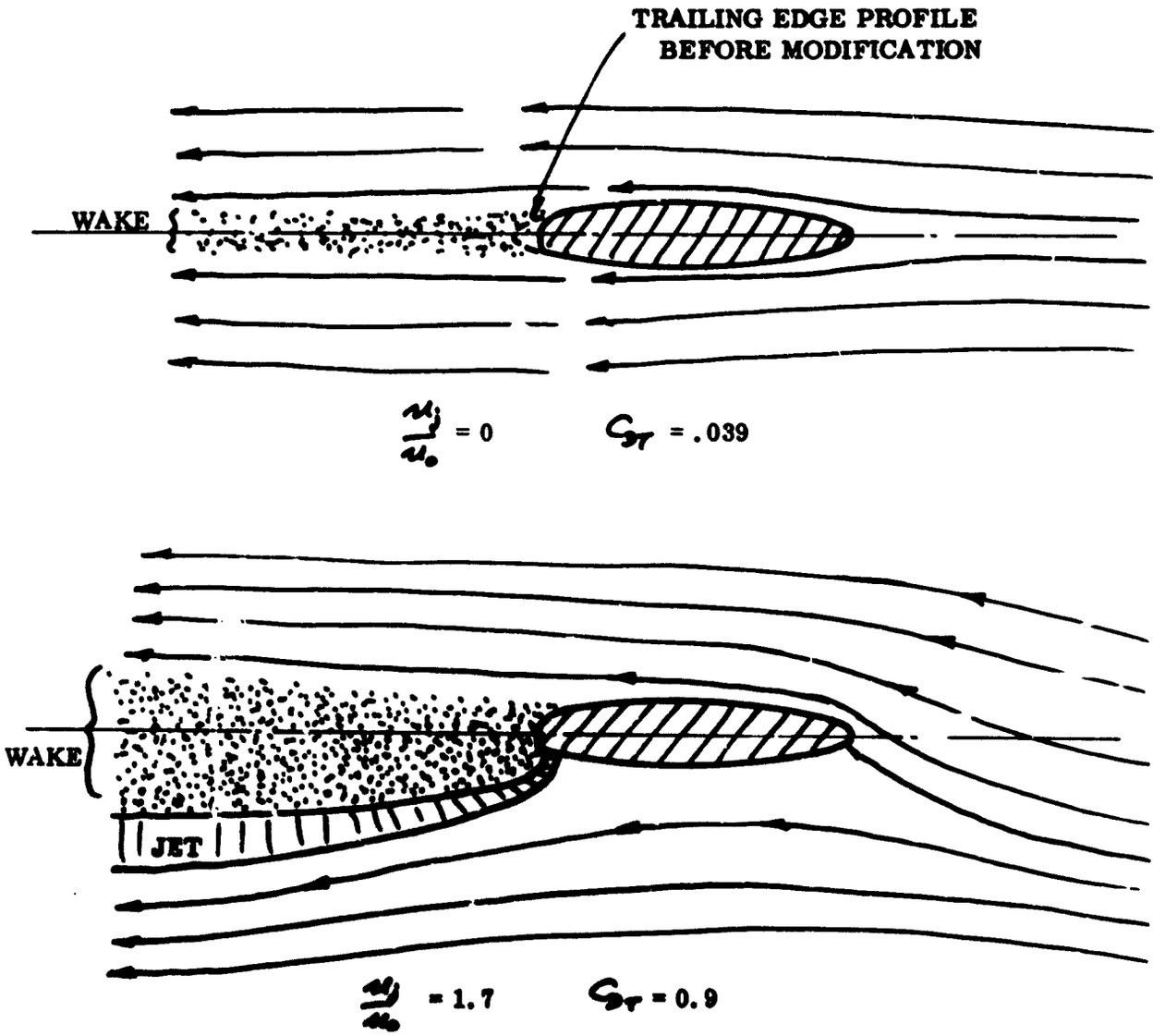

Figure 22. Observed Flow Patterns, With and Without Jet Flap Operating. (The trailing edge was modified in an effort to avoid flow separation).

If $\Delta p_c = 0$

$$J_a = \left(\frac{\int \Delta p_x \, dy}{h \, q_o}\right) h \, q_o .$$

and since $J_a = \left(\frac{J_a}{J_j}\right) \rho t u_j^2 ,$

$$\left(\frac{h}{t}\right) = \frac{2(u_j/u_o)^2 (J_a/J_j)}{\left(\frac{\int \Delta p_x \, dy}{h \, q_o}\right)} . \qquad (29)$$

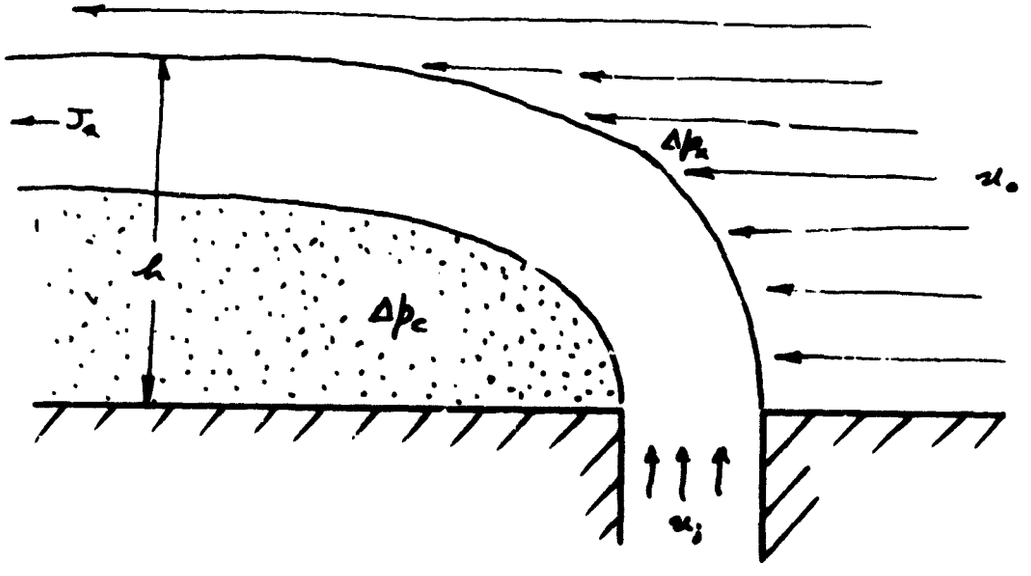

Figure 23. Assumed Geometry.

The parameter ($\int \Delta p_x \, dy / h \, q_o$) is studied in the main body of this report and is shown to be relatively insensitive to jet shape.

For the test conditions employed in the two-dimensional tunnel we obtained the following:

u_j/u_0	.56	1.34	2.88
Measured	---	5.0	7.5
Theoretical	0.94	75.0	169.0

The theoretical figures are based on the assumption of a constant radius curve, but even in the limit case they would be reduced by only two-thirds. Obviously, the theoretically predicted ℓ/t is an order of magnitude greater than the measured value.

A small part of this is attributable to assuming $\Delta p_c = 0$. From the test data we can see that $\Delta p_c < 0$, due to viscous entrainment of the cavity air. Most of it must be due to a reduction in J_a, however; part of which is attributable to mixing with the cavity air and part to mixing with the free-stream air.

Although some aspects of this problem have been studied briefly in Reference 3, we have not attempted to formalize the theory completely for this problem because of lack of time. Nevertheless, sufficient work has been done to indicate that it is probably amenable to the general techniques developed during this program.

Chapter Two

GENERAL DIFFUSION THEORY

THE FLOW OF A JET THROUGH A DISCONTINUITY IN STATIC PRESSURE

The flow of a jet through a change in static pressure is not well understood, perhaps because it rarely occurs in practice; or rather, it was rare until the advent of the jet flap and the annular jet. A one-dimensional solution due to Borda and Carnot is known for the case of an abrupt duct enlargement (the "Borda-Carnot loss" or the "Carnot impact formula") and gives very good agreement with experimental observations. However, this analysis has not been extended, and it is the purpose of the following sections to generalize the theory and to extend it to two-dimensional flow.

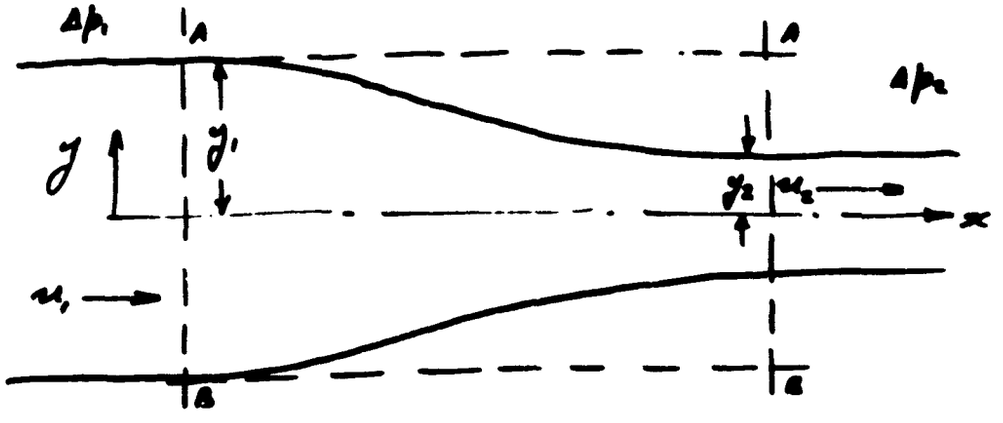

Figure 24. Geometry of Flow Through a Pressure Change.

SOLUTION FOR CONSERVATION OF TOTAL HEAD

In Reference 4, Payne assumed that, in the absence of a mechanism to account for losses, total head is conserved when a jet undergoes a change in static pressure. Referring to Figure 24, this amounts to assuming Bernoulli's equation for conservation of total head to apply along any streamline

$$\rho u_2^2 = \rho u_1^2 + 2(\Delta p_1 - \Delta p_2). \qquad (30)$$

For the one-dimensional case, the momentum flux is given by

$$J_1 = \dot{m} u_1, \qquad J_2 = \dot{m} u_2 .$$

Substituting into Equation (30),

$$\left(\frac{J_2}{\dot{m}}\right)^2 = \left(\frac{J_1}{\dot{m}}\right)^2 + \frac{2}{\rho}(\Delta p_1 - \Delta p_2)$$

$$J_2 = \left[J_1^2 + \frac{2}{\rho}(\Delta p_1 - \Delta p_2)\right]^{1/2}. \tag{31}$$

Since $\dot{m} = \frac{J_1}{u_1}$, this may also be written as

$$\frac{J_2}{J_1} = \left[1 + \frac{\Delta p_1 - \Delta p_2}{\frac{1}{2}\rho u_1^2}\right]^{1/2}. \tag{32}$$

In other words, an increase in static pressure reduces the momentum flux and vice versa.

THE GENERAL MOMENTUM SOLUTION

Consider the control boundary in AA and BB in Figure 24. The horizontal pressure forces on this boundary must equal the momentum flux in the system.

$$2y_1(\Delta p_1 - \Delta p_2) = \int_{-y_2}^{+y_2} \rho u_2^2 \, dy - \int_{-y_1}^{+y_1} \rho u_1^2 \, dy \tag{33}$$

$$= J_2 - J_1 \quad (\text{say}). \tag{34}$$

The mass flow is given by

$$\dot{m} = \int_{-y_1}^{+y_1} \rho u_1 \, dy = \int_{-y_2}^{+y_2} \rho u_2 \, dy$$

$$\dot{m} = y_1 \int_{-1}^{1} \rho u_1 \, d(y/y_1) = y_2 \int_{-1}^{1} \rho u_2 \, d(y/y_2)$$

$$= 2\rho y_1 \hat{u}_1 \qquad = 2\rho y_2 \hat{u}_2$$

$$\therefore \quad y_1 = \dot{m}/2\rho\hat{u}_1 \tag{35}$$

and $$J_2 = J_1 + \frac{\dot{m}}{\rho a_1}(\Delta p_1 - \Delta p_2) \tag{36}$$

$$\therefore \quad \frac{J_2}{J_1} = 1 + \frac{(\Delta p_1 - \Delta p_2)}{\int_{-1}^{+1} \rho u_1^2 \, d(y/y_1)} \tag{37}$$

$$= 1 + \frac{\Delta p_1 - \Delta p_2}{\rho u_1^2} \qquad \text{for uniform flow.} \tag{38}$$

Thus, as indicated in Figure 25, a reduction in pressure results in an increase in momentum flux, but the change is a little larger than that calculated by assuming conservation of total head. Because we use the dimension y_1 in Equation (33) the above analysis can only apply for accelerating flow.

We may summarize the results as follows:

> **"When there is no means of mechanically reacting a force in the direction of interest, momentum (rather than total head) is conserved in an inviscid jet."**

That is $$\int_{-y_n}^{+y_n} \Delta p_n \, dy_n + \int_{-y_n}^{+y_n} \rho u^2 \, dy_n = \text{constant.} \tag{39}$$

Thus, the energy (or total head) of the flow will diminish if it is slowed down (diffusion) and increase if it is accelerated. The principle of conservation of energy is not violated by this, because we have an essentially unbalanced system.

For the constrained flow case of Figure 26(a), the momentum balance is

$$2y_1\Delta p_1 - 2y_2\Delta p_2 - 2\int_{y_2}^{y_1} \Delta p \, dy = \int_{-y_2}^{+y_2} \rho u_2^2 \, dy - \int_{-y_1}^{+y_1} \rho u_1^2 \, dy \tag{40}$$

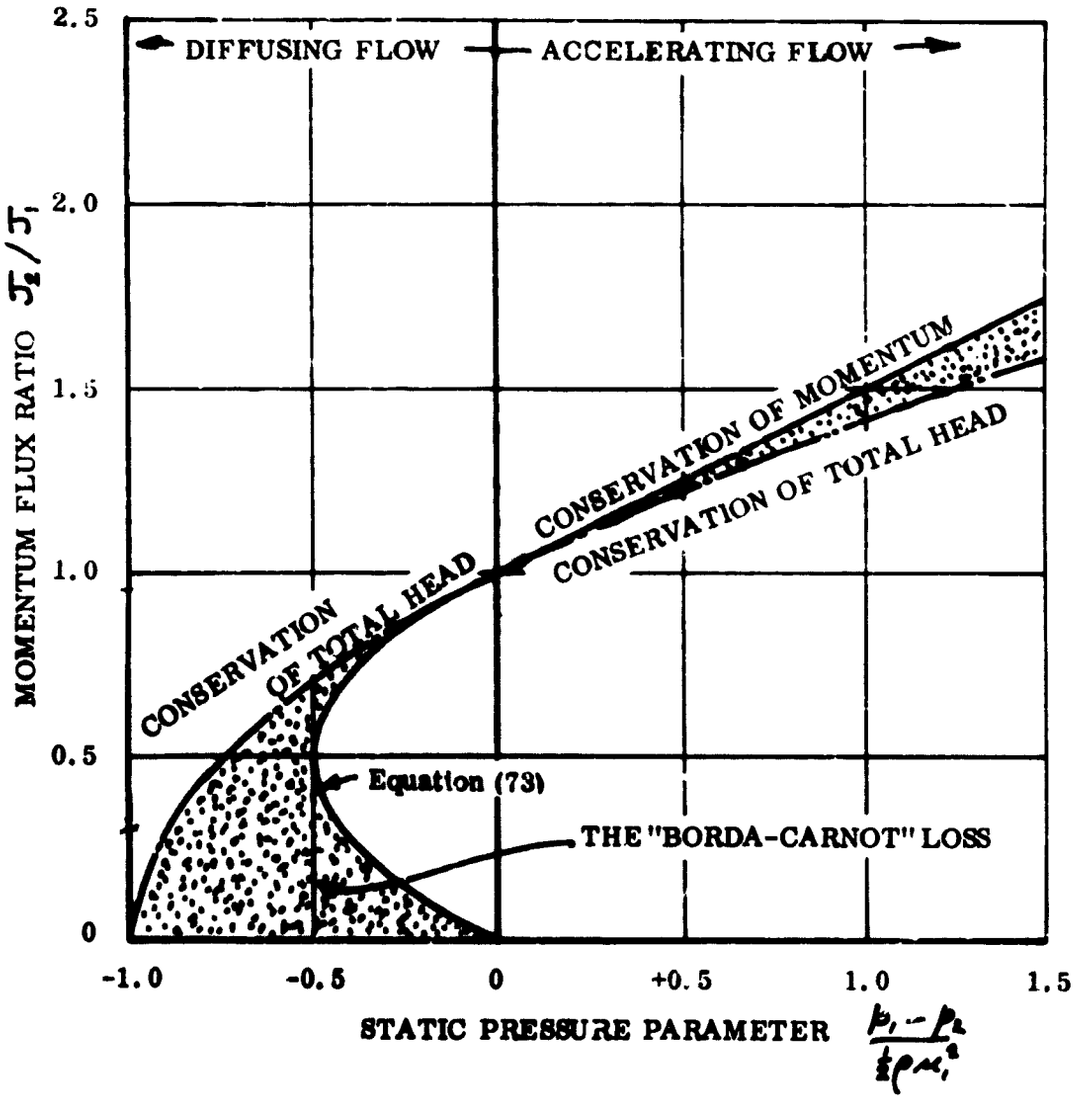

Figure 25. Change in Momentum Flux Through a Static Pressure Change for One-Dimensional Flow.

or

$$\int_{y_2}^{y_1} \Delta p \, dy = y_1 \Delta p_1 + \tfrac{1}{2} \int_{-y_1}^{+y_1} \rho u_1^2 \, dy - \left(y_2 \Delta p_2 + \tfrac{1}{2} \int_{-y_2}^{+y_2} \rho u_2^2 \, dy \right) \tag{41}$$

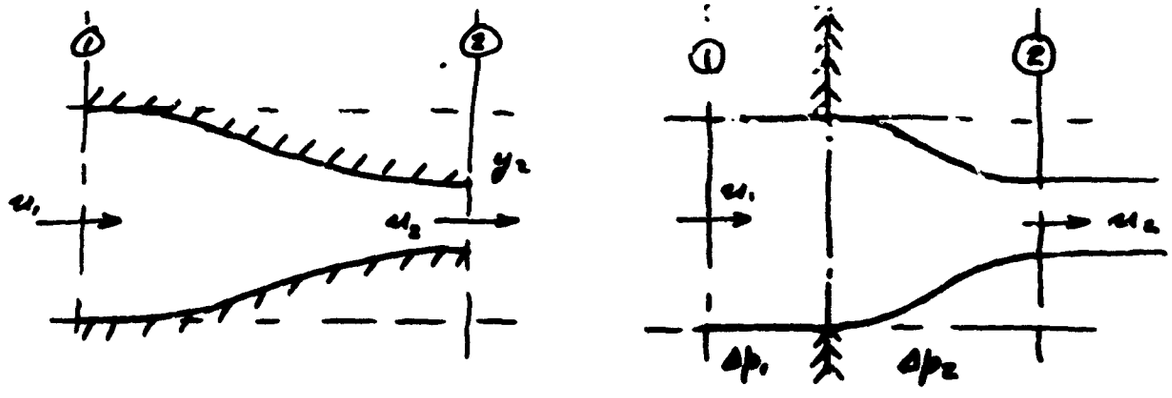

(a) Flow constrained by solid walls

(b) Unconstrained flow through a static pressure change

Figure 26. Constrained and Unconstrained Flow Through a Static Pressure Change.

As indicated in Figure 27, the integral on the left hand side of Equation (41) can have any value between zero and $(y_1 - y_2)(\Delta p_1 - \Delta p_2)$. If it is zero, we have the case of no applied mechanical force and Equation (41) is identical with Equation (39).

Referring to Figure 27, this implies that $f(\Delta p)$ follows the line (A-B-C). In other words, a contraction does not take place until after the pressure change has occurred, Figure 26(b), while an expansion occurs before a pressure increase.

The second case is certainly true of a sudden duct expansion. However, it is not clear that such a situation can exist for a reduction of static pressure.

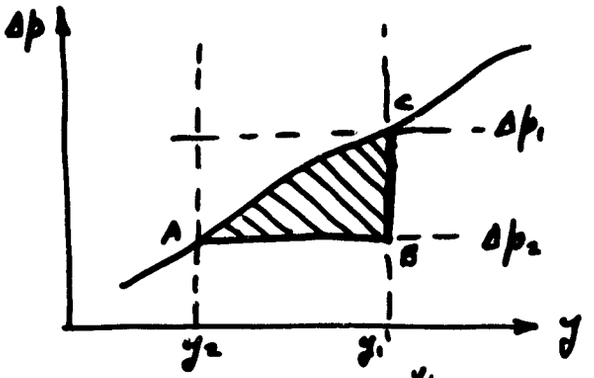

Figure 27. The Integral $\int_{y_2}^{y_1} \Delta p \, dy$

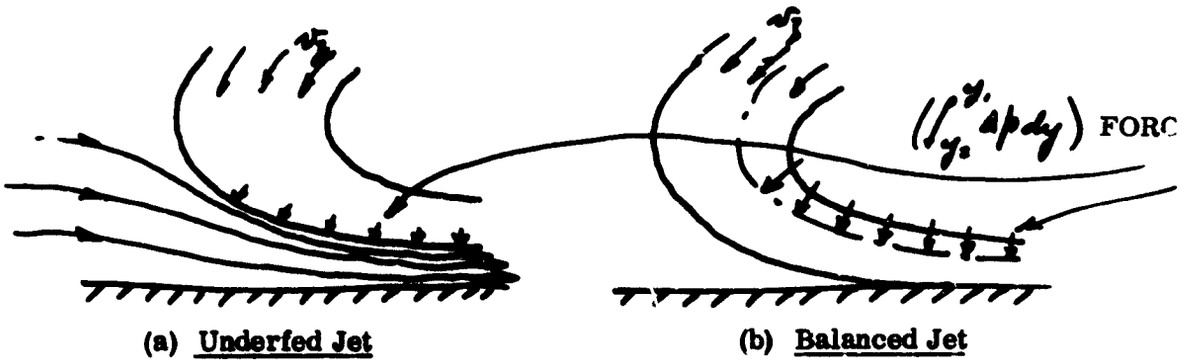

(a) Underfed Jet (b) Balanced Jet

Figure 28. Two Jet Flow Conditions.

We might imagine the condition of Figure 24 to exist for an annular jet. Indeed, most theories assume

$$\int_0^t \rho v_j^2 \, dz = \text{constant}$$

rather than

$$\int_0^t \rho v_j^2 \, dz + \int_0^t \Delta p_j \, dz = \text{constant.}$$

However, a closer examination of the jet flow indicates (Figure 28) that the local jet curvature itself provides a mechanism for providing the force ($\int_{y_2}^{y_1} \Delta p \, dy$) which we have seen to be essential to the conservation of total head.

We shall, therefore, continue to assume that when an annular jet accelerates to ambient static pressure, total head (and, therefore, power) is conserved.

BORDA-CARNOT DIFFUSION IN TWO-DIMENSIONAL FLOW

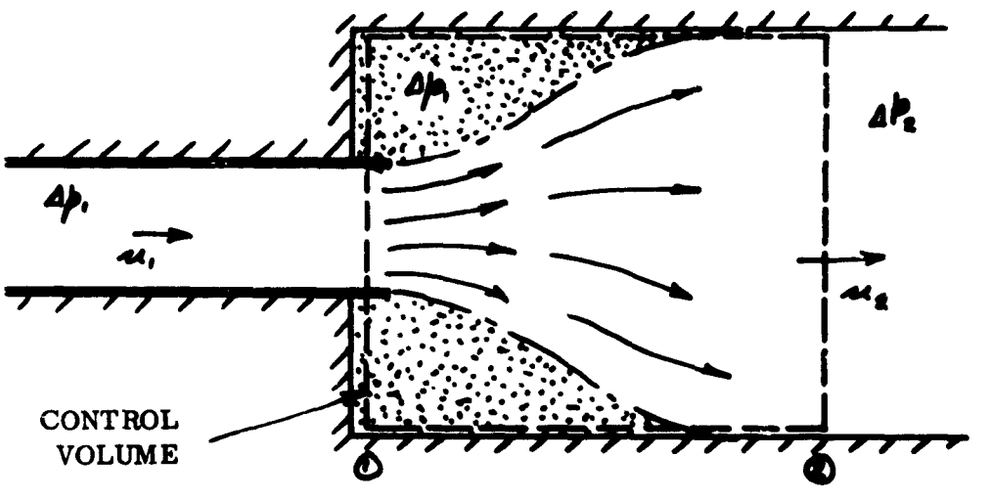

Figure 29. A Sudden Duct Expansion.

In this section we consider more formally the simple case of a sudden duct expansion, which was treated by Borda and Carnot for one-dimensional flow. Following the general considerations introduced in the previous section, we assume that the expansion of the flow boundary takes place before the pressure rise, as indicated in Figures 29 and 30.

Using the control boundaries shown in Figure 29, the sum of the pressure forces is

$$A_2(\Delta p_2 - \Delta p_1) \tag{42}$$

acting positively against the flow direction. (The static pressure at stations (1) and (2) must be constant across the duct, because the flow is assumed to be parallel.)

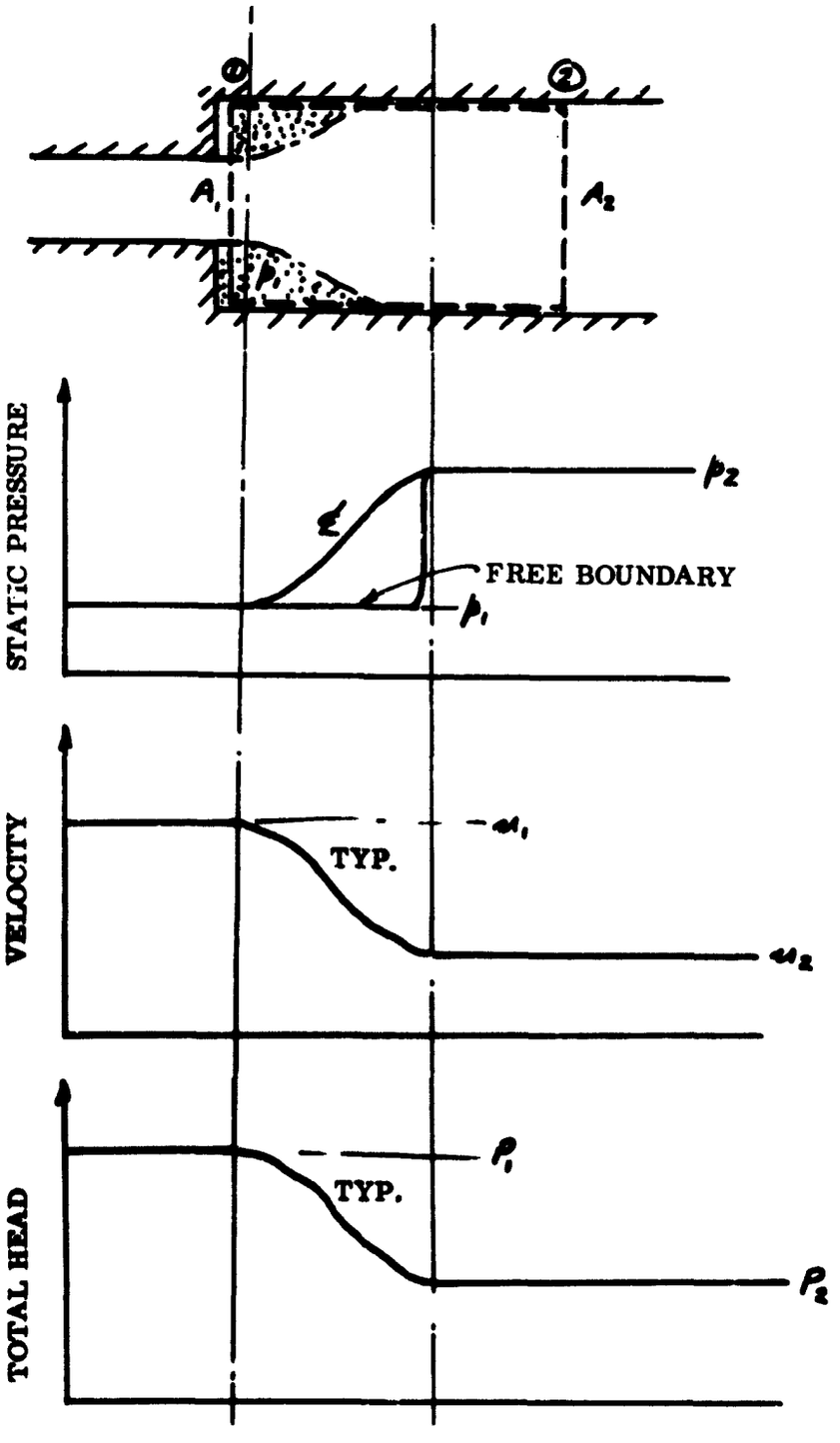

Figure 30. Variables in a Sudden Diffusion.

The momentum flux through the control volume is

$$\int_0^{A_2} \rho u_2^2 \, dA_2 - \int_0^{A_1} \rho u_1^2 \, dA_1. \tag{43}$$

Equating (42) and (43),

$$A_2(\Delta p_2 - \Delta p_1) = \int_0^{A_1} \rho u_1^2 dA_1 - \int_0^{A_2} \rho u_2^2 \, dA_2 . \tag{44}$$

For continuity of mass flow,

$$\int_0^{A_1} u_1 dA_1 = \int_0^{A_2} u_2 dA_2 . \tag{45}$$

The mean velocity is defined as

$$\hat{u}_n = \frac{1}{A_n} \int_0^{A_n} u_n dA_n \tag{46}$$

and we will define the momentum flux also in terms of $\hat{u}_n$.

That is,

$$\int_0^{A_n} \rho u_n^2 dA_n = \frac{\rho u_n^2 \int_0^{A_n} u_n^2 dA_n}{\left[\frac{1}{A_n} \int_0^{A_n} u_n dA_n\right]^2}$$

$$= \rho A_n \hat{u}_n^2 \lambda_n \tag{47}$$

where

$$\lambda = \frac{\frac{1}{A_n} \int_0^{A_n} u_n^2 dA_n}{\left[\frac{1}{A_n} \int_0^{A_n} u_n dA_n\right]^2} \tag{48}$$

Thus, Equations (44) and (45) now become

$$A_2(\Delta p_2 - \Delta p_1) = \rho A_1 \hat{u}_1^2 \lambda_1 - \rho A_2 \hat{u}_2 \lambda_2 \tag{49}$$

$$\rho A_1 \hat{u}_1 = \rho A_2 \hat{u}_2 . \tag{50}$$

We wish to determine the loss of energy occasioned by a sudden diffusion. Power is defined by

$$P_n = \int_0^{A_n} (\Delta p_n u_n + \tfrac{1}{2} \rho u_n^3) \, dA_n \tag{51}$$

$$= \Delta p_n A_n \bar{u}_n + \tfrac{1}{2} \rho A_n \hat{u}_n^3 \psi_n \tag{52}$$

where

$$\psi_n = \frac{\frac{1}{A_n} \int_0^{A_n} u_n^3 \, dA_n}{\left[\frac{1}{A_n} \int_0^{A_n} u_n \, dA_n \right]^3} . \tag{53}$$

Thus, we are interested in the ratio

$$\frac{P_2}{P_1} = \frac{\Delta p_2 A_2 \hat{u}_2 + \tfrac{1}{2} \rho A_2 \hat{u}_2^3 \psi_2}{\Delta p_1 A_1 \hat{u}_1 + \tfrac{1}{2} \rho A_1 \hat{u}_1^3 \psi_1} . \tag{54}$$

From (49) and (50),

$$\Delta p_2 = \Delta p_1 + \rho \hat{u}_1^2 \lambda_1 (A_1/A_2) - \rho \hat{u}_1^2 \lambda_2 (A_1/A_2)^2$$

$$= \Delta p_1 + \rho \hat{u}_1^2 (A_1/A_2) \left[\lambda_1 - \lambda_2 (A_1/A_2) \right] . \tag{55}$$

Substituting in (54),

$$\frac{P_2}{P_1} = \frac{\Delta p_1 + \rho \hat{u}_1^2 (A_1/A_2) [\lambda_1 - \lambda_2 A_1/A_2] + \tfrac{1}{2} \rho \hat{u}_1^2 \psi_2 (A_1/A_2)^2}{\Delta p_1 + \tfrac{1}{2} \rho \hat{u}_1^2 \psi_1} . \tag{56}$$

A convenient nondimensionalization is

$$\Delta\hat{p}_n = \frac{\Delta p_n}{\frac{1}{2}\rho u_n^2} . \tag{57}$$

Using this, Equation (56) becomes

$$\frac{p_2}{p_1} = \frac{\Delta\hat{p}_1 + \psi_2 + 2A_1/A_2\left[\lambda_1 - \lambda_2 A_1/A_2\right] - \left[1 - (A_1/A_2)^2\right]\psi_2}{\Delta\hat{p}_1 + \psi_1} \tag{58}$$

It is obviously convenient to assume similar velocity profiles at stations (1) and (2), so that $\psi_1 = \psi_2$ and $\lambda_1 = \lambda_2$. We should note that this is only an assumption of convenience, however, and that a rapid diffusion can be expected to alter the profile. We would intuitively expect that a uniform velocity at station (1) would become parabolic at station (2), for example. However, the similarity assumption can be expected to give at least a rough indication of the effects of profile.

Equation (58) becomes

$$\frac{\Delta p}{p_1} = 1 - \frac{p_2}{p_1}$$

$$= \frac{(1 - A_1/A_2)\left[(1 + A_1/A_2)\psi - 2\lambda A_1/A_2\right]}{\Delta\hat{p}_1 + \psi} . \tag{59}$$

It is often more convenient to write the demoninator in the form

$$\Delta\hat{p}_1 + \psi = p_1/\tfrac{1}{2}\rho\hat{u}_1^2 A_1$$

from Equation (52). Thus,

$$\frac{\Delta p}{p_1} \cdot \frac{p_1}{\frac{1}{2}\rho u_1^2 A_1} = \frac{\Delta p}{\frac{1}{2}\rho u_1^2 A_1} = (1 - A_1/A_2)\left[(1 + A_1/A_2)\psi - 2\lambda A_1/A_2\right] . \tag{60}$$

For uniform flow, $\psi = \lambda = 1.0$, and

$$\Delta p/p_1 = (1 - A_1/A_2)^2/(1 + \Delta\hat{p}_1)$$

or $$\frac{\Delta \mathcal{P}}{\frac{1}{2}\rho u_1^2 A_1} = \left(1 - A_1/A_2\right)^2. \qquad (61)$$

In other words, as $A_1/A_2 \to 0$, all the kinetic energy in the flow is lost.

Equation (61) is plotted in Figure 31.

Also in uniform flow

$$\mathcal{P}_n = \Delta P_n u_n A_n,$$

so that

$$\Delta P_n = \mathcal{P}_n / u_n A_n;$$

$$\therefore \quad \frac{\Delta P_1}{\Delta P_2} = \frac{\mathcal{P}_1}{u_1 A_1} \cdot \frac{u_2 A_2}{\mathcal{P}_2} = \frac{\mathcal{P}_1}{\mathcal{P}_2}.$$

Thus, the total head loss

$$\left.\frac{\Delta P_1 - \Delta P_2}{\Delta P_1}\right|_{\psi=\lambda=1} = \frac{\Delta \mathcal{P}}{\mathcal{P}_1} = \frac{\left(1 - A_1/A_2\right)^2}{1 + \Delta \hat{f}_1}. \qquad (62)$$

But

$$1 + \Delta \hat{f}_1 = \Delta P/(\Delta P - \Delta \phi);$$

$$\therefore \quad \left.\frac{\Delta P_1 - \Delta P_2}{\Delta P_1}\right|_{\psi=\lambda=1} = \left(1 - A_1/A_2\right)^2 \left(1 - \Delta \phi/\Delta P\right). \qquad (63)$$

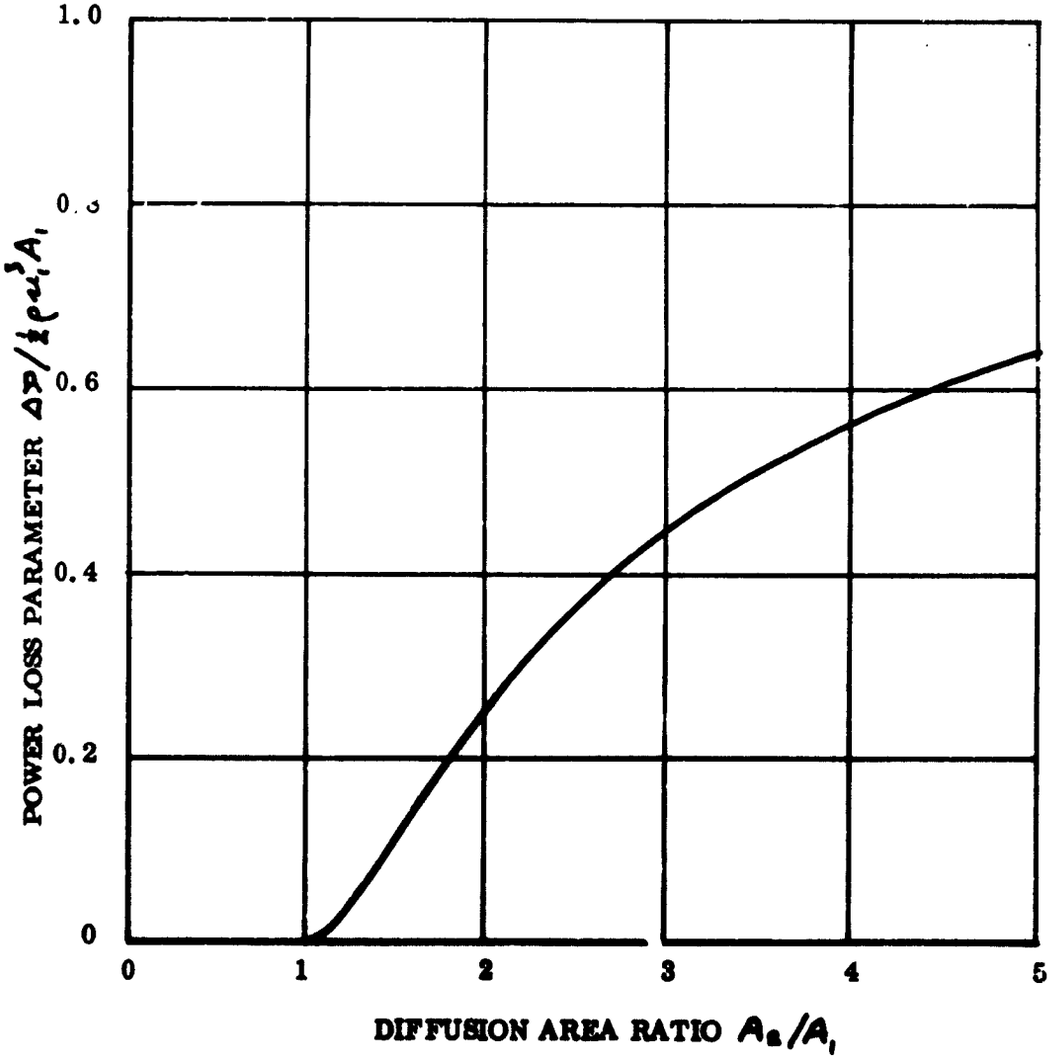

Figure 31. Power Lost in a Sudden Diffusion, for a Uniform Velocity Profile.

VALUES OF THE SHAPE FACTORS λ AND ψ

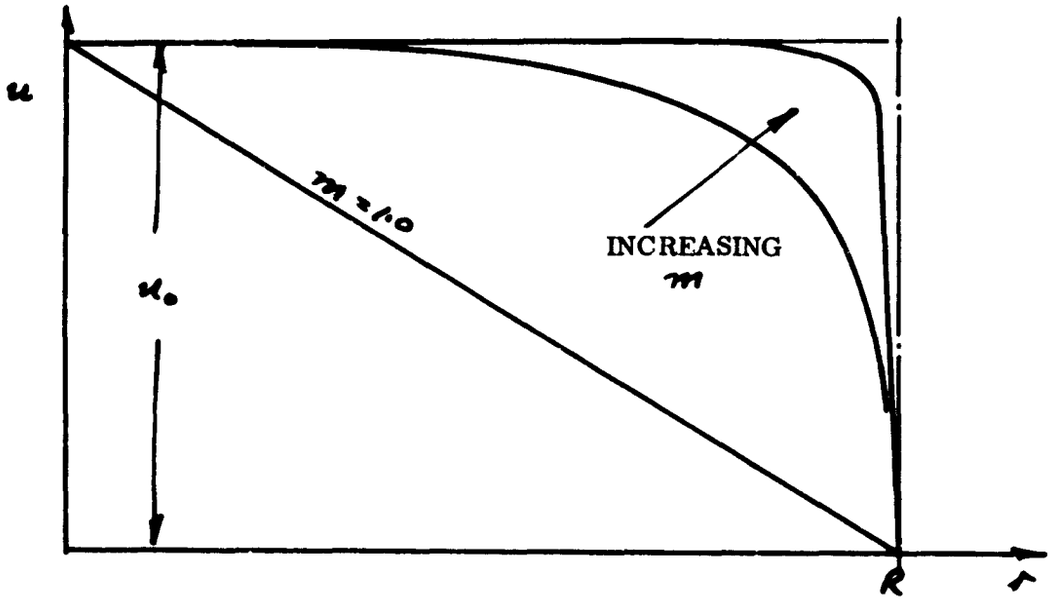

Figure 32. A Family of Radial Velocity Distributions in a Circular Duct.

We will consider the case of a circular duct with a velocity distribution of the type

$$u = u_0 \left[1 - (r/R)^m\right] \tag{64}$$

Obviously, this family tends to a uniform distribution as $m \to \infty$ and gives a triangular distribution where $n = 1.0$.

Now the area $A = \pi r^2$, $A_n = \pi R^2$

$$\frac{1}{A_n}\int_0^{A_n} u_n \, dA = u_0/A_n \cdot \int_0^{A_n} \left[1 - (r/R)^m\right] dA$$

$$= u_0/A_n \int_0^R \left[1 - (r/R)^m\right] \cdot 2\pi r \, dr$$

$$= 2u_0 \int_0^1 [1 - (r/R)^m](r/R)\,d(r/R)$$

$$= u_0 \left[1 - \frac{2}{2+m}\right]. \tag{65}$$

The momentum integral is

$$\frac{1}{A_n}\int_0^{A_n} u_n^2\,dA = \frac{u_0^2}{A_n}\int_0^{A_n} [1 - 2(r/R)^m + (r/R)^{2m}]\,dA$$

$$= u_0^2 \left[1 - \frac{4}{m+2} + \frac{1}{m+1}\right]. \tag{66}$$

Thus, from Equation (48)

$$\lambda = \frac{1 - \frac{4}{m+2} + \frac{1}{m+1}}{\left[1 - \frac{2}{2+m}\right]^2}. \tag{67}$$

Note that as $m \to \infty$, $\lambda \to 1.0$. For $m = 1.0$, $\lambda = 1.5$.

The power integral is

$$\frac{1}{A_n}\int_0^{A_n} u_n^3\,dA = \frac{u_0^3}{A_n}\int_0^{A_n} [1 - 3(r/R)^m + 3(r/R)^{2m} - (r/R)^{3m}]\,dA$$

$$= 2u_0^3 \int_0^1 [r/R - 3(r/R)^{m+1} + 3(r/R)^{2m+1} - (r/R)^{3m+1}]\,d(r/R)$$

$$= u_0 \left[1 - \frac{6}{m+2} + \frac{6}{2m+2} - \frac{2}{3m+2}\right]. \tag{68}$$

Thus, from Equation (53)

$$\psi = \frac{1 - \frac{6}{m+2} + \frac{6}{2m+2} - \frac{2}{3m+2}}{\left(1 - \frac{2}{2+m}\right)^3}. \tag{69}$$

As $m \to \infty$, $\psi \to 1.0$. For $m = 1$, $\psi = 3.7$.

Equations (67) and (69) are plotted in Figure 33, and the resultant power loss parameter, from Equation (60), in Figure 34.

THE LIMITING VELOCITY CHANGE

From Equations (49) and (50),

$$A_1 = A_2 \cdot \hat{u}_2 / \hat{u}_1 ;$$

$$\therefore \quad A_2(\Delta p_2 - \Delta p_1) = \rho A_2 \hat{u}_1 \hat{u}_2 \lambda_1 - \rho A_2 \hat{u}_2^2 \lambda_2 \qquad (70)$$

or

$$\left(\frac{\hat{u}_2}{\hat{u}_1}\right)^2 - \left(\frac{\lambda_1}{\lambda_2}\right)\left(\frac{\hat{u}_2}{\hat{u}_1}\right) + \frac{\Delta p_2 - \Delta p_1}{\rho \hat{u}_1^2 \lambda_2} = 0 . \qquad (71)$$

Writing

$$C_p = \frac{\Delta p_2 - \Delta p_1}{\tfrac{1}{2}\rho \hat{u}_1^2} ,$$

$$\frac{\hat{u}_2}{\hat{u}_1} = \tfrac{1}{2}\left[\frac{\lambda_1}{\lambda_2} \pm \left\{\left(\frac{\lambda_1}{\lambda_2}\right)^2 - \frac{2C_p}{\lambda_2}\right\}^{\frac{1}{2}}\right] . \qquad (72)$$

For similar profiles $\lambda_1 = \lambda_2 = \lambda$,

$$\frac{\hat{u}_2}{\hat{u}_1} = \tfrac{1}{2}\left[1 \pm \left\{1 - \frac{2C_p}{\lambda}\right\}^{\frac{1}{2}}\right] , \qquad (73)$$

an equation which is plotted in Figure 35.

If we write Equation (71) as

$$C_p = 2\left(\frac{\hat{u}_2}{\hat{u}_1}\right)\left[\lambda_1 - \lambda_2\left(\frac{\hat{u}_2}{\hat{u}_1}\right)\right] \qquad (74$$

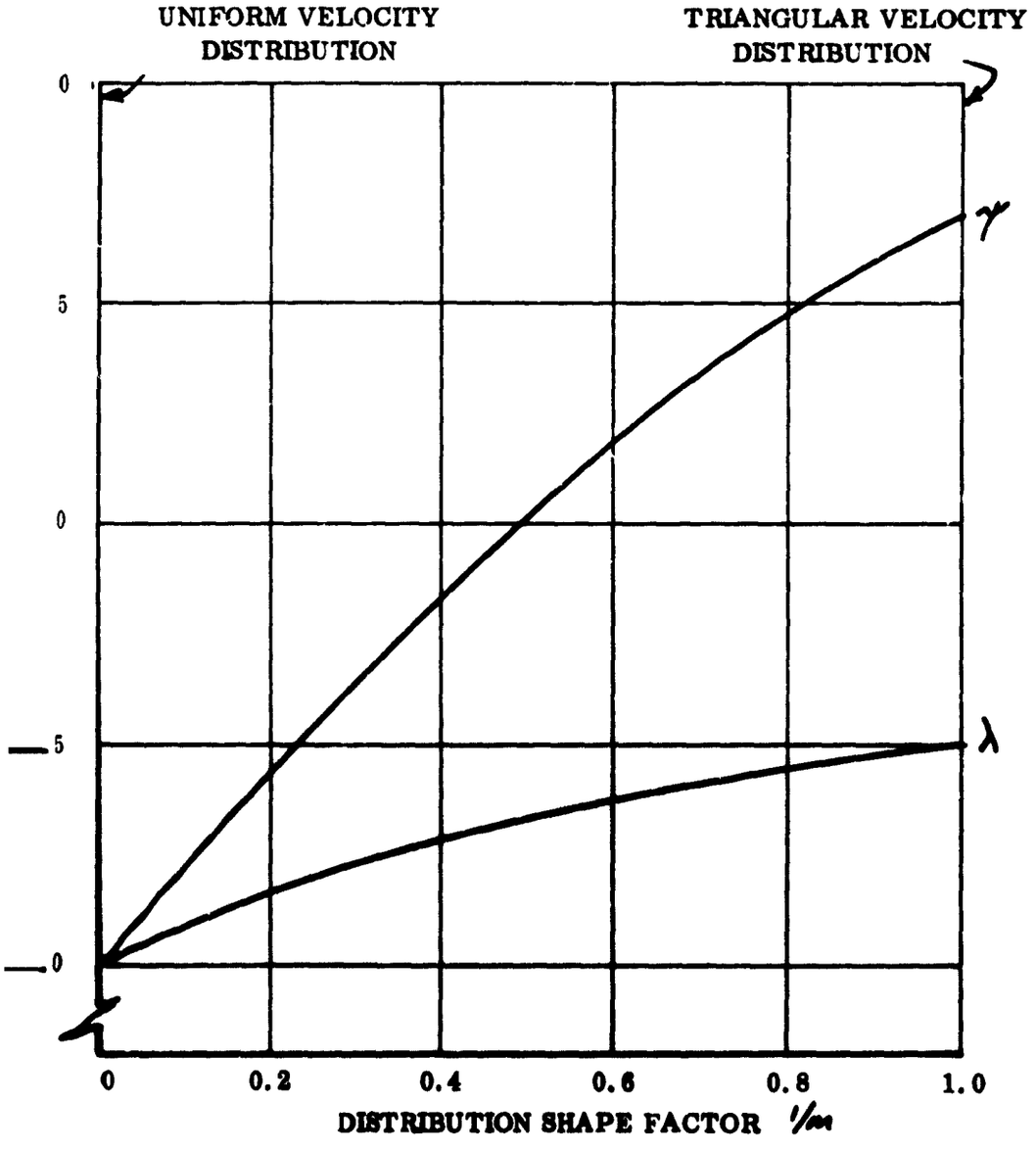

Figure 33. Variation of the Shape Integrals λ and ψ With the Shape Exponent m for the Power Law Family of Velocity Distributions.

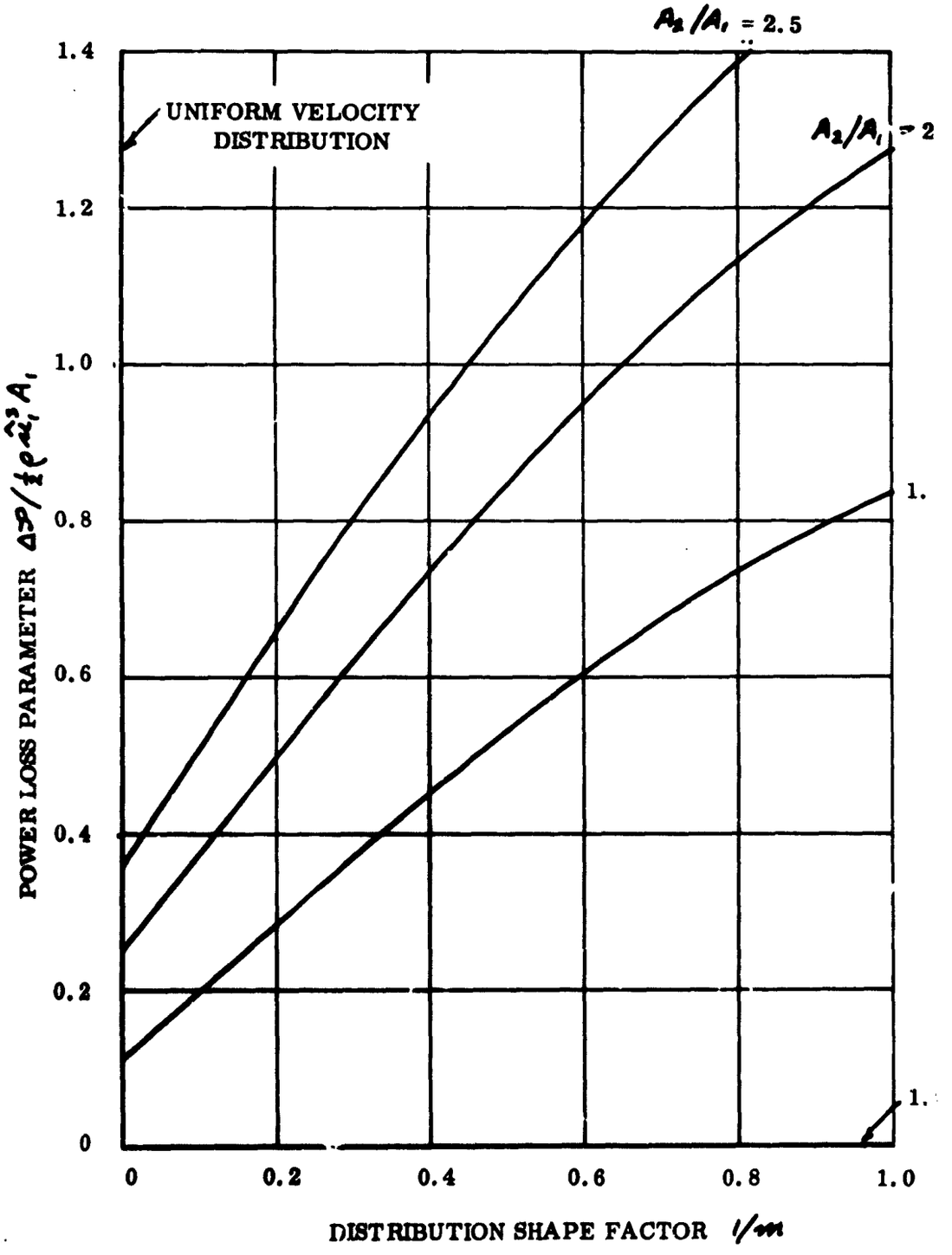

Figure 34. Power Lost in a Sudden Diffusion, as a Function of the Velocity Distribution Profile.

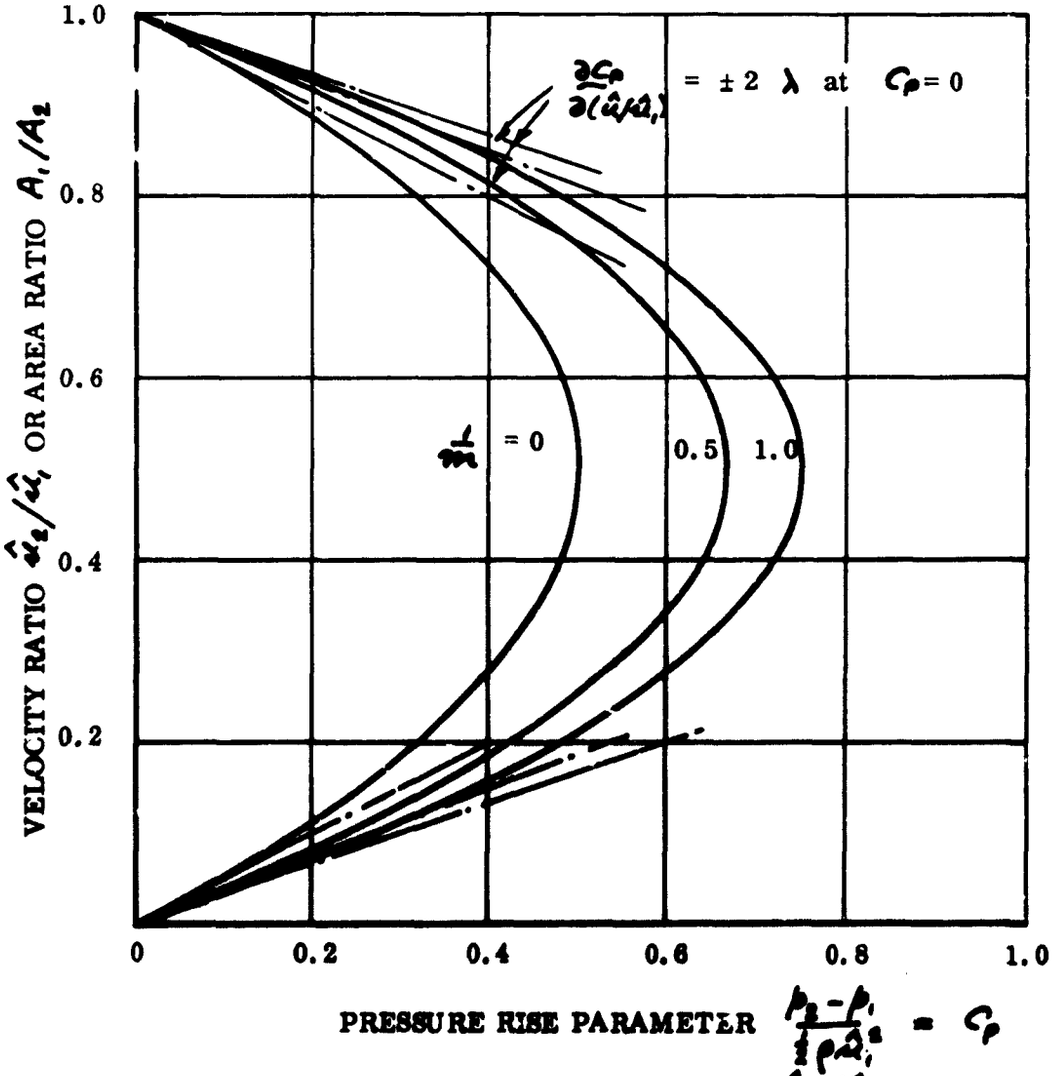

Figure 35. Variation of Velocity Ratio $\hat{u}_2/\hat{u}_1$, With the Pressure Rise Parameter C_p, for Similar Profiles.

and differentiate with respect to $\hat{u}_2/\hat{u}_1$, then equating to zero gives

$$\left.\frac{u_2}{u_1}\right|_{C_{p\,max}} = \frac{1}{2}\cdot\frac{\lambda_1}{\lambda_2}. \qquad (75)$$

Substituting in (74), :

$$C_{p\,max} = \left(\lambda_2 - \frac{1}{2}\right)\left(\frac{\lambda_1}{\lambda_2}\right)^2. \qquad (76)$$

Thus we see from (75) and (76) that, so long as the initial and final velocity profiles are similar ($\lambda_1 = \lambda_2$), $C_{p_{max}} = \lambda - \frac{1}{2}$ at a mean velocity ratio $\hat{u}_2/\hat{u}_1 = \frac{1}{2}$.

Thus increasing the flow distortion increases the pressure rise coefficient, although at the expense of increasing the associated energy loss.

Since λ increases in value with increasing deviation from uniform flow, however, we can expect $\lambda_2 > \lambda_1$, when the profiles are not similar. Thus, distortion of the flow profile <u>during</u> diffusion <u>reduces</u> the maximum obtainable pressure rise.

The corresponding total pressure loss for uniform flow is plotted against C_p in Figure 36.

The critical velocity ratio of $\hat{u}_2/\hat{u}_1 = \frac{1}{2}$ is extremely interesting, because this happens to be appropriately the limit for all diffusion processes. Ackeret's criterion of

$$C_p > 0.7 \text{ to } 0.8 \qquad (77)$$

for stall has been confirmed experimentally by Schlichting[5]. If η is a diffusion efficiency, we have from Bernoulli,

$$\Delta p_2 - \Delta p_1 = \frac{1}{A_1}\int_0^{A_1} \eta\,\tfrac{1}{2}\rho u_1^2\,dA_1 - \frac{1}{A_2}\int_0^{A_2} \tfrac{1}{2}\rho u_2^2\,dA_2$$

$$= \eta\lambda_1\,\tfrac{1}{2}\rho\hat{u}_1^2 - \lambda_2\cdot\tfrac{1}{2}\rho\hat{u}_2^2 ;$$

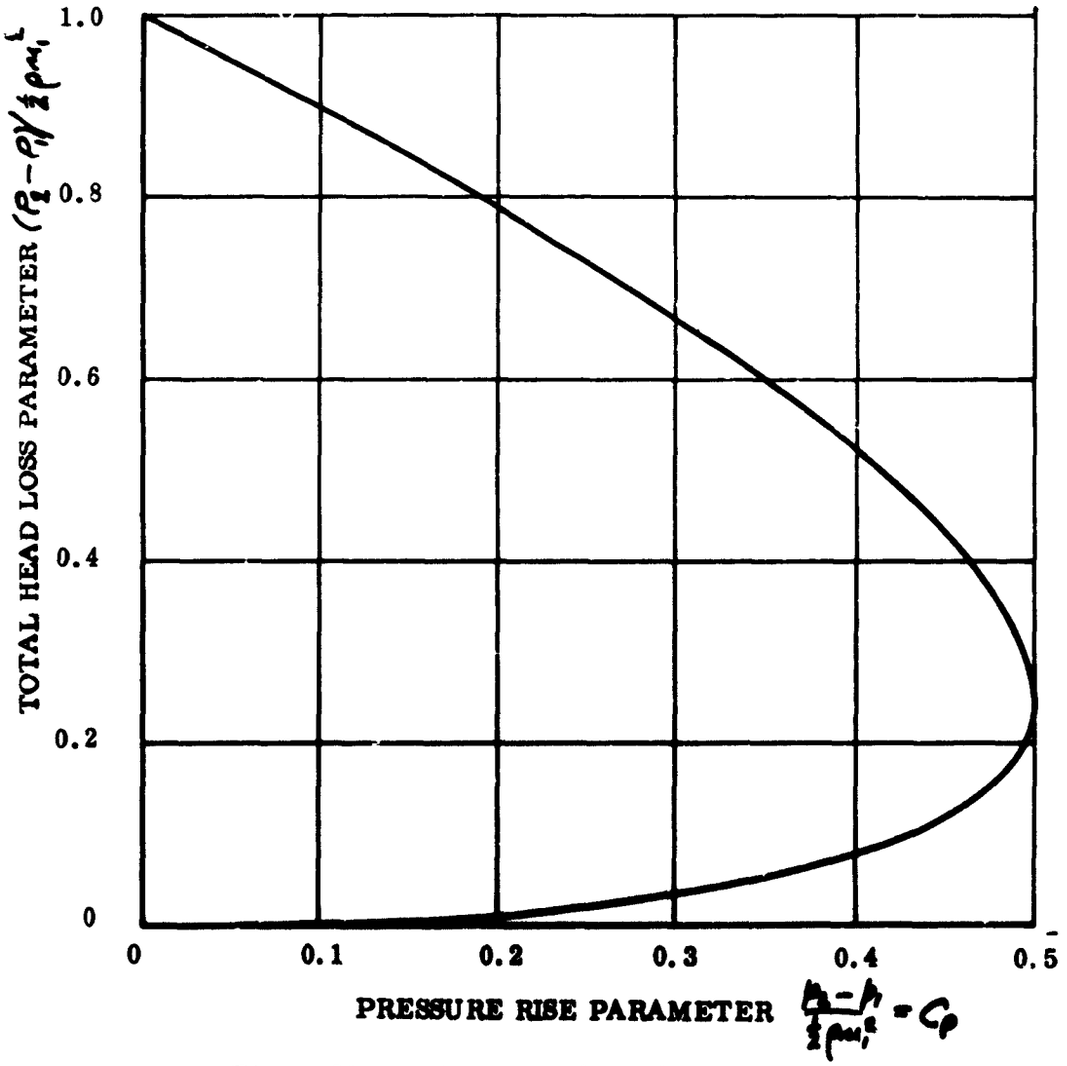

Figure 36. Variation of Total Pressure Loss With Static Pressure Rise, for the Case of Uniform Velocity Distribution.

$$\therefore \qquad C_p = \eta\lambda_1 - \left(\frac{\hat{u}_2}{\hat{u}_1}\right)^2\lambda_2 . \tag{78}$$

For uniform flow, and $\eta = 1.0$ (no diffusion loss), a value of $\hat{u}_2/\hat{u}_1 = 1/2$ gives $C_p = 0.75$, a value which is in excellent agreement with Ackeret's criterion.

Lieblein[6] has shown that flow separation occurs on compressor blades when the ratio ot the peak velocity to the trailing edge velocity exceeds 2.0.

Other examples of this limitation on diffusion have been cited by Senoo[7] who points out that all conical diffuser data combine to show a peak pressure recovery coefficient in the range 0.7 - 0.85, corresponding to velocity ratios of about 0.55 to 0.4. He also shows that, using numerical methods of determining the stability of a turbulent boundary layer, a uniform diffusion causes separation at a velocity ratio of around 0.6.

Finally, Goldschmied[8] has shown that stall can be correlated by the equation

$$C_p = 200\,\tau_o \tag{79}$$

where τ_o is the skin friction stress at the point of maximum velocity. Since τ_o cannot exceed .0048, C_p cannot exceed 0.86 under the most favorable conditions ($R_c = 5000$) and will be less for the higher Reynolds numbers encountered in most practical problems.

Thus, all the experimental evidence seems to point toward the essential correctness of Equations (75) and (76), even though we cannot at present see clearly why this should be so. There is obviously room for a great deal more research in this regard.

So far as the present program is concerned, we are principally interested in Equation (63), which can obviously be expressed as

$$\frac{\Delta H}{\Delta P_1} = \frac{\Delta P_1 - \Delta P_2}{\Delta P_1} = \left(1 - \frac{u_2}{u_1}\right)^2\left(1 - \frac{\Delta t_1}{\Delta t_2}\right). \tag{80}$$

Or, since $$\Delta P_1 \left(1 - \frac{\Delta p_1}{\Delta p_2}\right) = \tfrac{1}{2}\rho u_1^2 ,$$

$$\frac{\Delta H}{\frac{1}{2}\rho u_1^2} = \left(1 - \frac{u_2}{u_1}\right)^2 . \qquad (81)$$

When dealing with a curvilinear flow field which has a velocity gradient across the direction of flow, we shall assume that Equation (81) applies along individual streamlines. This implies that, even in the middle of a jet, diffusion takes place at constant static pressure (Figure 29 on an elemental scale); and this assumption is impossible to justify, at the moment, other than by the results of analysis based upon it.

Chapter Three

THE EQUATION FOR CURVILINEAR TWO-DIMENSIONAL FLOW

THE EQUATION OF MOTION

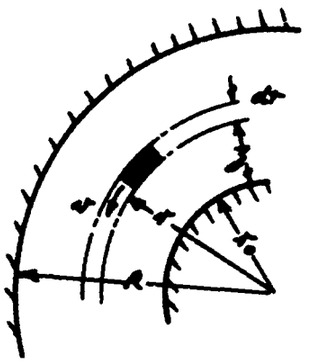

(a) Curved flow geometry.

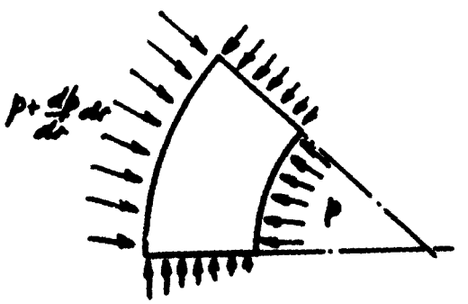

(b) Pressures acting on an element.

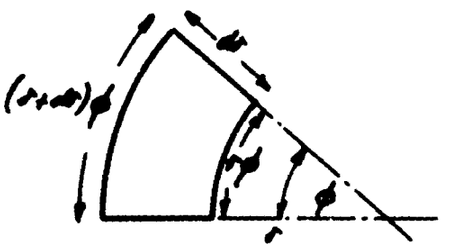

(c) Dimensions of an element.

Figure 37. The Elemental Geometry of the Curved Flow Field.

From Figure 37, the resultant pressure force acting (inward) on an element is, per unit length,

$$F_p = \left(p + \frac{dp}{dr}dr\right)(r+dr)\phi - pr\phi - 2\left(p + \frac{1}{2}\frac{dp}{dr}dr\right)\frac{1}{2}\phi\, dr. \quad (82)$$

Taking only first-order differentials, this simplifies to

$$F_p = +\phi \frac{d\phi}{dr} dr. \tag{83}$$

The mass per unit length of the element is

$$\rho r \phi \, dr, \tag{84}$$

so that the centrifugal force is

$$\rho r \phi \, dr \cdot \frac{v_r^2}{r}. \tag{85}$$

Since the centrifugal force must be balanced by the pressure force, we can equate (83) and (85)

$$\frac{dp}{dr} = \frac{\rho v_r^2}{r}. \tag{86}$$

The local velocity is related to the total head at radius r by Bernoulli's equation

$$P_r = p_r + \tfrac{1}{2}\rho v_r^2$$

$$\rho v_r^2 = 2(P_r - p_r).$$

Substituting for ρv_r^2 in Equation (86),

$$\frac{dp}{dr} + \frac{2}{r} p_r = \frac{2}{r} P_r \tag{87}$$

where P_r can be any function of r.

In order to solve this equation we need to specify one boundary condition; usually the static pressure at the r_0 or R boundary. For example, specifying ambient static pressure at the r_0 boundary would give the annular jet solution; specifying ambient pressure at the R boundary would correspond to Coanda flow around a curved surface.

It is convenient to use "gauge" pressures (that is, pressures measured with respect to some datum pressure, usually the ambient value), the definitions being

$$\Delta p = p - p_a$$
$$\Delta P = P - p_a \quad . \tag{88}$$

It follows that $\frac{d\Delta p}{dr} = \frac{dp}{dr}$. Thus Equation (87) becomes

$$\frac{dp}{dr} + \frac{2}{r}\Delta p_r = \frac{2}{r}\Delta P_r \quad . \tag{89}$$

A LINEAR TRANSFORMATION TO JET ORDINATES

Since the total pressure is specified with respect to the jet ordinate (z in Figure 37) it is convenient to transform Equation (89) to this variable. Such a transformation also enables us to introduce the concept of a jet which has a linear variation of curvature across its width, by writing

$$r = r_0 + \eta z \tag{90}$$

where η = 1.0 for free vortex flow.
η = 0 for the constant radius assumption used to derive "exponential theory".

In general, $0 < \eta < 1.0$ for an annular jet, for example.

Note that dr/dz = 1.0 in Equation (89), despite the transformation. It now becomes

$$\frac{dp}{dz} + \frac{2}{r_0 + \eta z}\Delta p_z = \frac{2}{r_0 + \eta z}\Delta P_z \quad . \tag{91}$$

The general solution is the familiar formula for a first order linear equation:

$$\Delta p_3 = e^{-2\int \frac{dz}{r_0+\eta z}} \left[\int e^{2\int \frac{dz}{r_0+\eta z}} \cdot \frac{2\Delta P_3}{r_0+\eta z} \cdot dz + K \right]. \quad (92)$$

Now $$2\int \frac{dz}{r_0+\eta z} = \frac{2}{\eta} \log |r_0+\eta z| ;$$

$$\therefore \quad e^{\pm \int \frac{2dz}{r_0+\eta z}} = e^{\pm \frac{2}{\eta} \log |r_0+\eta z|}$$

$$= (r_0+\eta z)^{\pm 2/\eta} . \quad (93)$$

Substituting in (92)

$$\Delta p_3 = (r_0+\eta z)^{-2/\eta} \left[2\int_0^z (r_0+\eta z)^{\frac{2}{\eta}-1} \Delta P_3 \, dz + K \right], \quad (94)$$

the constant K being zero if $\Delta p_3 = 0$ when $z = 0$, of course. The total static pressure rise across the jet is

$$\Delta p_c = (r_0+\eta t)^{-2/\eta} \left[2\int_0^t (r_0+\eta z)^{2/\eta-1} \Delta P_3 \, dz + K \right]. \quad (95)$$

NONLINEAR TRANSFORMATIONS

Although not germane to the problems of the present program, it is of interest to note that nonlinear transformations of Equation (89) have value in certain cases, one example being depicted in Figure 38.

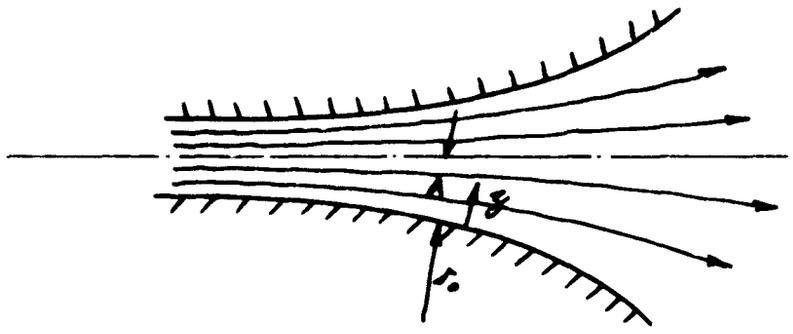

Figure 38. A Flow Which Has Infinite Radius of Curvature at the Center Line.

For this case, for example, we might reasonably use the transformation

$$\zeta = \frac{A r_0}{A - \zeta} \tag{96}$$

Thus Equation (89) becomes

$$\frac{d\phi}{d\zeta} + \frac{2}{A-\zeta}\Delta\phi_\zeta = \frac{2Ar_0}{(A-\zeta)^2}\Delta P_\zeta . \tag{97}$$

Chapter Four

INVISCID FLOW ANNULAR JET THEORY FOR CONSTANT TOTAL HEAD

In this chapter we shall apply the curvilinear jet theory first derived to the annular jet problem. Of all the common curved jet flows this has been studied most extensively, both theoretically and experimentally, and is therefore a very logical starting point.

As noted in the introduction, most theoretical analyses to date have been based on momentum equations. The well-known exception is Strand's[14] potential flow solution, which is known to give erroneous results at low ground clearance heights.

When an annular jet is close to ground plane, it approaches, in the limit, the case of a plenum chamber. The plenum chamber problem can be regarded as equivalent to a jet issuing from a slot in the wall of a large vessel, the ground plane replacing the axis of symmetry.

An extremely complete family of solutions for finite plenum chambers has been obtained by Gabbay[18], as part of a more general investigation, and the appropriate results are summarized in Figure 39. Since these results pass through the already known points for $\theta = +90^{\circ}$, 0° and -90°, and since these isolated cases are known to agree well with experiment, it is reasonable to feel a high level of confidence in all Gabbay's results.

In passing, it is of interest to note that the existence of these results now enables us to work out definitive solutions to the problem of the optimum wall angle for a plenum chamber GEM.

GENERAL MOMENTUM BALANCE CONSIDERATIONS

A Thin Jet Solution (Pinnes' Geometry)

When $t/R \ll 1.0$, we may postulate the geometry of Figure 40 for an annular jet. The assumption of constant radius of curvature along any streamline follows, of course, from the assumption of constant cushion and ambient static pressure.

We refer all pressures to ambient by the (Δ) notation. Considering the curved part of the jet (AABB), since the external pressure forces must be equal to the change in momentum, we resolve horizontally and vertically.

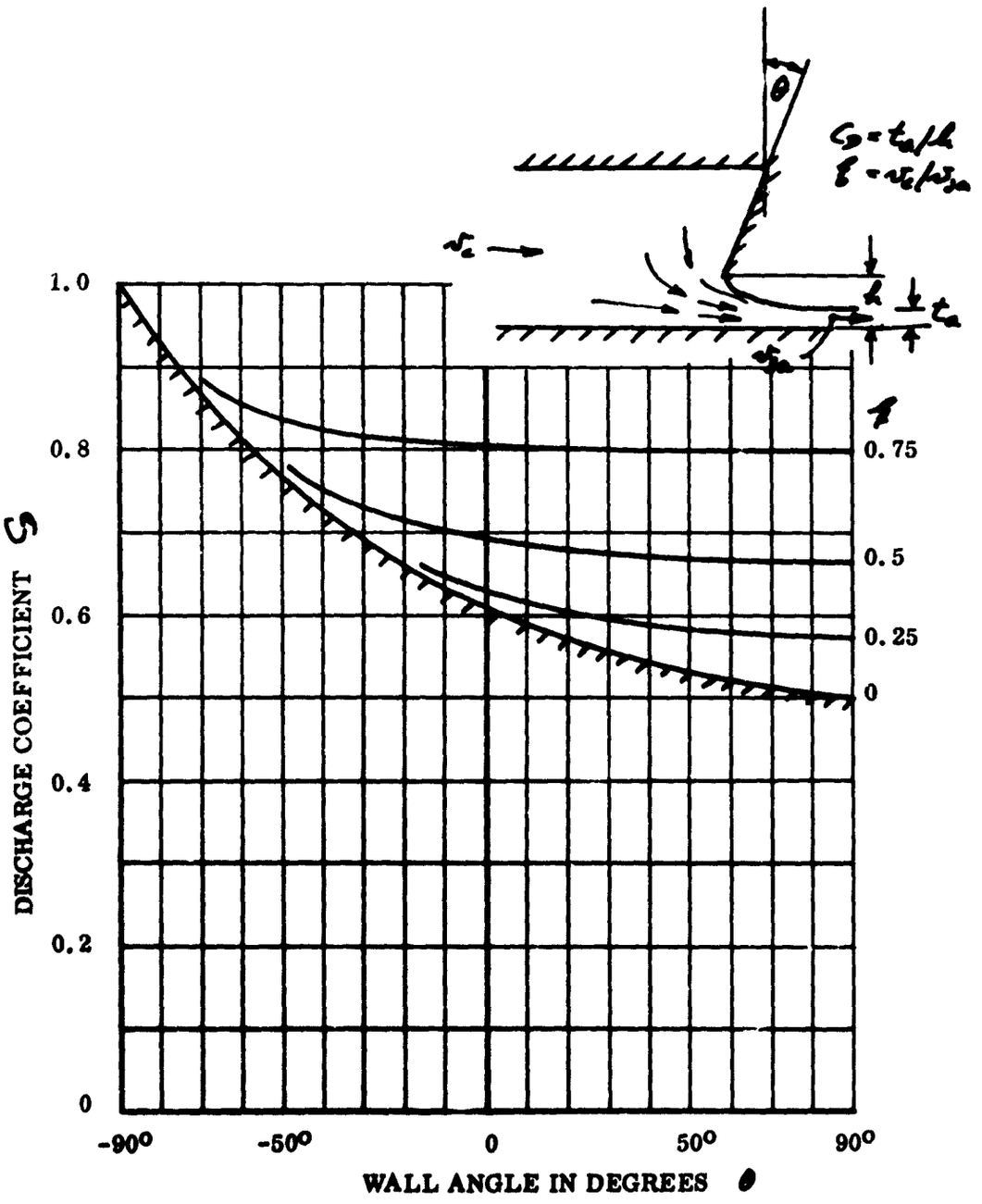

Figure 39. Potential Flow Solutions by Gabbay Applied to the Plenum Chamber Problem.

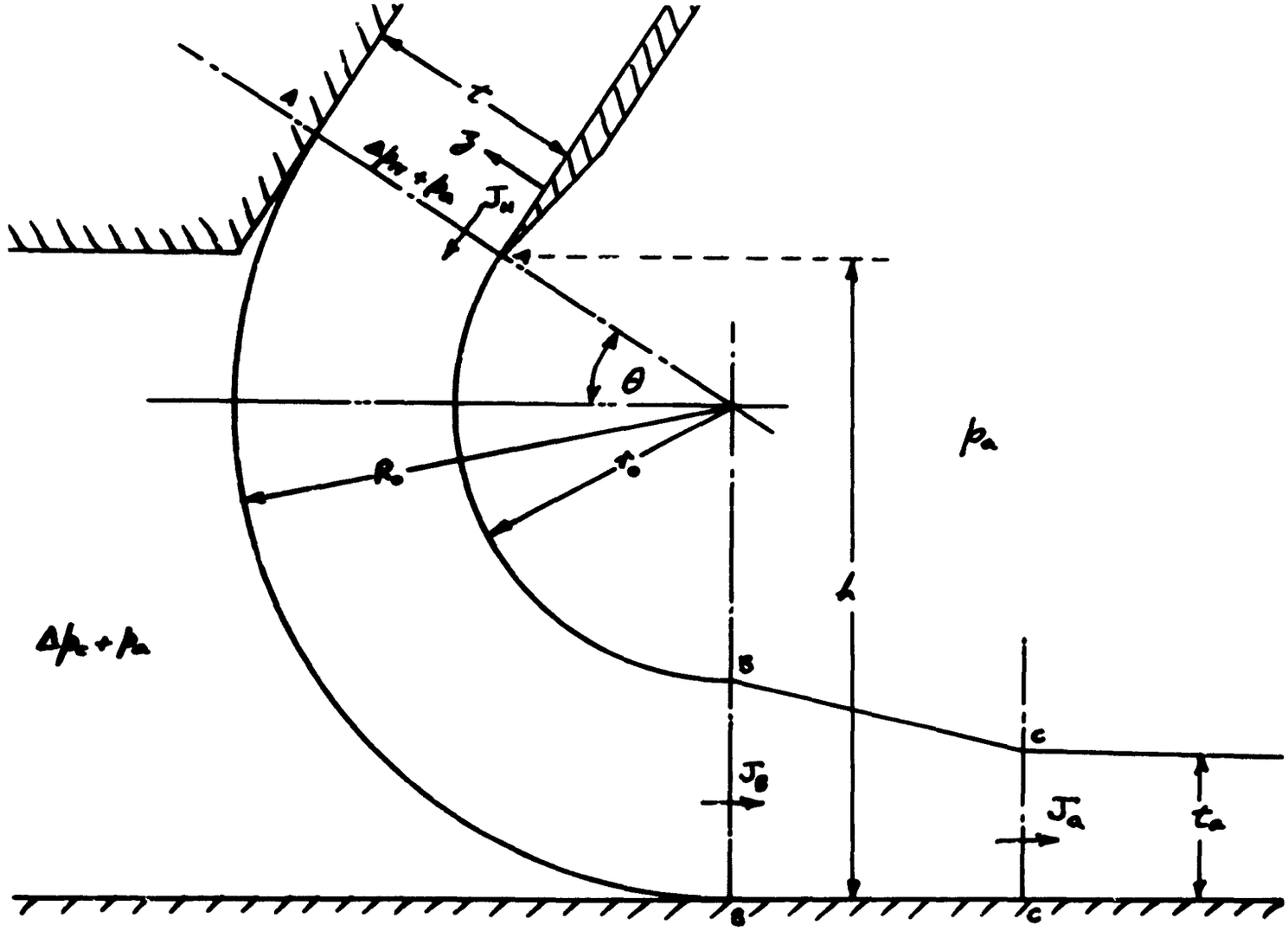

Figure 40. "Thin Jet" Geometry in the Absence of Viscous Mixing.

For the vertical resolution,

$$\Delta p_c R\,[1-(1-\cos\theta)] - \cos\theta \int_0^t \Delta p_N\, dz = \frac{J_N \cos\theta}{C_e};$$

$$\therefore \quad \int_0^t \Delta p_N\, dz = \Delta p_c R - \frac{J_N}{C_e}. \tag{98}$$

For the horizontal resolution,

$$\Delta p_c R(1+\sin\theta) - \sin\theta \int_0^t \Delta p_N\, dz - \int_0^t \Delta p_B\, dz = \frac{J_N \sin\theta}{C_e} + \frac{J_B}{C_e};$$

or, substituting from Equation (98) for $\int_0^t \Delta p_N\, dz$,

$$\Delta p_c R - \int_0^t \Delta p_B\, dz = \frac{J_B}{C_e}. \tag{99}$$

Considering now the momentum balance upon the accelerating flow section (BBCC), the horizontal resolution gives

$$\frac{J_a}{C_e} = \frac{J_B}{C_e} + \int_0^t \Delta p_B\, dz. \tag{100}$$

Substituting for $\int_0^t \Delta p_B\, dz$ in Equation (99)

$$\Delta p_c = \frac{J_a}{R C_e}. \tag{101}$$

It should be noted that no assumptions have had to be made for the form of the static pressure distribution across the jet or for the total pressure variation. Thus Equation (101) should hold for any theory.

The present analysis does not completely define the effective jet periphery C_e, of course, except in the two-dimensional flow case. However, a three-dimensional momentum balance is easy to do for a given three-dimensional planform, using the concepts introduced above.

A Thick Jet Solution

As the jet nozzle approaches closer to the ground, we cannot expect the region (BBCC) in Figure 40 to be physically separated from the curved jet flow. Rather, as Strand has shown in his elegant potential flow solution, the acceleration to ambient conditions will take place during the curved flow regime, and the jet shape will resemble Figure 41.

Equation (98) is obviously still applicable to this case, so an expression defining the nozzle pressure integral is available. For the horizontal resolution we have

$$\Delta p_e R(1+\sin\theta) - \sin\theta \int_0^t \Delta p_N \, dz = \frac{J_N}{C_e}\sin\theta + \frac{J_a}{C_e}. \quad (102)$$

Substituting Equation (98) for $\int_0^t \Delta p_N dz$, we find that Equation (101) still applies.

The Variation of Curvature Across a Thick Jet

The outer (cushion boundary) radius is always defined by

$$R = R(1+\sin\theta) - t\sin\theta \quad (103)$$

on the assumption that the radius along any streamline is constant.

For the geometry of Figure 40

$$r_0 = R - t \quad (104)$$

and the flow pattern is completely defined. Note however, that in previous work the ($t\sin\theta$) term in Equation (103) has been omitted.

For the thick-jet case of Figure 41, we must make an additional assumption; to whit, that the ambient boundary streamline is tangential to the nozzle wall. Then from Figure 41

$$R = t_a + r_0 + (r_0 + t - R)\sin\theta$$

or

$$R(1+\sin\theta) = t\left(\frac{t_a}{t} + \sin\theta\right) + r_0(1+\sin\theta). \quad (105)$$

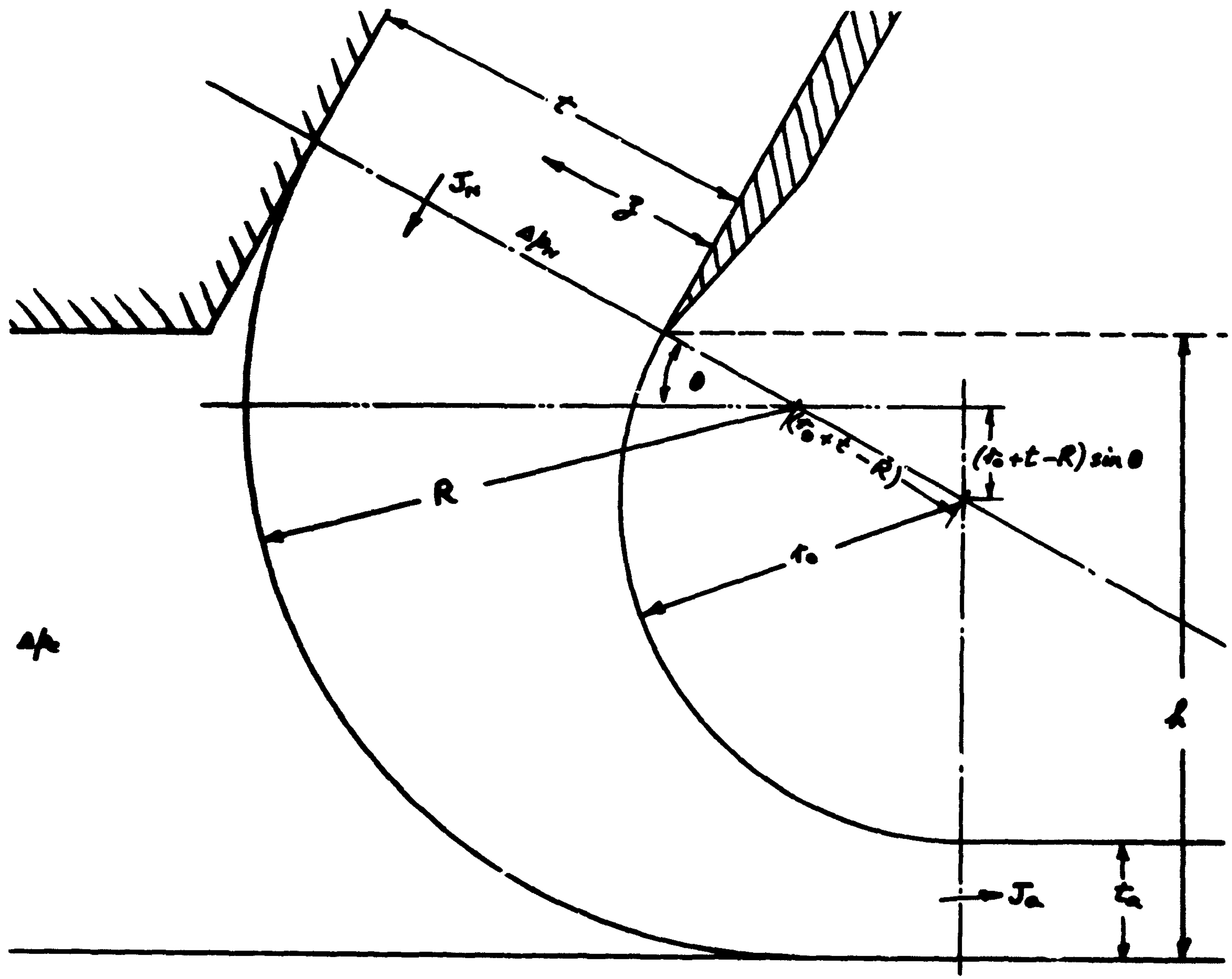

Figure 41. Geometry of Thick Annular Jet With N[illegible]

If $r = r_0 + \eta 3$, as discussed in the previous chapter,

$$R = r_0 + \eta t$$

and

$$\eta = (R - r_0)/t . \tag{106}$$

But, from Equation (105),

$$r_0 = R - \frac{t(\frac{t_a}{t} + \sin\theta)}{1 + \sin\theta} ;$$

$$\therefore \quad \eta = \frac{\frac{t_a}{t} + \sin\theta}{1 + \sin\theta} . \tag{107}$$

The ratio t_a/t is a discharge coefficient, of course. As

$$h/t \to 0 \quad , \quad t_a/t \to 0, \quad \eta \to \frac{\sin\theta}{1 + \sin\theta} .$$

The Height Parameter t/R

We shall find that the fundamental parameter which defines the characteristics of an annular jet is

$$t/R = \frac{\text{Jet thickness at the nozzle}}{\text{Radius of curvature of the outer streamline}} .$$

From Equation (103) this is given by

$$t/R = \frac{t_a}{t} \cdot \frac{(1 + \sin\theta)}{1 + \frac{t_a}{t}\sin\theta} . \tag{108}$$

Previously, most writers have used the parameter

$$\alpha = \frac{t_a}{t} \cdot (1 + \sin\theta) \tag{109}$$

which is evidently erroneous, for $\theta > 0$, from the geometry of Figures 40 and 41.

Three-Dimensional Effects

The principal geometric effect of three-dimensional flow is to modify the jet curvature and hence the cushion pressure. From Figure 41 it is obvious that the radius R will not be influenced, whatever the planform. When the jet is curved in the third dimension, however, as in a circular planform GEM, for example, its effective periphery increases as it moves away from the vehicle, so that its thickness (t_a) on the ground plane is accordingly reduced, leading to an increase in the ambient side radius r_a .

It is important to realize that this effect applies only to annular jets which do not have straight nozzles in planform. The jets of a rectangular GEM would behave (on this postulation) exactly as if they were two-dimensional, the "three-dimensional effects" being confined to their junctions at the corners. There is some experimental evidence[19] to indicate that, in such a case, the interaction of two peripheral jets at a corner gives an increase in cushion pressure rather than a loss.

As the most common example of a curved jet, the circular planform illustrated in Figure 42 is considered here.

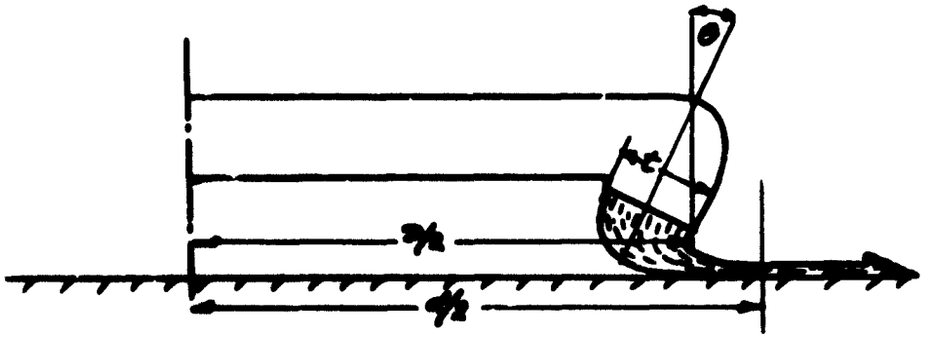

Figure 42. Geometry of a Circular GEM.

The effective circumference C of the jet is given by evaluating the area of the frustum of the right circular cone made by the jet exit.

$$Ct = \pi\left[\tfrac{D}{2} + \tfrac{B}{2} - t\cos\theta\right]\left[t^2\sin^2\theta + \left\{\tfrac{D}{2} - \left(\tfrac{B}{2} - t\cos\theta\right)\right\}^2\right]^{1/2}$$

$$C_t = \pi D t \left[1 - \frac{t}{D}\cos\theta\right]$$

$$C = \pi D \left[1 - \frac{t}{D}\cos\theta\right]. \tag{110}$$

The jet radius on the cushion side is unaffected by the planform. The radius defined by the r_o arc becoming parallel to the ground is

$$\frac{d}{2} = \frac{D}{2} + r_o(1 - \cos\theta). \tag{111}$$

Thus the effective periphery is

$$C_e = \pi D\left[1 + \frac{2r_o}{D}(1 - \cos\theta)\right]. \tag{112}$$

The analysis then proceeds as before. However, t_a is now defined as

$$t_{a_{3\text{-}D}} = t_{a_{2\text{-}D}} \times \frac{1 - \frac{t}{D}\cos\theta}{1 + 2\frac{r_o}{D}\cdot\frac{t}{D}(1-\cos\theta)} \tag{113}$$

or

$$\frac{t_a}{t}_{3\text{-}D} = \frac{t_a}{t}_{2\text{-}D} \times \frac{1 - \frac{t}{D}\cos\theta}{1 + 2\frac{r_o}{D}\cdot\frac{t}{D}(1-\cos\theta)}. \tag{114}$$

The limit case of a very thin jet is provided, of course, by assuming

$$\frac{t_a}{t}_{2\text{-}D} = 1.0.$$

SOME GENERAL RELATIONS FOR THE FLOW PARAMETERS OF AN ANNULAR JET

In the most general case, the total head variation across a jet is a function only of the distance (ζ) across the jet.

$$\Delta P_\zeta = f_1(\zeta). \tag{115}$$

The local static pressure Δp_3 is also a function of ζ . It is therefore possible to define completely general relationships for the various performance parameters of interest, in terms of these two variables.

The Local Jet Velocity v_3

In the nozzle exit plane, the local velocity is

$$v_3 = \left[\frac{2}{\rho} (\Delta P_3 - \Delta p_3) \right]^{1/2}. \tag{116}$$

The Jet Mass Flow $\dot{m}_j$

$$d\dot{m}_j = \rho C v_3 \, d\zeta$$

$$= C \left[2\rho (\Delta P_3 - \Delta p_3) \right]^{1/2} d\zeta$$

$$\frac{\dot{m}_j}{t C (2\epsilon)^{1/2}} = \int_0^1 (\Delta P_3 - \Delta p_3)^{1/2} \, d(\zeta/\epsilon) . \tag{117}$$

The Nozzle Momentum Flux J_j

$$dJ_j = \rho C v_3^2 \, d\zeta$$

$$\frac{J_j}{2C} = \int_0^\epsilon (\Delta P_3 - \Delta p_3) \, d\zeta$$

$$\frac{J_j}{2C\epsilon} = \int_0^1 \Delta P_3 \, d(\zeta/\epsilon) - \int_0^1 \Delta p_3 \, d(\zeta/\epsilon). \tag{118}$$

Total Nozzle Force F_N

$$dF_N = \rho C v_3^2 \, d\zeta + C \Delta p_3 \, d\zeta$$

$$= C \left[2\Delta P_3 - \Delta p_3 \right] d\zeta$$

$$\frac{F_N}{tC} = \int_0^1 (2\Delta P_3 - \Delta p_3) \, d(\zeta/\epsilon) . \tag{119}$$

Jet Power P_j

Power is defined at the nozzle

$$P_j = \int_0^A v \Delta P \, dA$$

$$dP_j = C d\zeta_3 \cdot \Delta P_3 \left[\tfrac{2}{\rho}(\Delta P_3 - \Delta p_3)\right]^{1/2}$$

$$\frac{P_j}{tC(\frac{2}{\rho})^{1/2}} = \int_0^1 \Delta P_3 (\Delta P_3 - \Delta p_3)^{1/2} d(\zeta/\ell). \qquad (120)$$

Total Lift

Total lift = jet lift + cushion lift

$$= F_N \cos\theta + A_c \Delta p \qquad (121)$$

in inviscid flow.

SOLUTION OF THE CURVED JET EQUATION FOR CONSTANT TOTAL PRESSURE

We come now to the solution of Equation (94) for the case

ΔP_3 = constant = ΔP_j (say).

This gives

$$\frac{\Delta p_3}{\Delta P_j} = 2(r_0 + \eta_3)^{-3/\eta} \int_0^3 (r_0 + \eta_3)^{3/\eta - 1} d\zeta_3 , \qquad (122)$$

the constant of integration vanishing because of the boundary condition $\Delta p_3 = 0$ at $\zeta_3 = 0$. Integrating (122), we obtain

$$\frac{\Delta p_3}{\Delta P_j} = 1 - \left(\frac{r_0}{r_0 + \eta_3}\right)^{3/\eta} \qquad (123)$$

and, of course, the cushion pressure is

$$\frac{\Delta p_c}{\Delta P_j} = 1 - \left(\frac{\tau_0}{\tau_0 + \gamma k}\right)^{2/\gamma} . \qquad (12)$$

Local Jet Velocity v_3

$$v_3 = \left[\frac{2}{\rho}\Delta P_j\left(1 - \frac{\Delta p_3}{\Delta P_j}\right)\right]^{1/2}$$

$$\frac{v_3}{\left(\frac{2}{\rho}\cdot\Delta P_j\right)^{1/2}} = \left(\frac{\tau_0}{\tau_0 + \gamma z_3}\right)^{1/\gamma} . \qquad (13)$$

Jet Mass Flow $\dot{m}_j$

$$d\dot{m}_j = \rho C dz_3 v_3$$

$$\frac{\dot{m}_j}{C\left(2\rho\Delta P_j\right)^{1/2}} = \int_0^t \left(\frac{\tau_0}{\tau_0 + \gamma z_3}\right)^{1/\gamma} dz_3$$

$$\frac{\dot{m}_j}{Ct\left(2\rho\Delta P_j\right)^{1/2}} = \frac{\tau_0/t}{1-\gamma}\left[1 - \left(\frac{\tau_0/t}{\tau_0/t + \gamma}\right)^{\frac{1-\gamma}{\gamma}}\right] = t_m/t . \qquad (14)$$

The Nozzle Momentum Flux J_m

$$\frac{J_m}{2C} = \int_0^t (\Delta P_3 - \Delta p_3)\, dz_3$$

$$\frac{J_m}{2C\Delta P_j} = \int_0^t \left(\frac{\tau_0}{\tau_0 + \gamma z_3}\right)^{2/\gamma} dz_3$$

$$\frac{J_m}{2Ct\,\Delta P_j} = \frac{\tau_0/t}{2-\gamma}\left[1 - \left(\frac{\tau_0/t}{\tau_0/t + \gamma}\right)^{\frac{2-\gamma}{\gamma}}\right] . \qquad (15)$$

Total Jet Force F_N

$$F_N = J_m + C\int_0^t \Delta p_3\, dz_3$$

$$\frac{F_N}{2C\Delta P_j} = \frac{J_N}{2C\Delta P_j} + \frac{1}{2}\int_0^t \frac{\Delta p_3}{\Delta P_j}\, d\xi$$

$$= \frac{t}{2}\left[1 + \frac{J_N}{2Ct\Delta P_j}\right]$$

From the preceding section;

$$\therefore \frac{F_N}{2Ct\Delta P_j} = \frac{1}{2}\left[1 + \frac{r_0/t}{2-\eta}\left\{1 - \left(\frac{r_0/t}{r_0/t+\eta}\right)^{\frac{2-\eta}{\eta}}\right\}\right]. \qquad (128)$$

The Jet Curvature Parameter η

After the jet has accelerated to ambient, its thickness is t_a.

Thus, for continuity

$$\dot{m}_j = \rho t_a C v_{ja}$$

or

$$\frac{t_a}{t} = \frac{\dot{m}_j}{\rho C t v_{ja}}. \qquad (129)$$

There are two possible assumptions for calculating v_{ja}. If total head is conserved, then

$$v_{ja} = \left(\frac{2}{\rho}\Delta P_j\right)^{\frac{1}{2}};$$

$$\therefore \frac{t_a}{t} = \frac{\dot{m}_j}{Ct(2\rho\Delta P_j)^{\frac{1}{2}}} = \frac{r_0/t}{1-\eta}\left[1 - \left(\frac{r_0/t}{r_0/t+\eta}\right)^{\frac{1-\eta}{\eta}}\right] \qquad (130)$$

from Equation (126).

If total momentum is conserved, then v_{ja} is not necessarily constant across the jet. The conservation of total momentum assumption only states that

$$J_a = F_N = C\int_0^{t_a} \rho v_{ja}^2\, d\xi. \qquad (131)$$

For the present analysis we will assume v_{ja} = a constant, while noting the limitations of this assumption. Thus, Equation (131) becomes

$$F_N = \rho t_a C v_{ja}^2 ;$$

$$\therefore \quad v_{ja} = \left(\frac{F_N}{\rho C t_a} \right)^{\frac{1}{2}} . \tag{132}$$

Substituting Equations (126) and (128)

$$\frac{t_a}{t} = \frac{2\left(\frac{r_o/t}{1-\eta}\right)^2 \left[1 - \left(\frac{r_o/t}{r_o/t + \eta} \right)^{\frac{1-\eta}{\eta}} \right]^2}{1 + \frac{r_o/t}{2-\eta} \left[1 - \left(\frac{r_o/t}{r_o/t + \eta} \right)^{\frac{2-\eta}{\eta}} \right]} . \tag{133}$$

The jet thickness ratio t_a/t is also defined by the jet gometry. If we assume that the inner and outer boundaries are circular arcs, then from Figure 41

$$\eta = \frac{t_a/t + \sin\theta}{1 + \sin\theta} . \tag{134}$$

By cross-plotting Equation (134) with Equations (130) or (133), we can obtain solutions for η in terms of r_o/t . This has been done in Figure 43, assuming conservation of total head. The resulting values of η and t_a/t are plotted in Figures 44 and 45. The agreement with Strand's potential flow solution is notable in Figure 45.

Momentum Balance

From Equation (126), assuming conservation of total head

$$J_a = \dot{m}_j v_{ja}$$

$$= \left(\frac{g}{\rho} \Delta P_j \right)^{\frac{1}{2}} t C (\rho \Delta P_j)^{\frac{1}{2}} \frac{r_o/t}{1-\eta} \left[1 - \left(\frac{t_a/t}{r_o/t + \eta} \right)^{\frac{1-\eta}{\eta}} \right] . \tag{135}$$

From Equation (101)

$$\frac{\Delta p_c}{\Delta P_j} = \frac{J_a}{\Delta P_j \cdot C t (r_o/t + \eta)} \tag{136}$$

$$\text{——·——}\quad \eta = \frac{(r_c/t) + \sin\theta}{(1 + \sin\theta)}$$

$$\text{———}\quad \left(\frac{t_a}{t}\right) = \frac{r_c/t}{(1-\eta)}\left\{1 - \left(\frac{r_c/t}{\frac{r_c}{t}+\eta}\right)^{\frac{1-\eta}{\eta}}\right\}$$

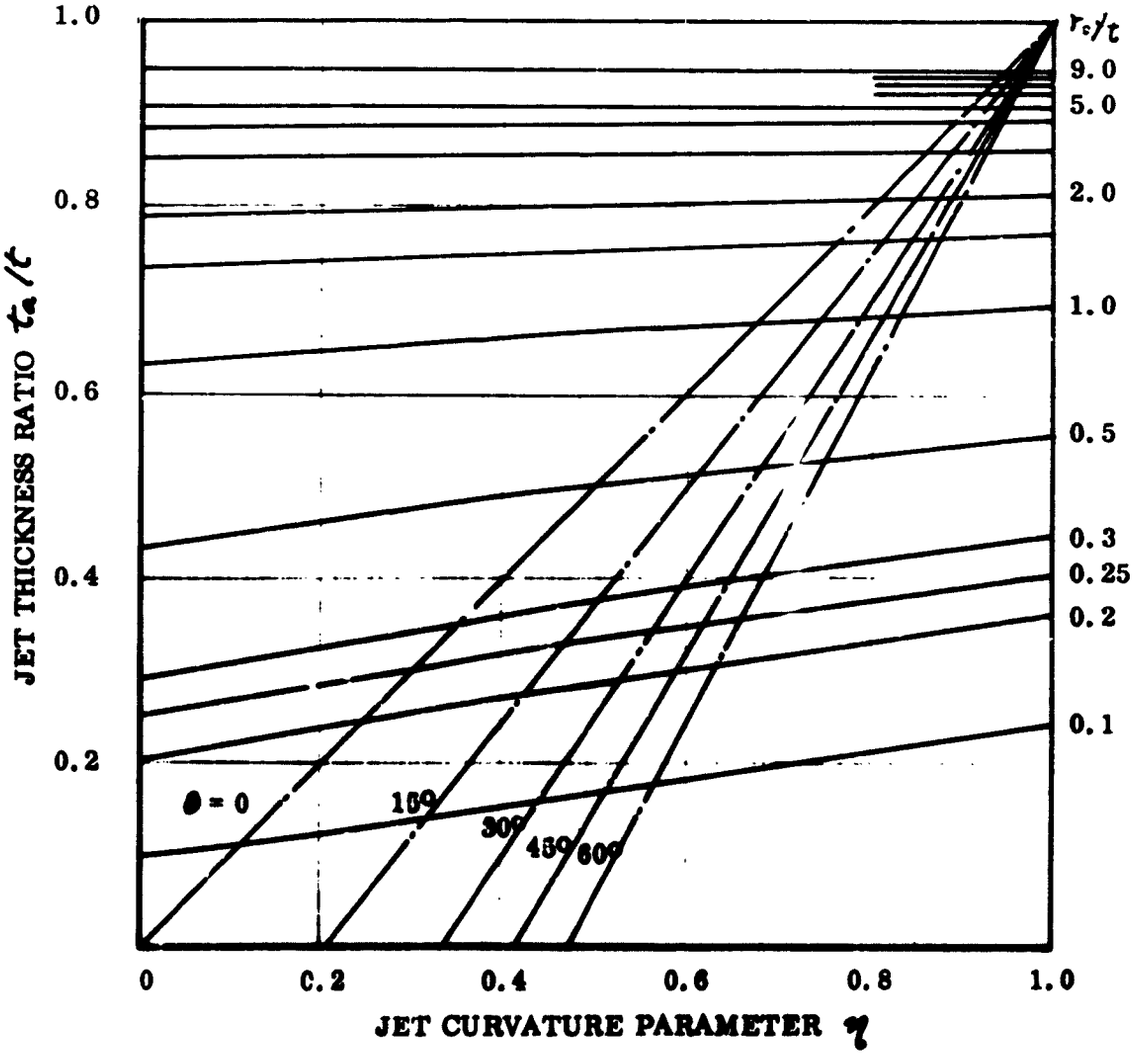

Figure 43. Cross-Plot of Equations (130) and (134) To Determine Values for the Jet Curvature Parameter η . (Solution for Conservation of Total Head.)

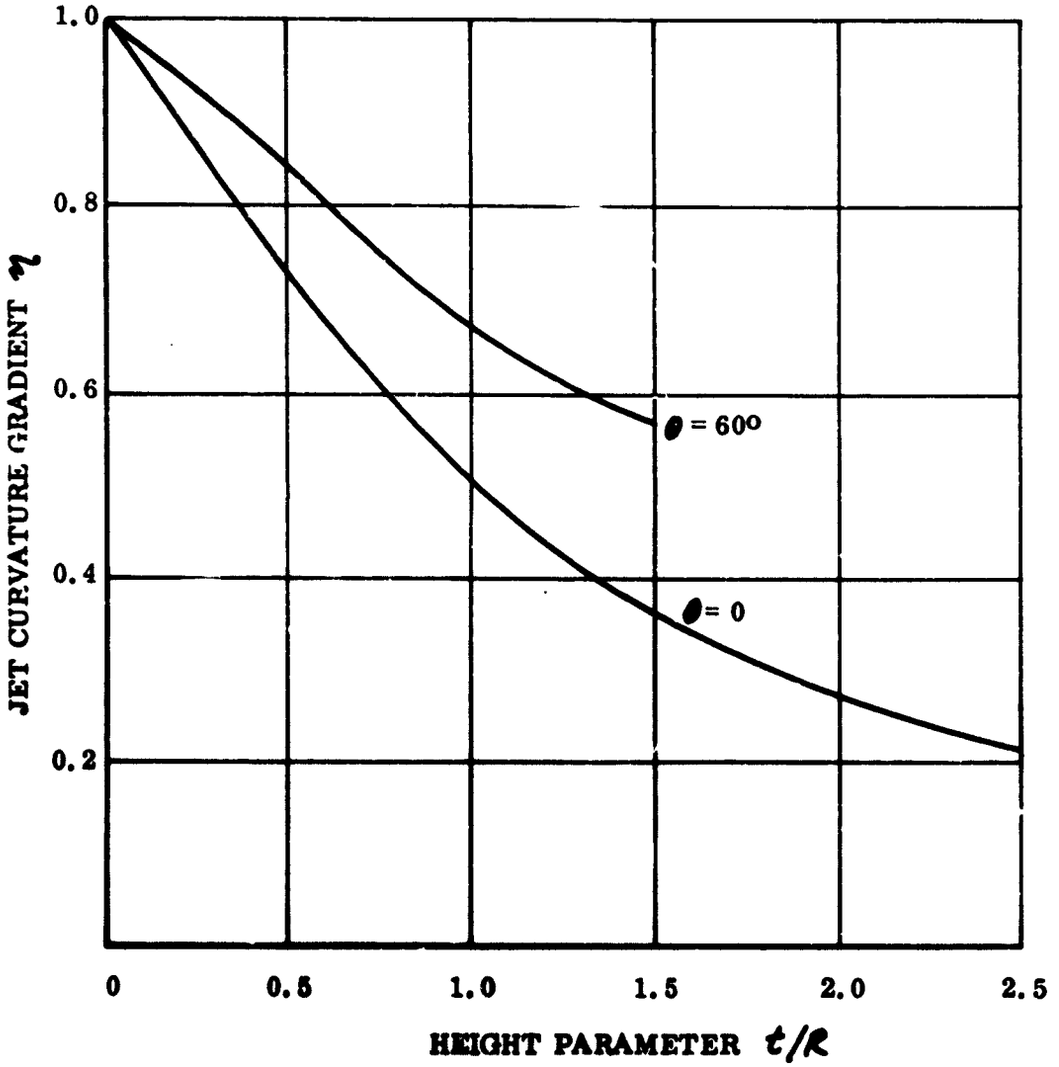

Figure 44. Variation of Jet Curvature Parameter η With the Height Parameter t/R .

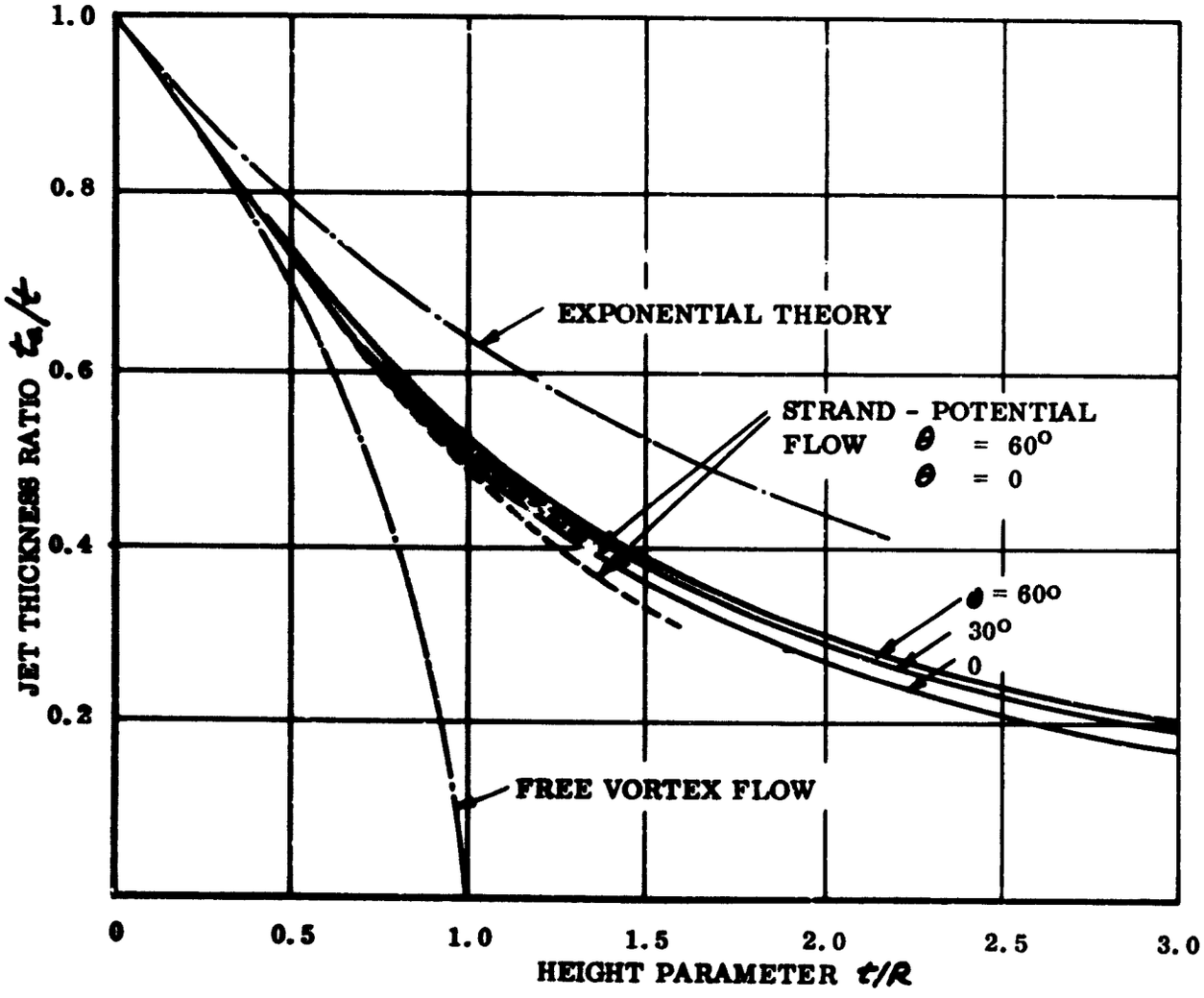

Figure 45. **Jet Thickness at Ambient Pressure, as a Function of the Height Parameter t/R . (Based on Continuity of Mass Flow.)**

$$\frac{\Delta p_c}{\Delta p_j} = \frac{2}{1-\eta}\left(\frac{r_0/t}{r_0/t+\eta}\right)\left[1-\left(\frac{r_0/t}{r_0/t+\eta}\right)^{\frac{1-\eta}{\eta}}\right] \qquad (137)$$

Comparing this with Equation (117) we have

$$\frac{\text{(Momentum Balance)}}{\text{(Curved Jet Theory)}} = \phi = \frac{2}{1-\eta}\left(\frac{r_0/t}{r_0/t+\eta}\right)\left[\frac{1-\left(\frac{r_0/t}{r_0/t+\eta}\right)^{\frac{1-\eta}{\eta}}}{1-\left(\frac{r_0/t}{r_0/t+\eta}\right)^{3/\eta}}\right] \qquad (138)$$

Equation (138) is plotted in Figure 46. Although the momentum balance breaks down as $R/t \to 0$, the new formulation is obviously much more satisfactory than previous theories. It should also be noted that the divergence from $\phi = 1.0$ as $R \to 0$ may not indicate a departure from balance, but only a departure from the assumption of circular curvature.

Other Results

Knowing the variation of η with R/t, we can calculate the values of the other quantities derived earlier in this chapter.

In Figure 47 the cushion pressure parameter $\Delta p_c/\Delta p_j$ behaves just as we would expect, falling between the free-vortex and exponential theory results.

The discharge coefficient plotted in Figure 48 is particularly interesting, because, in contrast to previous results, it obviously agrees well with the known potential flow solutions for a plenum chamber. For the case $\theta = 0$ on the curve obviously fairs well into the point $C_D = 0.61$ which is established for a jet issuing from an orifice in a plane wall, while the $\theta = 90^\circ$ curve would obviously fair into the Borda mouthpiece solution of $C_D = 0.5$.

It will be recalled that a major criticism of Strand's potential flow solution was the limit $C_D \to 0.5$ as $R \to 0$ in contrast to the known result $C_D = 0.61$.

A more detailed comparison of the discharge coefficient predicted by the various theories is given in Figures 49 - 51, which also include an analogous solution by Gabbay[18].

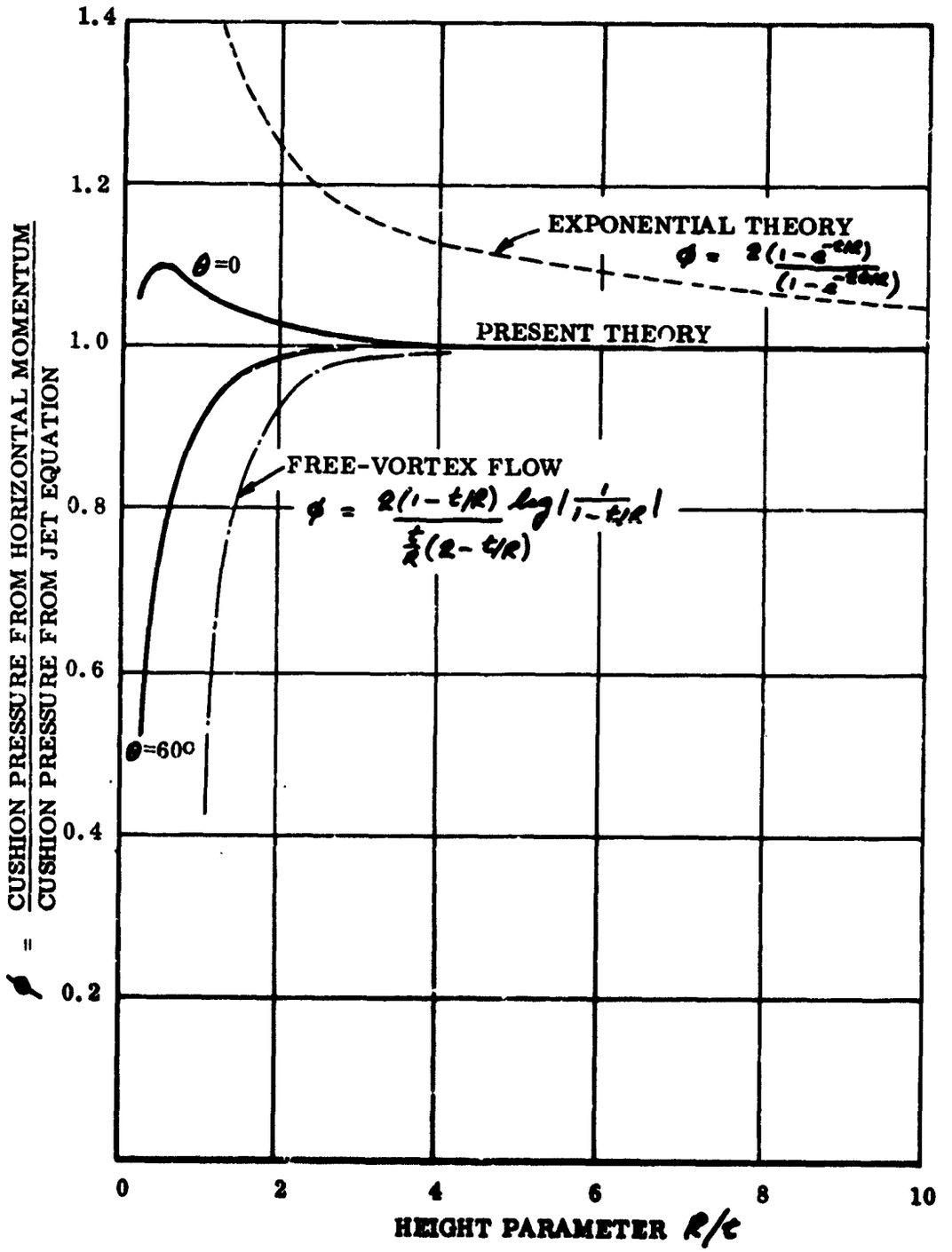

Figure 46. Momentum Balance as a Function of the Height Parameter R/t.

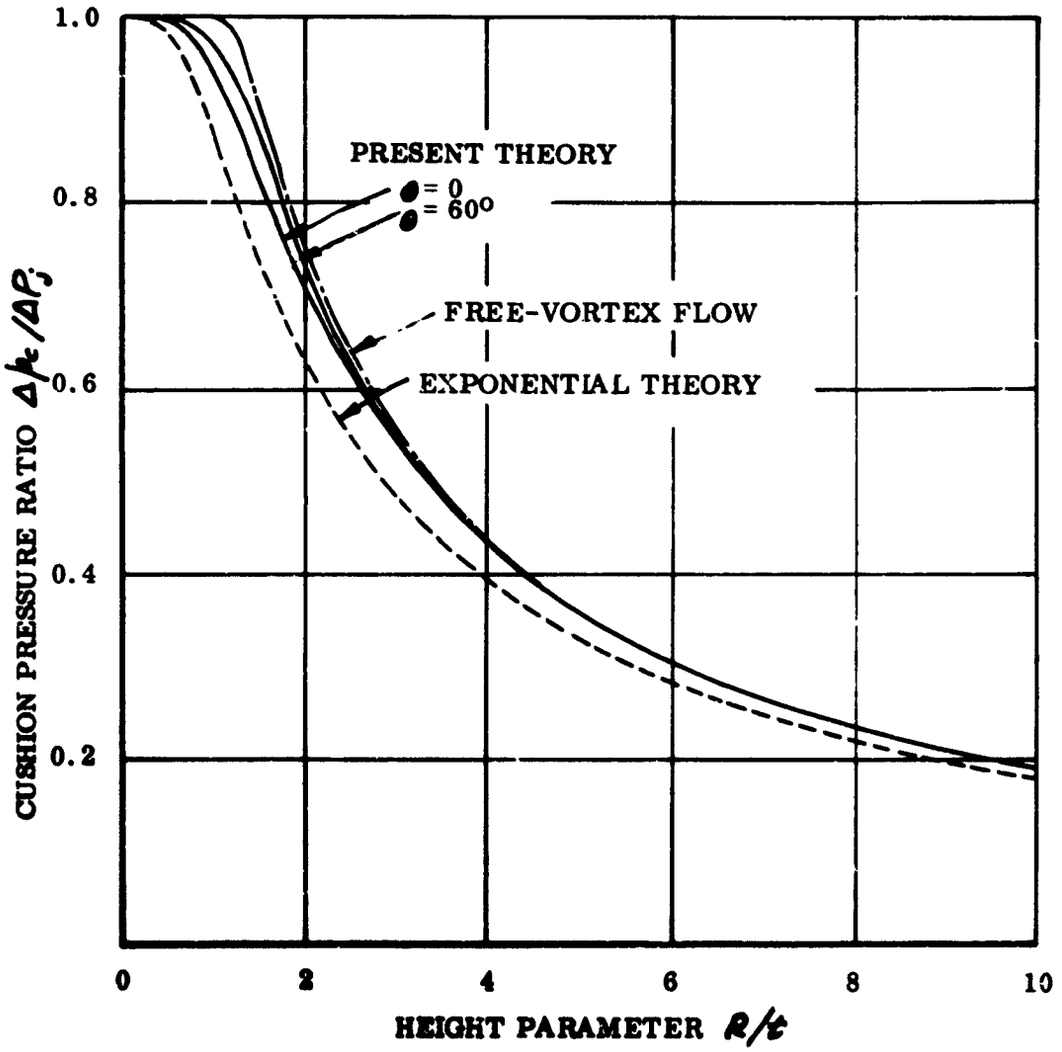

Figure 47. Variation of Cushion Pressure With the Height Parameter R/t.

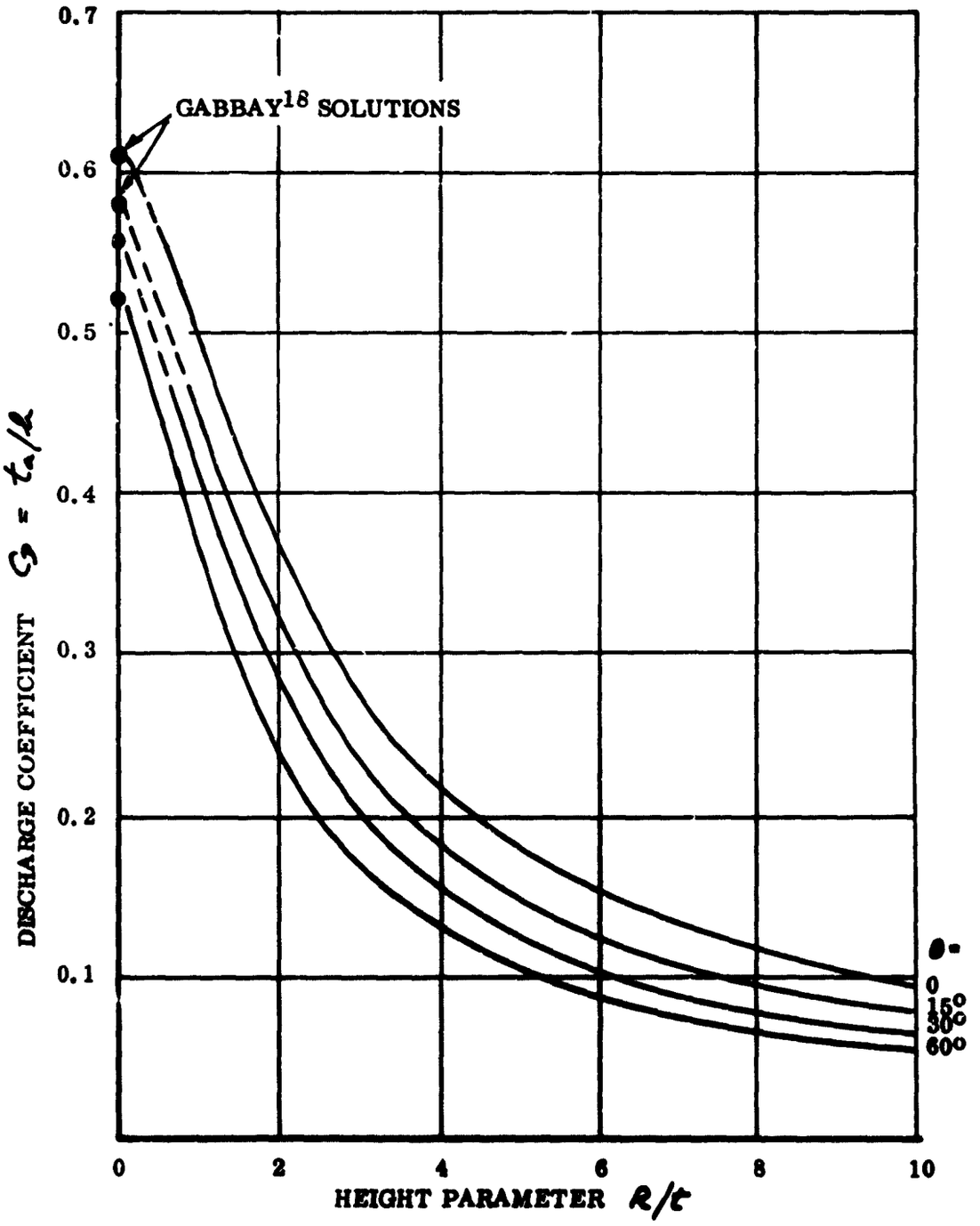

Figure 48. Discharge Coefficient C_D as a Function of the Height Parameter R/t.

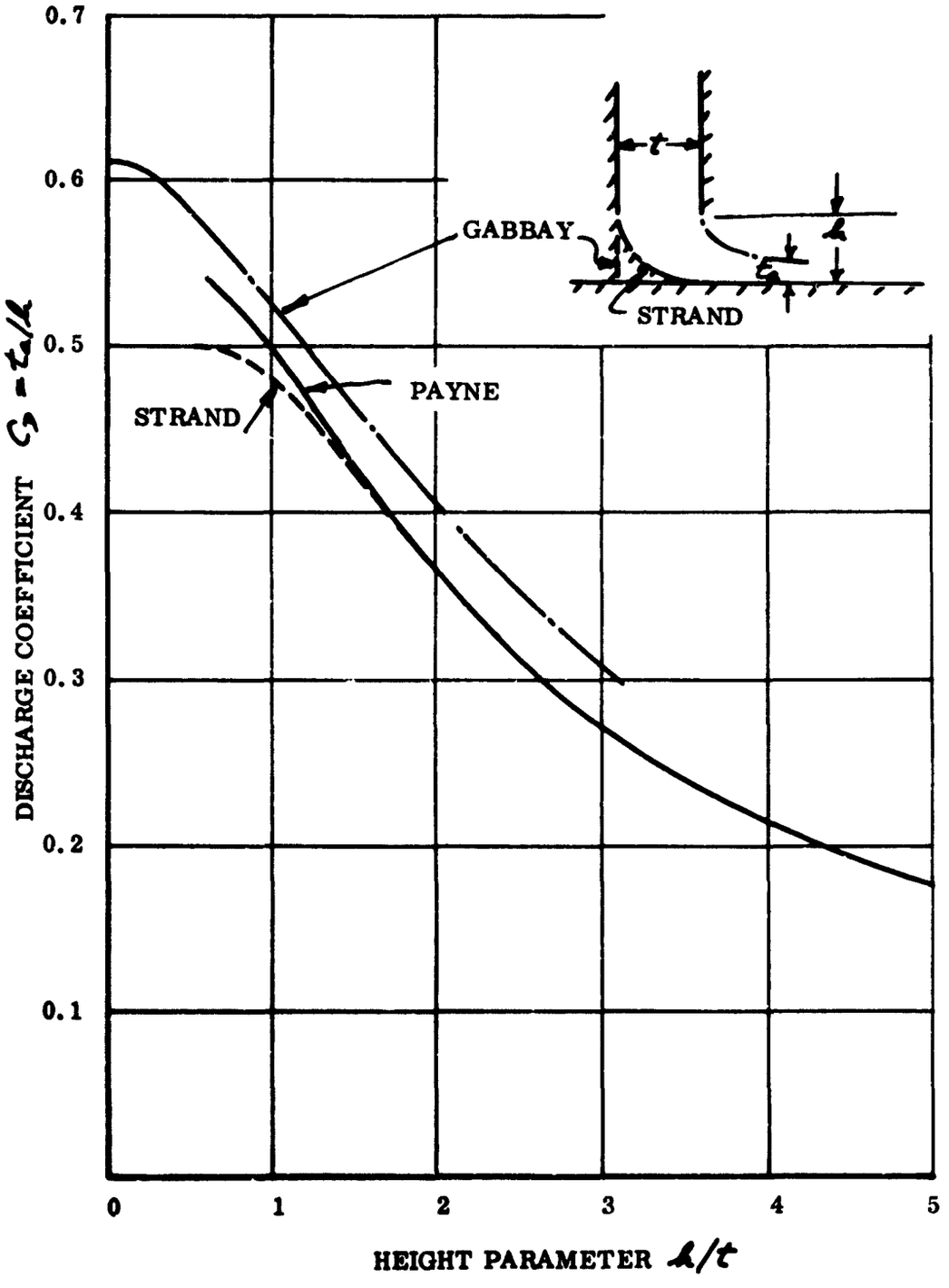

Figure 49. Comparison of Theoretical Discharge Coefficients for $\theta = 0$.

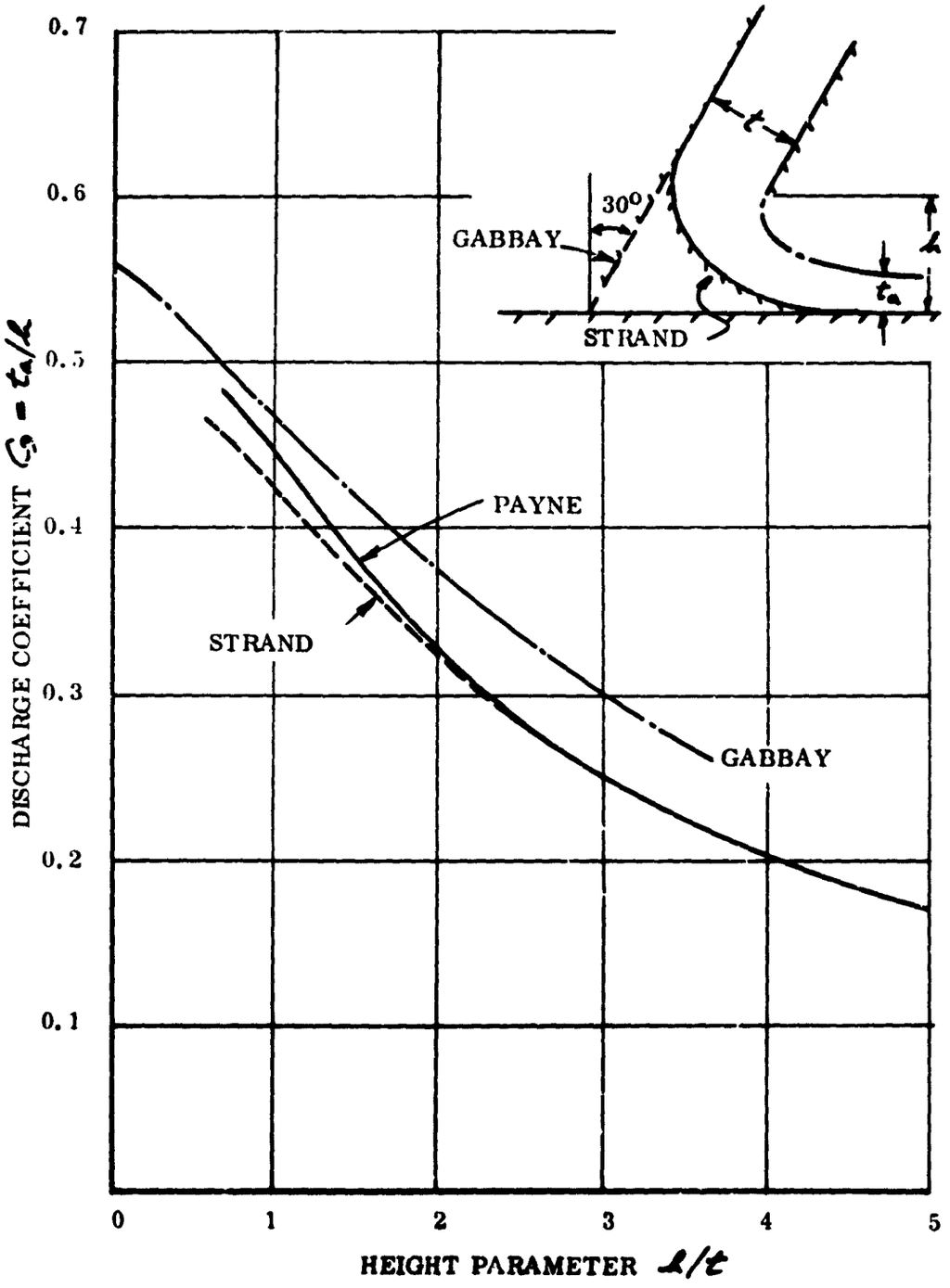

Figure 50. Comparison of Theoretical Discharge Coefficients for $\theta = 30^{\circ}$.

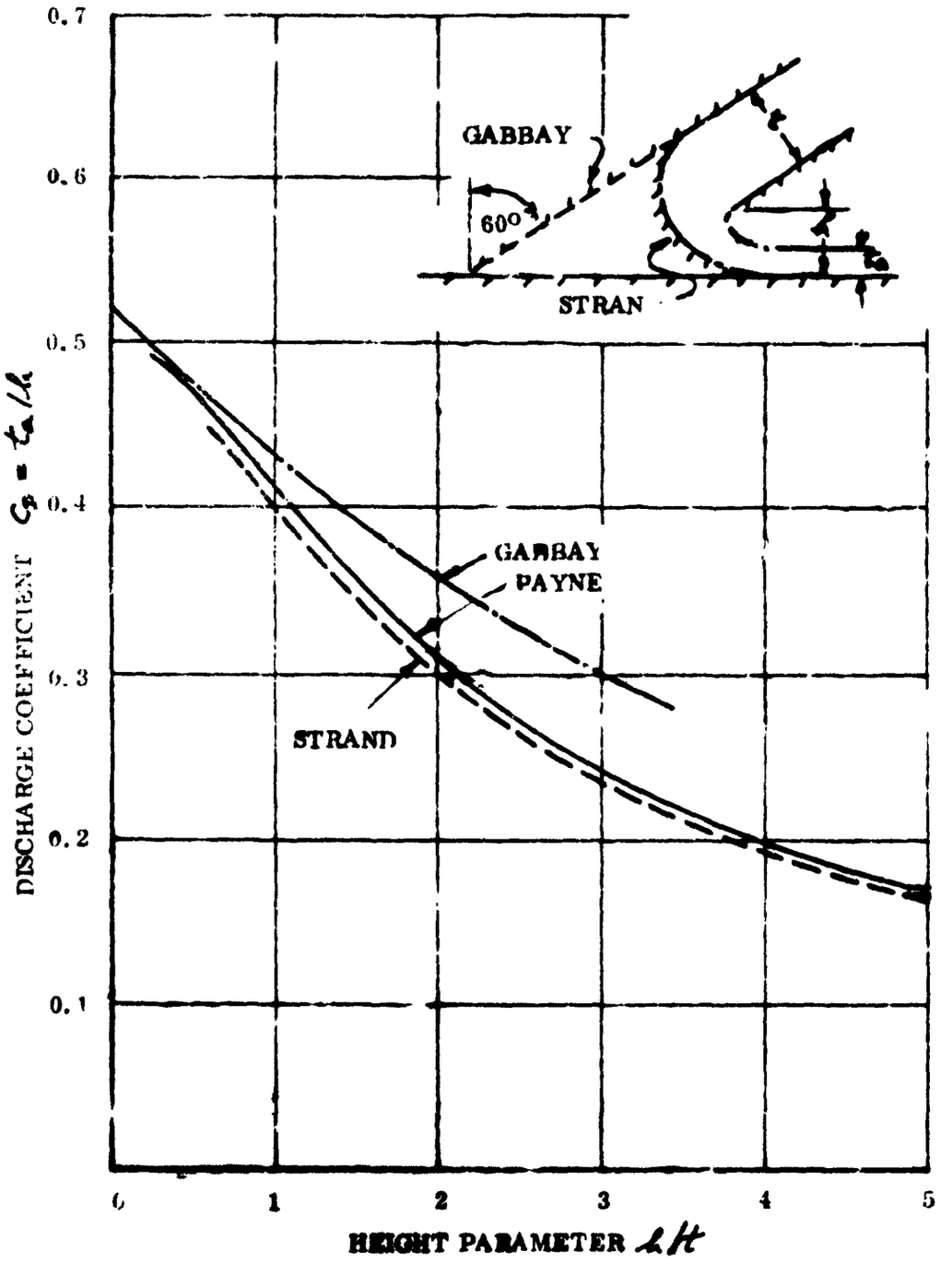

Figure 31. Comparison of Theoretical Discharge Coefficients for $\theta = 60^0$.

Gabbay's problem involves a straight wall as the inner (cushion side) boundary instead of a constant static pressure streamline. Since the static pressure along his boundary is not necessarily constant. his result approximates to the annular jet case only in the limit $h/t \to 0$. But at large values of the jet angle θ the approximation will presumably be valid at finite small values of h/t.

We see that, in general, the present theory agrees with Strand's for $h/t > 1$ and tends towards Gabbay's for $0.5 < h/t < 1$. At values of $h/t < 0.5$, the solution breaks down because the implied geometrical assumptions are no longer tenable; but the extrapolation from higher values points quite convincingly towards Gabbay's limits for $h/t = 0$.

For practical GEMs the range of interest is $0.5 < h/t < 2$ or 3. The elegant and sophisticated potential flow treatments of Gabbay and Strand apply respectively below and above this range. Within the range, this relatively simple theory of this report is apparently more applicable than either.

We should hasten to add that Gabbay was not considering the annular jet problem in his analysis and never intended his solution to apply to it.

The nozzle force parameter plotted in Figure 52 is noteworthy because the pressure lift term is generally ignored in the calculation of total lift, yet is seen to make an important contribution at low ground clearance heights.

Some of the calculated two-dimensional solutions are given numerically in Table 1.

The same procedures apply to the calculation of jet characteristics in the three-dimensional case, using Equation (114).

As an example, we calculate the values of η and $\Delta p_c/\Delta p_j$ for a circular planform GEM, for the case $\theta = 0$, $h/D = 0.1165$. The results are plotted in Figures 53 and 54, and we see that, although there is a significant variation in η (and therefore t_o/t), the cushion pressure remains almost completely unaffected by the change of planform.

THE CUSHION PRESSURE PARAMETER $\overline{\Delta p_c}$

We shall see later that the conventional cushion pressure parameter

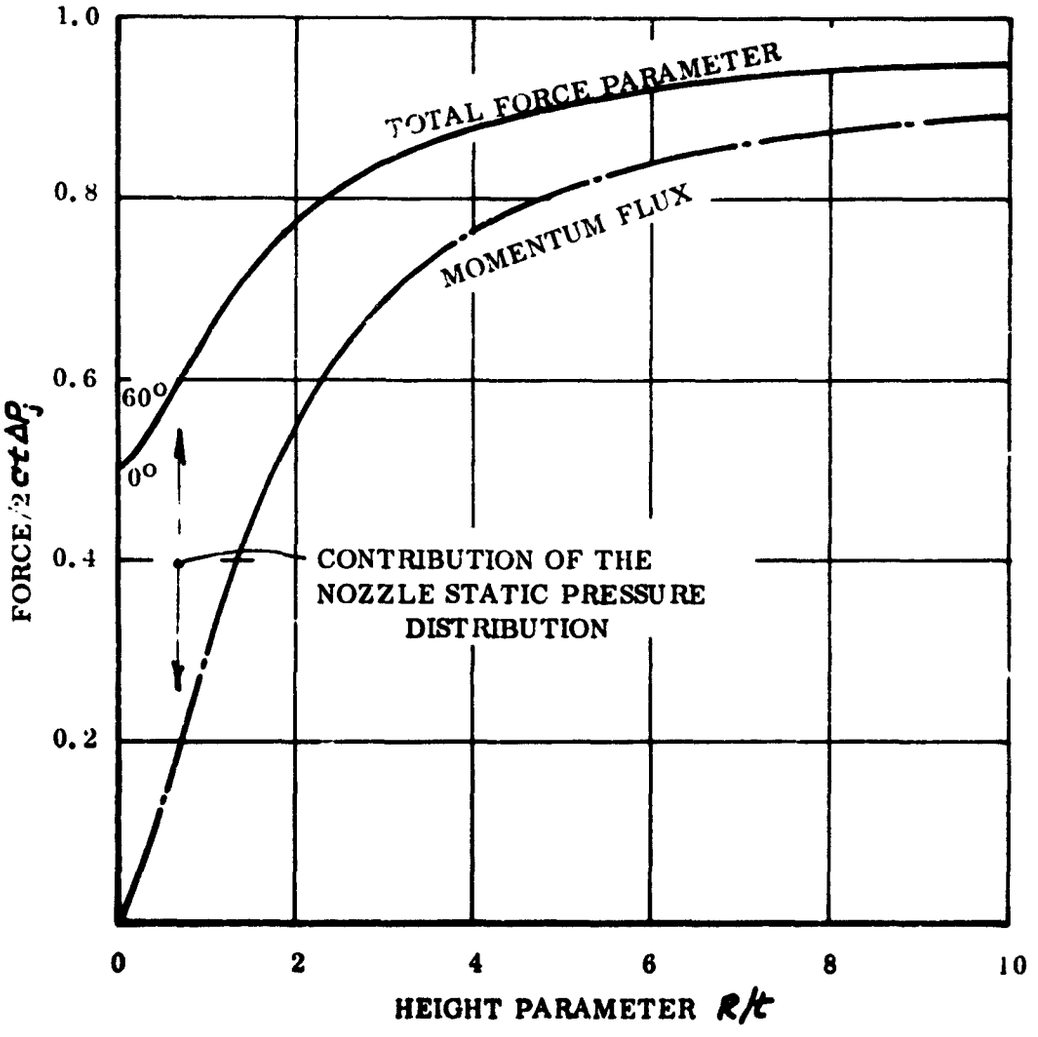

Figure 52. Total Nozzle Force, Measured Parallel to the Nozzle Axis, as a Function of the Height Parameter R/t .

TABLE 1. COMPUTED VALUES OF SOME ANNULAR JET FUNCTIONS

t/R	R/t	t_0/t	t_a/t	η	$\frac{\Delta p_c}{\Delta P_j}$	$\frac{J_i}{2ct\Delta P_j}$	$\frac{F_N}{2ct\Delta P_j}$
4.65	0.215	0.10	0.115	0.115	1.00	0.053	0.526
2.25	0.445	0.20	0.245	0.245	0.999	0.114	0.557
1.82	0.550	0.25	0.300	0.300	0.995	0.145	0.572
1.54	0.650	0.30	0.350	0.350	0.988	0.177	0.588
1.00	1.00	0.50	0.500	0.500	0.937	0.292	0.646
0.597	1.68	1.0	0.675	0.675	0.783	0.479	0.740
0.443	2.26	1.5	0.760	0.760	0.660	0.590	0.795
0.357	2.80	2.0	0.803	0.803	0.570	0.665	0.832
0.259	3.86	3.0	0.860	0.860	0.444	0.750	0.875
0.205	4.89	4.0	0.890	0.890	0.365	0.805	0.902
0.169	5.91	5.0	0.910	0.910	0.307	0.825	0.912
0.101	9.95	9.0	0.945	0.945	0.191	0.895	0.950
1.492	0.67	0.10	0.175	0.570	0.999	0.068	0.534
1.202	0.832	0.20	0.305	0.632	0.986	0.139	0.570
1.104	0.905	0.25	0.355	0.655	0.981	0.173	0.590
1.018	0.982	0.30	0.403	0.682	0.969	0.205	0.602
0.744	1.345	0.50	0.525	0.745	0.914	0.312	0.656
0.545	1.835	1.0	0.685	0.835	0.768	0.495	0.750
0.421	2.375	1.5	0.765	0.875	0.652	0.600	0.800
0.345	2.900	2.0	0.810	0.900	0.562	0.662	0.831
0.254	3.930	3.0	0.860	0.930	0.440	0.746	0.873
0.202	4.945	4.0	0.890	0.945	0.362	0.795	0.900
0.168	5.950	5.0	0.910	0.950	0.307	0.848	0.924
0.1002	9.970	9.0	0.945	0.970	0.191	0.870	0.935

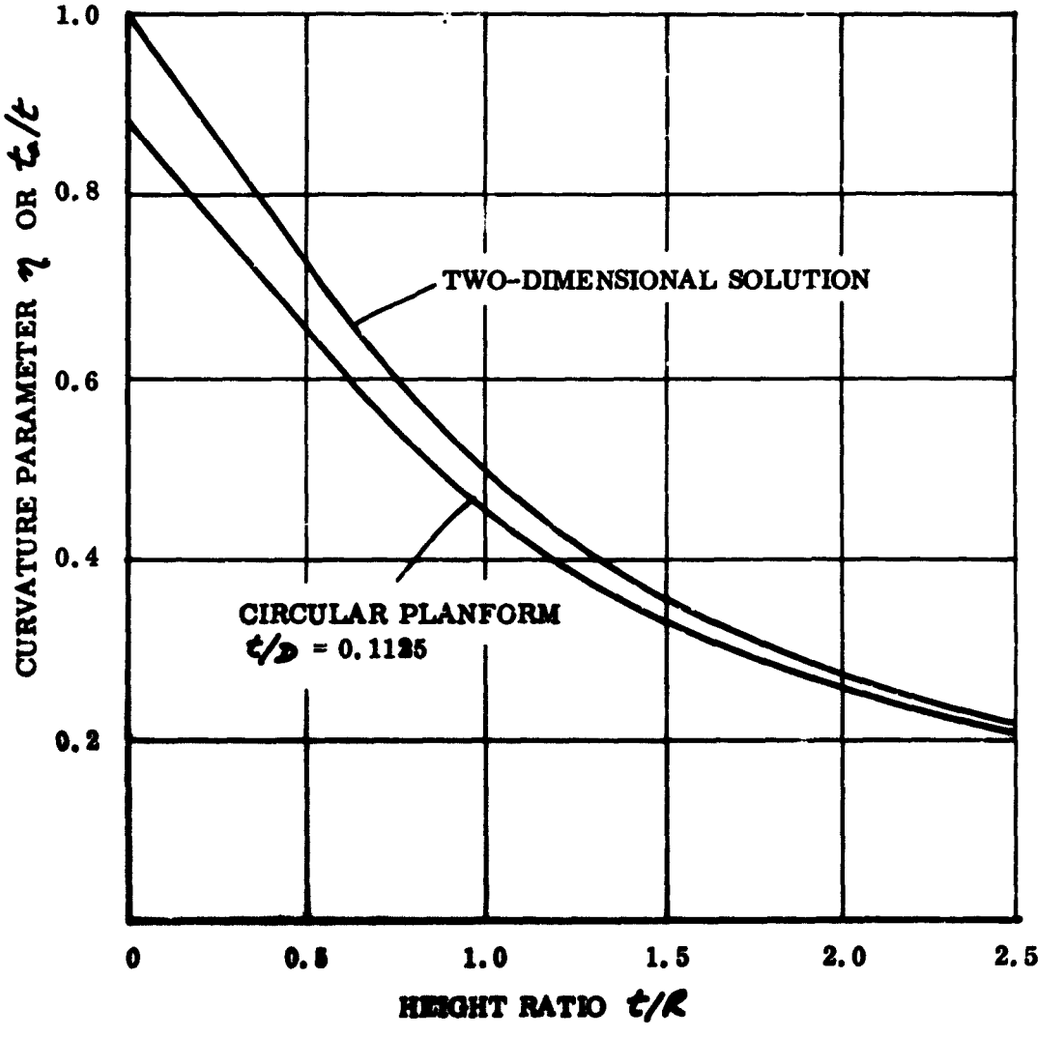

Figure 53. Comparison of Discharge Coefficient Ratio C_b/C for Two-Dimensional and Circular Planform GEMs ($\theta = 0^{\circ}$).

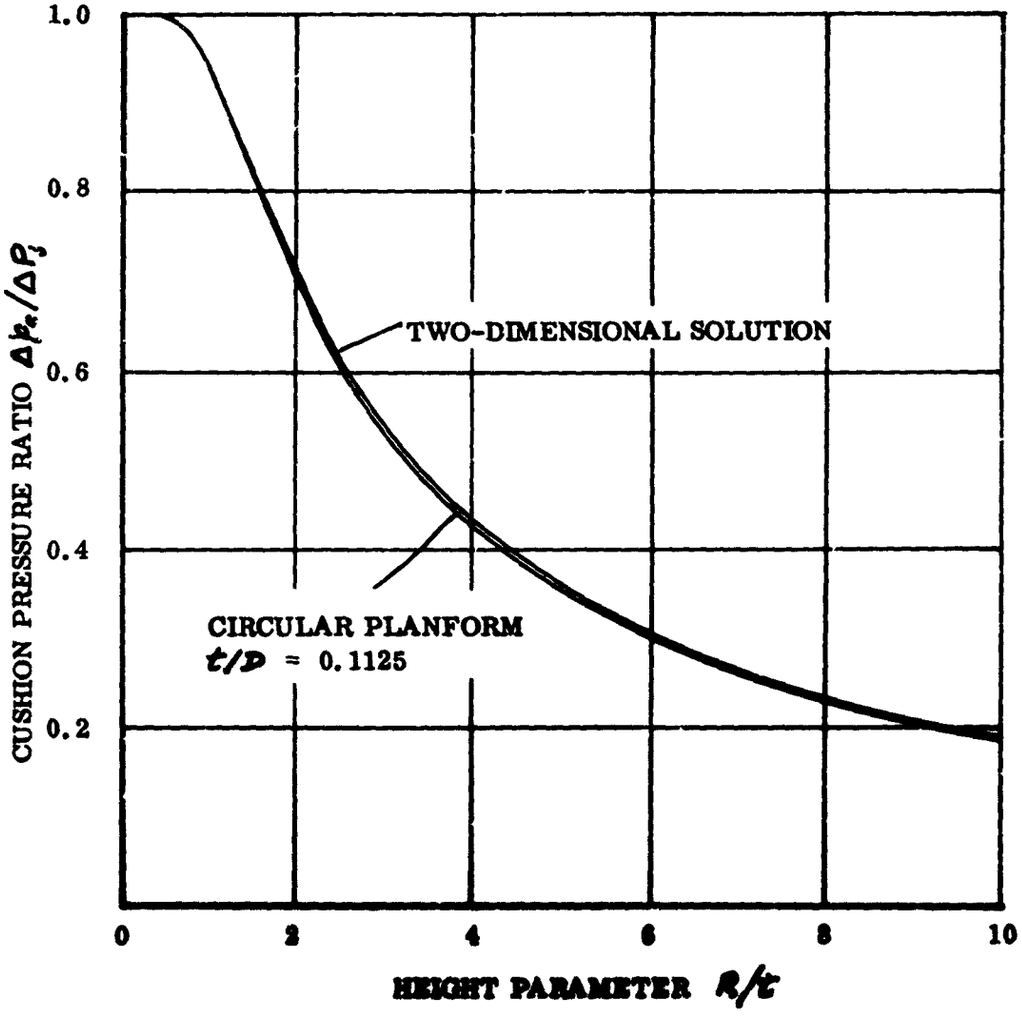

Figure 54. Effect of Planform on the Cushion Pressure Parameter $\Delta p_c/\Delta p_j$.

$$\frac{\Delta p_c}{\Delta P_j} = \frac{\text{cushion pressure}}{\text{mean jet total pressure}}$$

is not a very meaningful index of annular jet performance, nor is it a good parameter for correlating test data.

The fundamental performance parameter in hover is the ratio of the total lift developed to the power lost in the jet, but this introduces extraneous variables related to the planform and geometry of the vehicle. A closely related index is the ratio of the cushion pressure to the jet power, however, and this seems to be the most useful parameter for general use.

From Equation (120) the general expression for jet power is seen to be

$$\mathcal{P}_j = \tfrac{1}{2} C \left(\tfrac{2}{\rho}\right)^{1/2} \int_0^1 \Delta P_j \left(\Delta P_j - \Delta p_j\right)^{1/2} d(j/t)$$

$$= \tfrac{1}{2} C \left(\tfrac{2}{\rho}\right)^{1/2} \int_0^1 \Delta P_j^{3/2} \left(1 - \frac{\Delta p_j}{\Delta P_j}\right)^{1/2} d(j/t). \qquad (139$$

Since $$\Delta p_c \propto \int_0^1 \Delta P_j \, d(j/t),$$

we may expect that

$$\frac{\Delta p_c^{3/2}}{\mathcal{P}_j} = \text{constant.}$$

We can formalize this result by considering an ideal (very deep) plenum chamber at an edge clearance height of h. The mass flow out is

$$\dot{m}_j = \rho C h C_D v_{ja} = \rho C h C_D \left(\tfrac{2}{\rho} \Delta p_c\right)^{1/2}; \qquad (140$$

$$\therefore \quad \mathcal{P}_j = \tfrac{1}{2} \dot{m} v_{ja}^2 = C h C_D \left(\tfrac{2}{\rho}\right)^{1/2} \Delta p_c^{3/2}; \qquad (141$$

$$\therefore \quad \Delta p_c / \mathcal{P}_j = (C h C_D)^{-1} \left(\tfrac{2}{\rho} \Delta p_c\right)^{-1/2}.$$

The obvious non-dimensionalization is

$$\Delta \bar{p}_c = C h \left(\tfrac{2}{\rho} \Delta p_c\right)^{1/2} \frac{\Delta p_c}{\mathcal{P}_j} = \frac{1}{C_D}. \qquad (142$$

$\Delta\bar{p}_c$ can thus be calculated for any GEM configuration, provided that p_j and Δp_c are known. Although $\Delta\bar{p}_c$ is the reciprocal of C_p', this is an effective discharge coefficient. In the general case, it will differ from the actual discharge coefficient, which is defined as

$$C_D = \frac{\dot{m}_j}{\rho_j C v_{ja}} = \frac{\dot{m}_j}{h C (2\rho \Delta p_c)^{1/2}} . \quad (143)$$

Naturally, although we have derived this relationship from plenum chamber theory, it can be applied to an annular jet. Indeed, at very low edge clearance heights ($h/b \to 0$), there is no difference between the two configurations. As lift increases, the annular jet may be regarded as a special case of the plenum, where ducting is employed to reduce the discharge coefficient.

The General Expression for $\Delta\bar{p}_c$

From Equations (139) and (142),

$$\Delta\bar{p}_c = \frac{h/c \cdot \Delta p_c^{3/2}}{\int_0^1 \Delta P_3 (\Delta P_3 - \Delta p_3)^{1/2} d(x/c)} . \quad (144)$$

Substituting for Δp_c and Δp_3 from Equations (94) and (95),

$$\Delta\bar{p}_c = \frac{h/c (r_0 + \eta t)^{-3/\gamma} \left[2 \int_0^t (r_0 + \eta\zeta)^{\frac{3}{\gamma}-1} \Delta P_3 \, d\zeta \right]^{3/2}}{\int_0^1 \Delta P_3 \left[\Delta P_3 - (r_0 + \eta\zeta)^{-3/\gamma} \left\{ 2 \int_0^\zeta (r_0 + \eta\zeta)^{\frac{3}{\gamma}-1} \Delta P_3 \, d\zeta \right\} \right]^{1/2} d(x/c)} . \quad (145)$$

An optimum total head distribution will be one which maximizes this expression.

The Constant Total Head Solution

If ΔP_3 = a constant, it vanishes from the expression, and

$$\Delta\bar{p}_c = \frac{h/c (r_0 + \eta t)^{-3/\gamma} \left[2 \int_0^t (r_0 + \eta\zeta)^{\frac{3}{\gamma}-1} d\zeta \right]^{3/2}}{\int_0^1 \left[1 - (r_0 + \eta\zeta)^{-3/\gamma} \left\{ 2 \int_0^\zeta (r_0 + \eta\zeta)^{\frac{3}{\gamma}-1} d\zeta \right\} \right]^{1/2} d(x/c)} ;$$

that is, $$\Delta\bar{p}_c = \frac{\frac{\rho}{2}\left[1 - \left(\frac{r_0}{r_0 + \eta z}\right)^{2/\eta}\right]^{3/2}}{\frac{1}{z}\int_0^z \left(\frac{r_0}{r_0 + \eta z}\right)^{1/\eta} dz} \tag{146}$$

$$= (1-\eta)\cdot\frac{\rho}{2}\cdot\frac{z}{r_0}\left[1 - \left(\frac{r_0/z}{r_0/z + \eta}\right)^{2/\eta}\right]^{3/2} \Big/ \left[1 - \left(\frac{r_0/z}{r_0/z + \eta}\right)^{1-\eta}\right]. \tag{147}$$

<u>The Solution for Free-Vortex Flow (η = 1.0)</u>

For the case η = 1.0,

$$\Delta p_3 = (r_0 + 3)^{-2}\cdot 2\int_0^3 (r_1 + 3)\,\Delta P_3\, dz. \tag{148}$$

Substituting in Equation (144), this reduces to

$$\Delta\bar{p}_c = \frac{\frac{z}{r_0}\cdot\left(2\frac{r_0}{z} + 1\right)}{\left(\frac{r_0}{z} + 1\right)^2 \log\left|1 + \frac{z}{r_0}\right|}, \tag{149}$$

which can be written as

$$\frac{z}{R}\Delta\bar{p}_c = \frac{(z/R)^{5/2}(2 - z/R)^{3/2}}{(1 - z/R)\log\left|\frac{1}{1 - z/R}\right|}. \tag{150}$$

<u>The Solution for Exponential-Theory Flow (η = 0)</u>

In this case it can be shown that

$$\frac{z}{R}\Delta\bar{p}_c = z/R\,\frac{(1 - e^{-2z/R})}{(1 - e^{-z/R})}. \tag{151}$$

GENERAL SOLUTIONS FOR FREE-VORTEX FLOW WITH CONSTANT TOTAL PRESSURE

For the special case of free-vortex flow, the jet curvature parameter is $\eta = 1.0$. Thus, from Equation (94),

$$\frac{\Delta p_z}{\Delta P_j} = (r_0 + z)^{-2} \cdot 2\int_0^z (r_0 + z)\, dz \tag{152}$$

$$= 2(r_0 + z)^{-2} \cdot (r_0 z + \tfrac{z^2}{2}) . \tag{153}$$

Calculation of Mass Flow $\dot{m}_j$

From Equation (117),

$$\frac{\dot{m}_j}{C(2\rho \Delta P_j)^{\frac{1}{2}}} = \int_0^t [1 - 2(r_0 + z)^{-2}(r_0 z + \tfrac{1}{2} z^2)]^{\frac{1}{2}} dz$$

$$= \int_0^t \frac{dz}{1 + z/r_0} ; \tag{154}$$

$$\therefore \frac{\dot{m}_j}{tC(2\rho \Delta P_j)^{\frac{1}{2}}} = \frac{r_0}{t} \log |1 + t/r_0| \tag{155}$$

writing $R = r_0 + t$, $1 + t/r_0 = \frac{1}{1 - t/R}$

and $$\frac{\dot{m}_j}{tC(2\rho \Delta P_j)^{\frac{1}{2}}} = \frac{1 - t/R}{t/R} \log \left| \frac{1}{1 - t/R} \right| . \tag{156}$$

Calculation of the Local Velocity v_z

$$\frac{v_z}{(\frac{1}{2}\rho \Delta P_j)^{\frac{1}{2}}} = \frac{1}{1 + z/r_0} \tag{157}$$

$$= \frac{1 - t/R}{1 - t/R + z/r_0} . \tag{158}$$

Note that as $t/R \to 1.0$, $v_3 \to 0$.

The Nozzle Momentum Flux J_j

Since

$$dJ_j = \rho C\, dz_3\, v_3^2 = \frac{\rho C\, dz_3}{(1+3/r_0)^2}\frac{2}{\rho}\Delta P_j ,$$

$$\frac{J_j}{2Ct\Delta P_j} = \frac{1}{t}\int_0^t \frac{dz_3}{(1+3/r_0)^2}$$

$$= \frac{1}{1+t/r_0} = 1 - t/R . \qquad (159)$$

The Total Jet Force F_N

From Equation (119),

$$\frac{F_N}{2Ct\Delta P_j} = \frac{1}{2t}\int_0^t \left(2 - \frac{\Delta p_3}{\Delta P_j}\right) dz_3$$

$$= \frac{1}{2} + \frac{1}{2t}\int_0^t \frac{r_0^2 + 2r_0 z_3 + z_3^2 - (2r_0 z_3 + z_3^2)}{(r_0+z_3)^2}\, dz_3$$

$$= \frac{1}{2} + \frac{1}{1+t/r_0} = \frac{3}{2} - t/R . \qquad (160)$$

The Jet Power P_j

From Equations (117) and (120) it is obvious that the jet power parameter is the same as the mass flow parameter.

Momentum Balance

The momentum flux to ambient, assuming conservation of total head, is

$$J_a = \dot{m}_{ja} v_{ja} = \left(\frac{2}{\rho}\Delta p_j\right)^{\frac{1}{2}} \cdot ct \left(2\rho\Delta p_j\right)^{\frac{1}{2}} \cdot \frac{1-\epsilon/R}{\epsilon/R} \log\left|\frac{1}{1-\epsilon/R}\right|; \quad (161)$$

$$\therefore \quad \frac{\Delta p_a \text{ (Momentum Theory)}}{\Delta p_c \text{ (Curved Jet Theory)}} = \phi = \frac{2(1-\epsilon/R)\log\left|\frac{1}{1-\epsilon/R}\right|}{\epsilon/R\,(2-\epsilon/R)}. \quad (162)$$

GENERAL SOLUTIONS FOR CONSTANT RADIUS FLOW (EXPONENTIAL THEORY) WITH CONSTANT TOTAL PRESSURE

The exponential theory is concerned with the solution to Equation (94) when $\eta = 0$. We then have, from Equation (91),

$$\Delta p_3 = e^{-\frac{2}{R}\int dz}\left[\frac{2}{R}\int e^{\frac{2}{R}\int dz}\Delta p_3 dz + k\right]$$

$$= e^{-2z/R}\cdot\left[\frac{2}{R}\int e^{2z/R}\Delta p_3 dz + k\right]. \quad (163)$$

When $z = 0$, $\int_0^3 e^{2z/R}\Delta p_3 dz = 0$; $\therefore k = 0$;

$$\therefore \Delta p_3 = \frac{2}{R} e^{-2z/R}\cdot\int_0^3 e^{2z/R}\Delta p_3 dz. \quad (164)$$

When Δp_3 = a constant = Δp_j, Equation (164) becomes

$$\frac{\Delta p_3}{\Delta p_j} = \frac{2}{R} e^{-2z/R}\int_0^3 e^{2z/R} dz$$

$$= 1 - e^{-2z/R} \quad (165)$$

and, of course, the cushion pressure is

$$\frac{\Delta p_c}{\Delta p_j} = 1 - e^{-2\epsilon/R}. \quad (166)$$

The Local Jet Velocity v_{z_j}

Since $$v_{z_j} = \left(\frac{2}{\rho}\Delta P_j\right)^{\frac{1}{2}}\left(1 - \frac{\Delta P_z}{\Delta P_j}\right)^{\frac{1}{2}},$$

$$\frac{v_{z_j}}{\left(\frac{2}{\rho}\Delta P_j\right)^{\frac{1}{2}}} = e^{-z/R} . \tag{167}$$

The Jet Mass Flow $\dot{m}$

Since $$dm_j = \rho C dz v_z ,$$

$$\frac{\dot{m}_j}{C(2\rho\Delta P_j)^{\frac{1}{2}}} = \int_0^t e^{-z/R} dz ;$$

$$\therefore \quad \frac{\dot{m}_j}{Ct(2\rho\Delta P_j)^{\frac{1}{2}}} = \frac{1 - e^{-t/R}}{t/R} = \frac{t_a}{t} . \tag{168}$$

The Nozzle Momentum Flux J_j

Since $$dJ_j = \rho C dz v_z^2$$

$$= \rho C dz \cdot \frac{2}{\rho}\Delta P_j e^{-2z/R} ,$$

$$\frac{J_j}{2Ct\Delta P_j} = \frac{1}{t}\int_0^t e^{-2z/R} dz$$

$$= \frac{1 - e^{-2t/R}}{2t/R} . \tag{169}$$

The Total Jet Force F_N

$$F_N = J_j + C_f \int_0^t \Delta P_z dz ;$$

$$\therefore \quad \frac{F_N}{2Ct\Delta P_j} = \frac{J_j}{2Ct\Delta P_j} + \frac{1}{2t}\int_0^t \frac{\Delta P_z}{\Delta P_j} dz$$

$$= \frac{1}{2} + \frac{1 - e^{-2t/R}}{4t/R} . \tag{170}$$

The Jet Power P_j

From Equation (120),

$$\frac{P_j}{C t \Delta P_j \left(\frac{2}{\rho}\Delta P_j\right)^{\frac{1}{2}}} = \frac{1}{t}\int_0^t \left(1 - \frac{\Delta p_z}{\Delta P_j}\right)^{\frac{1}{2}} dz \ .$$

This expression is the same as for the mass flow, of course, so that

$$\frac{P_j}{C t \Delta P_j \left(\frac{2}{\rho}\Delta P_j\right)^{\frac{1}{2}}} = \frac{\dot{m}_j}{C t (\Delta P_j 2\rho)^{\frac{1}{2}}} = \frac{t_0}{t} = \frac{1 - e^{-t/R}}{t/R} \ . \qquad (171)$$

Momentum Balance

The momentum flux to ambient, assuming conservation of total head, is

$$J_a = \dot{m}_j v_{ja} = \left(\frac{2}{\rho}\Delta P_j\right)^{\frac{1}{2}} C t (2\rho \Delta P_j)^{\frac{1}{2}} \left(\frac{1 - e^{-t/R}}{t/R}\right) .$$

From Equation (101),

$$\frac{\Delta p_c}{\Delta P_j} = \frac{J_a}{\Delta P_j C R}$$

$$= 2\left(1 - e^{-t/R}\right) . \qquad (172)$$

Comparing this with Equation (166),

$$\frac{\Delta p_c \text{ (Momentum Theory)}}{\Delta p_c \text{ (Curved Jet Theory)}} = \phi = \frac{2\left(1 - e^{-t/R}\right)}{1 - e^{-2t/R}} \ . \qquad (173)$$

SOME EXPERIMENTAL RESULTS AT CONSTANT TOTAL PRESSURE

The Annular Jet Test Rig

The annular jet test rig shown in Figure 55 is based on a concept by Dr. Harvey Chaplin of the David Taylor Model Basin. The novelty lies chiefly in the use of an air supply at room ambient conditions aspirated through the test section to artificially low "ambient" conditions created by a centrifugal blower.

This arrangement has the advantage that, since the supply air is initially still, the distribution of total pressure at the nozzle is very uniform and losses and distortions arising from boundary layer effects are minimized. The use of a constant static pressure streamline intake assists in the creation of these desirable flow characteristics.

The appearance of the rig, and of the nozzle geometry used for the present series of measurements, is shown in the photograph, Figure 55. The internal dimensions and location of the measurement stations are shown in Figure 56. The rig is practically two-dimensional, being contained between the sideboards 11.5 inches apart. All the measurements were made in the central plane and quantities such as mass flow, volume flow, and power are referred to a unit width ($\mathcal{C}$ = 1 foot). Thus, flow volume appears as cubic feet per second per foot and power as foot pounds per second per foot.

The Experiment

The principal experimental subject is, of course, the behavior of the air at the nozzle exit. The air conditions prior to entering the nozzle were known absolutely, being the ambient room conditions. The principal measurements were at the outlet, where total and static pressures and the angle of flow were obtained. A further series of measurements were made a little lower downstream, traversing the jet and deep into the cushion to examine the behavior of the cushion air mass.

Instrumentation

Total and static pressures in the jet were sensed with a probe which detected also the local direction of the flow. The sensing head of this type of probe is wedge shaped, with the total pressure tap in the thin leading edge and a static tap in each slant face. The observed static pressures equalize at the true static when the wedge is pointing upstream, subject to a correction for error in manufacture and for pitch angle of the flow. The probe was inserted through the side of the rig,and the traverse was obtained by swinging the probe about

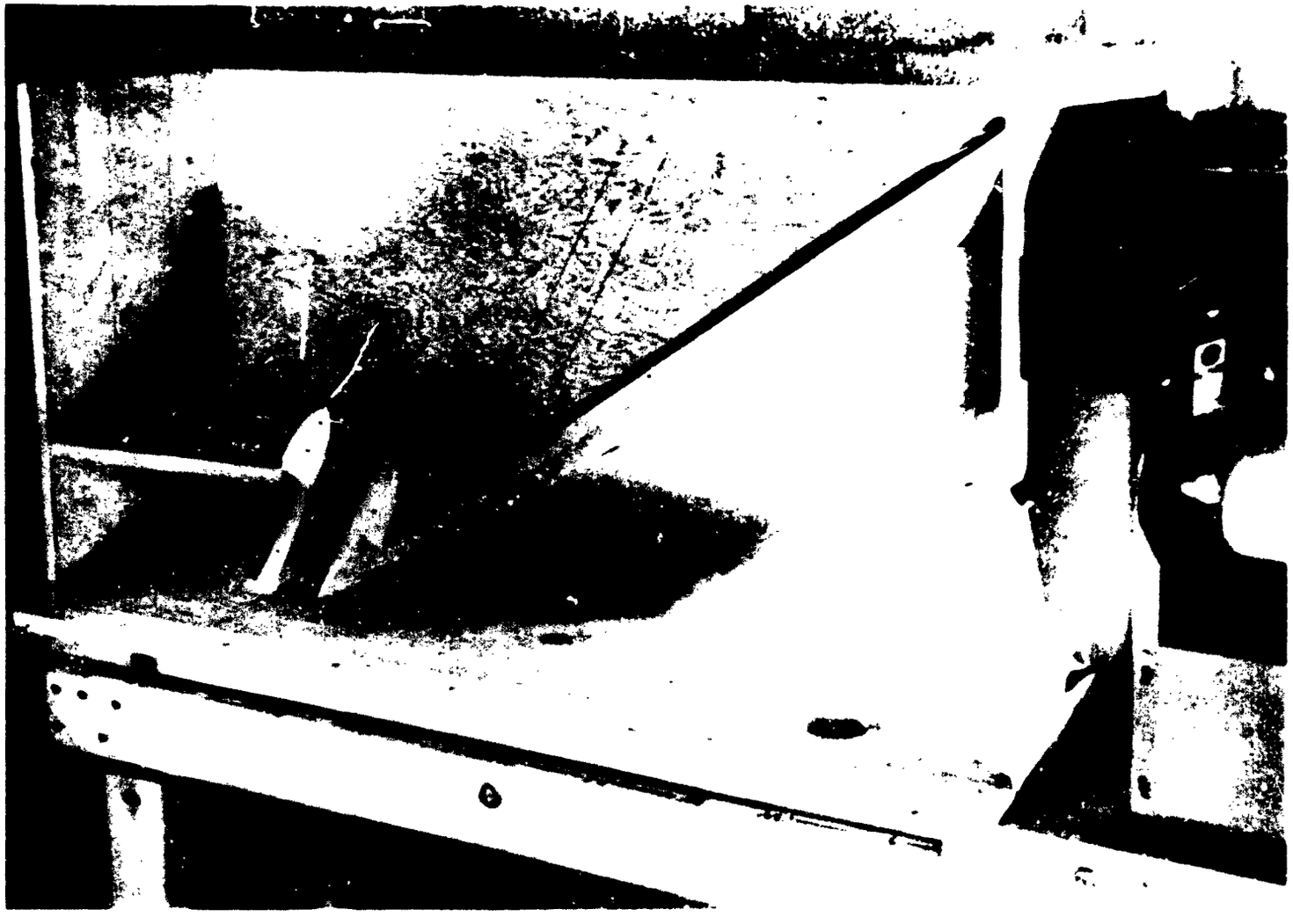

Figure 55. The Annular Jet Test Rig With Side Panel Removed To Show Nozzle Configuration ($d/t = 1.0$, $\theta = 30^{o}$).

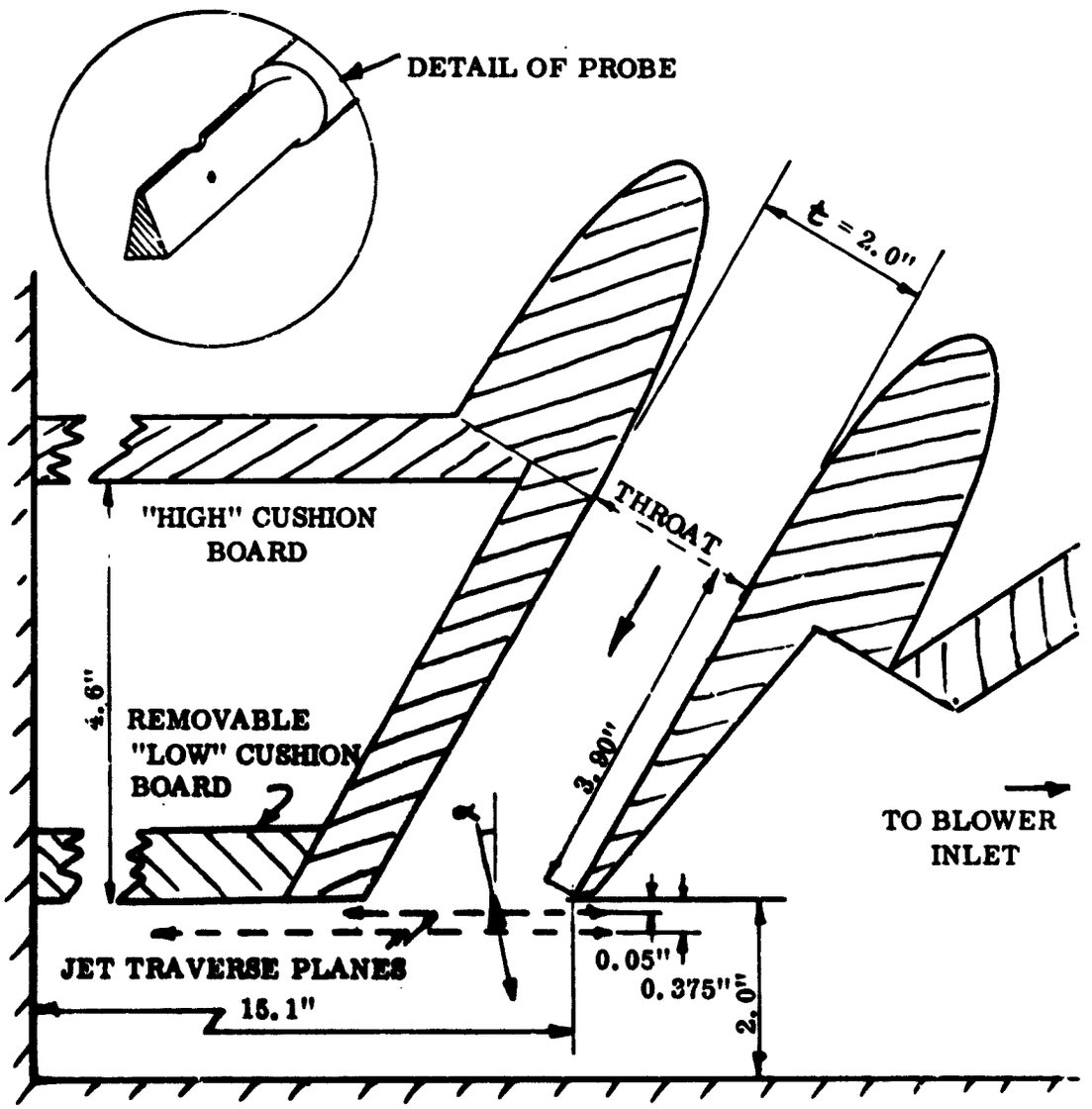

Figure 56. Internal Dimensions of Annular Jet Test Rig.

the point of penetration of the side wall. Thus, we obtained the angle of the flow in the central plane, as well as the pressures, and were able to correct for the pitch component due to the probe angle relative to the central plane by using the calibration. (Actually, this correction was very small at all positions.) Pressures were measured on inclined manometers. The readings were always consistent and repeatable and are believed to be free from random error within ± 1 percent of the maxima, including transcription and computation errors. Systematic errors, if any, are unknown and are inherent in the method.

The pressure and velocity at the nozzle throat and outlet are shown in Figures 57 and 58. The experimental data are given in Table 2. These have been reduced from manometer readings to pressures in inches of water and velocity in feet per second. No smoothing has been applied, either by alteration or by omission. Values for the flow volume and flow power were derived by numerical integration of these data.

Flow at the Throat (Figure 57)

The total pressure at the throat was virtually zero (relative to room ambient) because of the negligibly small loss incurred by the flow in the entry. The static pressure across the throat was nearly uniform with a roughly linear increase outward from the cushion side. The mean velocity was [illegible] 3 feet per second, and the volume flow was 9.00 cubic feet per second per foot. This value is probably slightly low because of the inability of the probe to penetrate the very thin boundary layers and the consequent omission of some small part of the flow from the integration. Similarly, the flow power, at 137 foot-pounds per foot, may also be low.

Flow at the Nozzle

At the nozzle outlet (Figure 58) the flow pattern is greatly changed. There is a velocity gradient running from a sharp peak value at the nozzle lip down to zero at a point 2.25 inches nearer the cushion. The flow angle is, in the main, normal to the traverse axis, indicating that the air has already turned through the nozzle angle (30°) and more toward the lip. Numerical integration of this velocity across the traverse gives a flow volume of 9.06 cubic feet per second per foot in the very fair agreement with the throat value.

The static pressure beyond the lip drops sharply to a depression of 2.94 inches of water. This is artificial "ambient" created by the inlet to the blower. The pressure scale in the figure is referred to this datum, giving a cushion pressure of +2.63 inches of water and a supply pressure of +2.94 inches of water. The total pressure loss across the jet is greatest at the cushion side and diminishes to

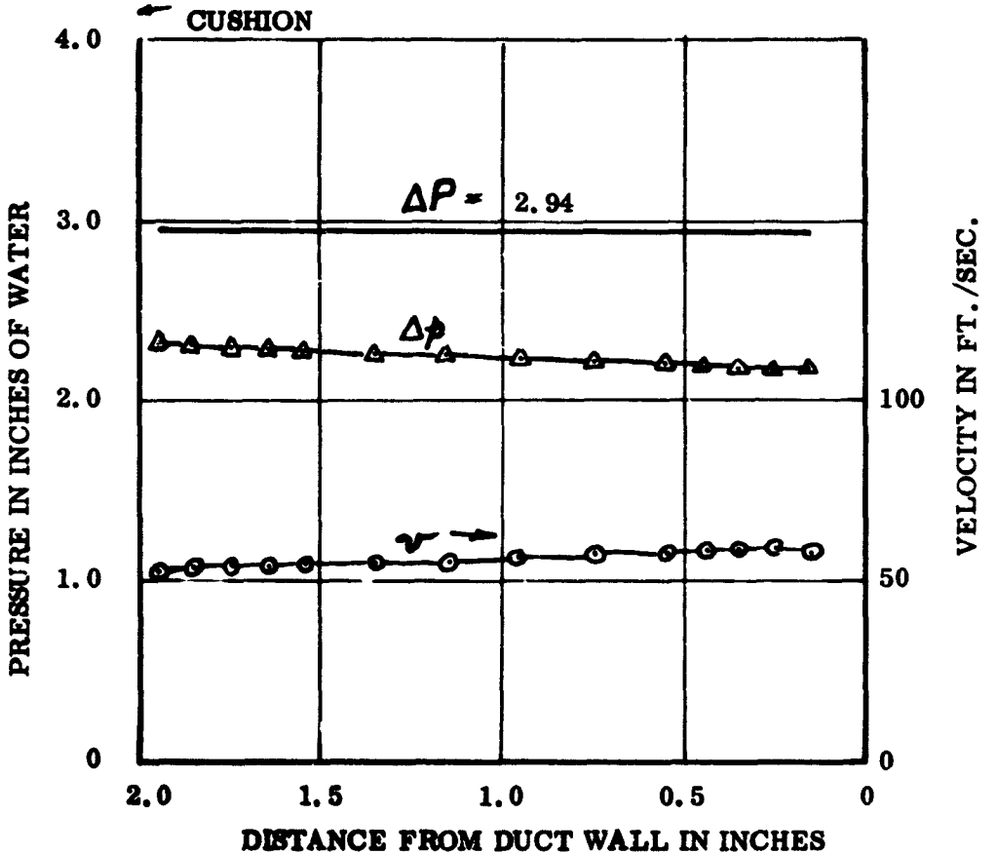

Total pressure ΔP and static pressure Δp are relative to the artificial ambient pressure at outlet.

Mean velocity = 56.6 ft/sec.
Flow volume = 9.00 ft^2/sec.
Flow power = 137.0 ft-lb/sec. ft.

Figure 57. Velocity and Pressure Distribution in the Throat of the Annular Jet.

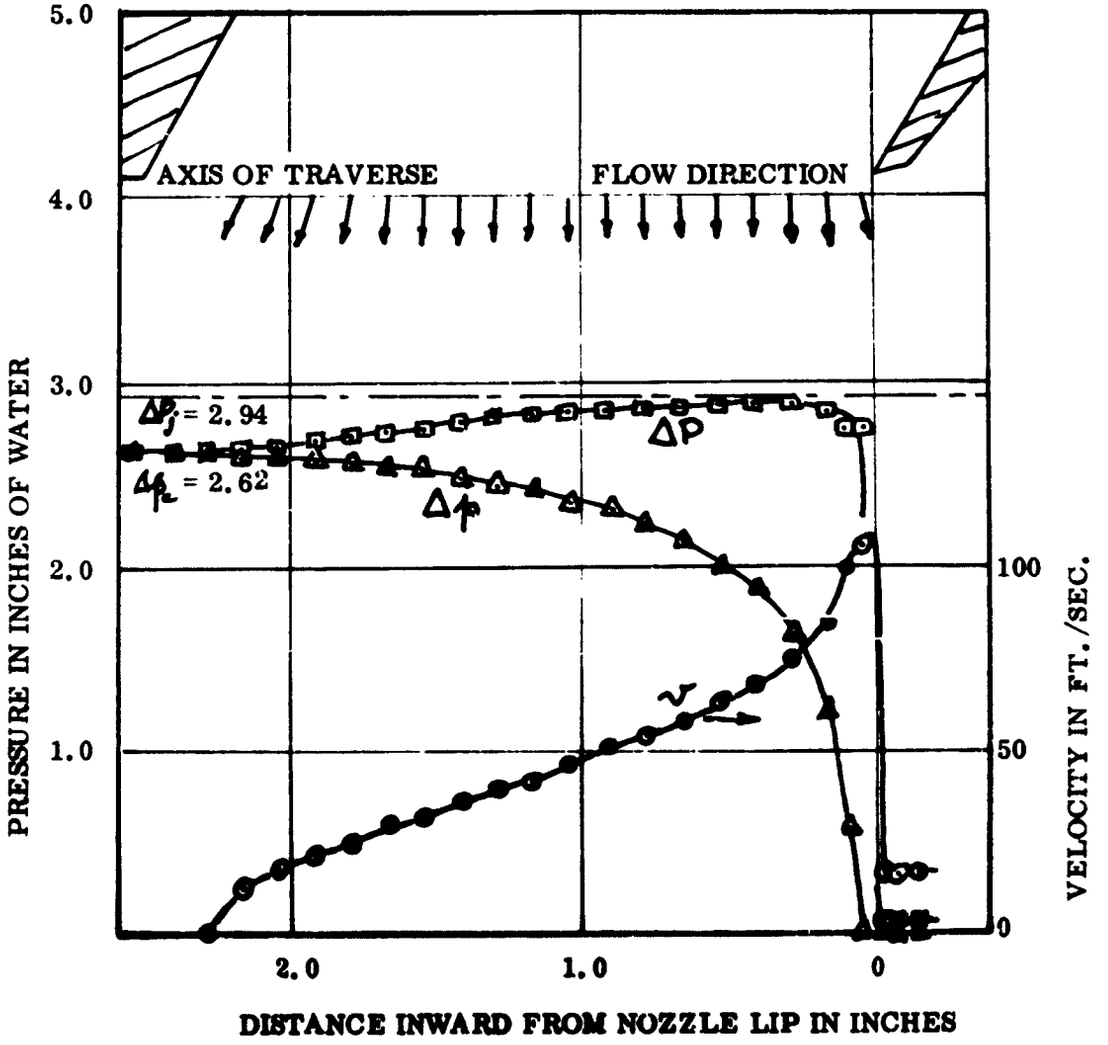

Figure 58. **Pressures and Velocity at Nozzle Exit**
t/ℓ = 1.0 θ = 30° ℓ = 2.0 Inches.

TABLE 2

EXPERIMENTAL DATA - ANNULAR JET TEST RIG

Location Inches Inward From Lip	Static Pressure Inches Water	Total Pressure Inches Water	Flow Angle Degrees	Velocity Feet Per Second
THROAT				
0.15	2.19	2.94	-	57.6
0.25	2.17	2.94	-	58.5
0.35	2.18	2.94	-	58.0
0.45	2.18	2.94	-	58.0
0.55	2.20	2.94	-	57.3
0.65				
0.75	2.20	2.94	-	57.3
0.85				
0.95	2.23	2.94	-	56.2
1.05				
1.15	2.25	2.94	-	55.4
1.25				
1.35	2.26	2.94	-	55.0
1.45				
1.55	2.28	2.94	-	54.2
1.65	2.28	2.94	-	54.2
1.75	2.29	2.94	-	53.8
1.85	2.31	2.94	-	53.0
1.95	2.32	2.94	-	52.5
NOZZLE EXIT				
0.14	0.000	0.070	-	16.5
0.08	0.000	0.070	-	16.5
0.02	0.040	0.070	-	9.5
0.04	0.000	2.768	+10	111.0
0.10	0.590	2.770	-	99.0
0.16	1.220	2.850	+3	85.0
0.29	1.640	2.886	+1.5	75.0
0.43	1.880	2.884	+1.5	67.0
0.54	2.023	2.885	+6	62.0

0.66	2.150	2.877	+6	57.0
0.79	2.223	2.864	+6	53.5
0.91	2.310	2.855	+1.5	50.0
1.04	2.361	2.846	+1.5	46.5
1.16	2.425	2.824	-1	42.0
1.29	2.459	2.824	-1	40.5
1.43	2.490	2.792	-1	37.0
1.54	2.535	2.757	-1	31.5
1.66	2.544	2.747	-6	30.0
1.79	2.570	2.716	-11	25.5
1.91	2.580	2.694	-18	22.5
2.04	2.596	2.663	-19	17.0
2.16	2.598	2.636	-26	13.0
2.29	2.609	2.609	-	0.0
2.43	2.615	2.609	-	-
2.54	2.631	2.631	-	0.0

NOZZLE EXIT AND CUSHION - LOW CUSHION BOARD

-0.41	0.00	0.10	90	21
-0.29	0.00	0.10	63	21
-0.16	0.09	2.21	48	97
-0.10	0.35	2.62	37	100.5
-0.04	0.70	2.62	30	92.5
+0.08	1.165	2.82	25	86
0.21	1.48	2.84	23	77.7
0.33	2.745	2.85	20	70
0.46	1.925	2.82	12	63
0.58	2.080	2.829	15	56
0.71	2.178	2.827	12.5	54
0.83	2.275	2.816	12.5	49
0.96	2.332	2.798	12.5	46
1.08	2.399	2.776	11	41
1.21	2.426	2.758	8	39
1.33	2.460	2.743	6.5	36
1.46	2.494	2.722	2.5	32
1.58	2.515	2.697	-2.5	28
1.71	2.529	2.695	-3	27
1.83	2.542	2.650	-5	22
1.96	2.550	2.639	-7.5	20
2.08	2.559	2.639	-10	19
2.21	2.569	2.612	-20	13.8

2.33	2.573	2.590	-22	9.2
2.46	2.572	2.583	-25	9.0
2.58	2.569	2.569	-	0
2.71	2.569	2.569	-	0
2.83				
2.96	2.569	2.569	-	0
3.08				
3.21	2.569	2.569	-	0
3.33	2.567	2.574	+75	5.6
3.46	2.567	2.574	+80	5.6
3.58				
3.71	2.574	2.574	-	0
3.83				
3.96	2.577	2.577	-	0
4.08				
4.21	2.571	2.573	+90	3.0

NOZZLE EXIT AND CUSHION - HIGH CUSHION BOARD

-0.41	0.00	0.30	90	36
-0.29	0.00	0.28	60	35
-0.16	0.17	1.25	51	63
-0.10	0.30	2.833	40	106
-0.04	0.63	2.825	29	99
+0.08	1.20	2.833	26	85
0.21	1.545	3.060	24	82
0.33	1.870	3.026	19	77.1
0.46	2.075	3.008	19	64
0.58	2.207	3.008	17	59.2
0.71	2.320	2.999	17	54.6
0.83	2.408	2.968	16.5	49.6
0.96	2.495	2.920	15	45.7
1.08	2.538	2.928	15	41.4
1.21	2.604	2.929	10	37.8
1.33	2.604	2.929	10	37.8
1.46	2.675	2.860	8	28.5
1.58	2.675	2.860	8	28.5
1.71	2.719	2.806	4	19.5
1.83	2.732	2.825	-	20.2
1.96	2.745	2.816	-	17.6
2.08	2.749	2.780	-	11.6
2.21	2.757	2.771	-	7.8

2.46	2.746	2.751	-	4.7
2.58	2.757	2.757	-	0.0
2.71	2.762	2.762	160	0.0
2.83				
2.96	2.758	2.771	112	3.6
3.08				
3.21	2.758	2.776	87	8.9
3.33				
3.46	2.789	2.789	47	10.0
3.58				
3.71	2.789	2.789	29	5.1
3.83				
3.96	2.789	2.789	24	5.1
4.08				
4.21	2.789	2.789	24	5.1

very small values toward the outer edge.

The power loss between the throat and the nozzle is simply the integral of $P_v r dx$ across the jet at the nozzle. This was computed as 5.49 foot-pounds per foot, equal to 4.01 percent of the throat power. The total pressure loss is plotted in Figure 59. The power distribution in the jet, like the velocity of the flow, is weighted heavily away from the cushion. It is given by the product of velocity and total pressure referred to the artificial ambient; that is to say, by the product of ΔP and v as they appear in Figure 58. This is also plotted in Figure 59.

The static pressure variation across the jet at the nozzle outlet, as given in Figure 58, is replotted in Figure 60 as the ratio $\Delta p_j/\Delta P_o$ for comparison with theory. In this display the unitized jet width is taken as 2-1/8 inches, this being the greatest width at which a finite velocity was observed on the cushion side.

From the comparison of Figure 60, it is evident that the present theory gives a very fair approximation to the experimental observation. The theory appears to predict (1) a higher pressure at the cushion side of the jet than was obtained experimentally and (2) a lower pressure, implying a higher velocity, on the lip side of the jet. This is entirely plausible as the result of viscous and diffusion losses in the real case, not taken into account in the theories. Also, since the measurements are not across a truly normal plane, some distortion of the axis must be present.

Flow Adjacent to the Annular Jet

In the attempt to determine the flow patterns beyond the boundaries of the jet proper, we made an extended traverse reaching from outside the jet through the jet and beyond for a distance of one jet thickness into the cushion. The experiment was exploratory in concept. We wanted to get some measurements in proximity to the jet boundary in the high-speed region around the nozzle lip, to see if the secondary flow inside the cushion could be detected, and, as a practical objective, to see if the variation in height of the cushion cavity would influence the performance. Accordingly, the measurements were made, firstly, with the cushion flush with the end of the nozzle, as in all the preceding experiments, and secondly, with the cushion board high in relation to the nozzle as featured in the illustration, Figure 55.

To clear the nozzle and low cushion board, the traverse axis was slightly lower than in the nozzle measurements of Figure 58. The answers to the questions are evident in the plots of the measurements in Figures 61 and 62.

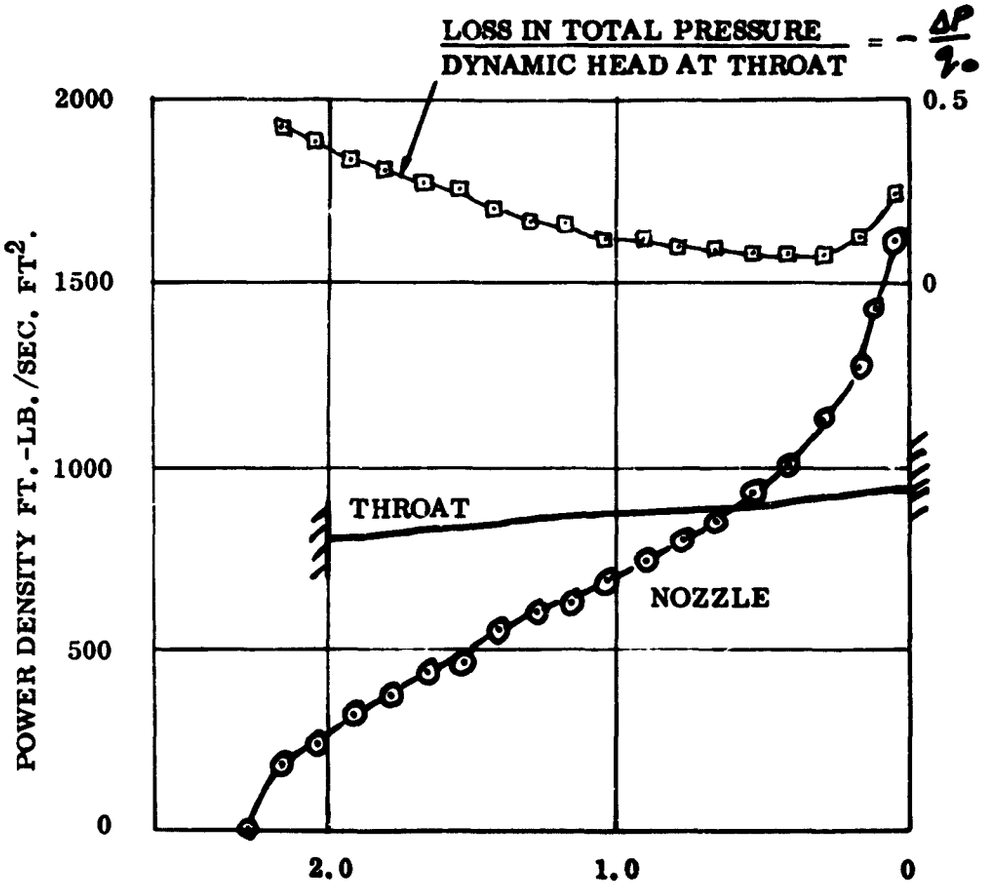

Power at throat = $\int_0^{.5} \rho V \Delta P \, dx$ = 137 ft-lb/sec ft.

Power at nozzle = $\int_{.5}^{2.5} \rho V \Delta P \, dx$ = 132.4 ft-lb/sec ft.

Power loss = difference = 4.6 ft-lb/sec ft.

Power loss computed as $\int_0^{2.5} \rho V \Delta P \, dx$ = 5.49 ft-lb/sec ft.

Figure 59. Redistribution of Power in Annular Jet.

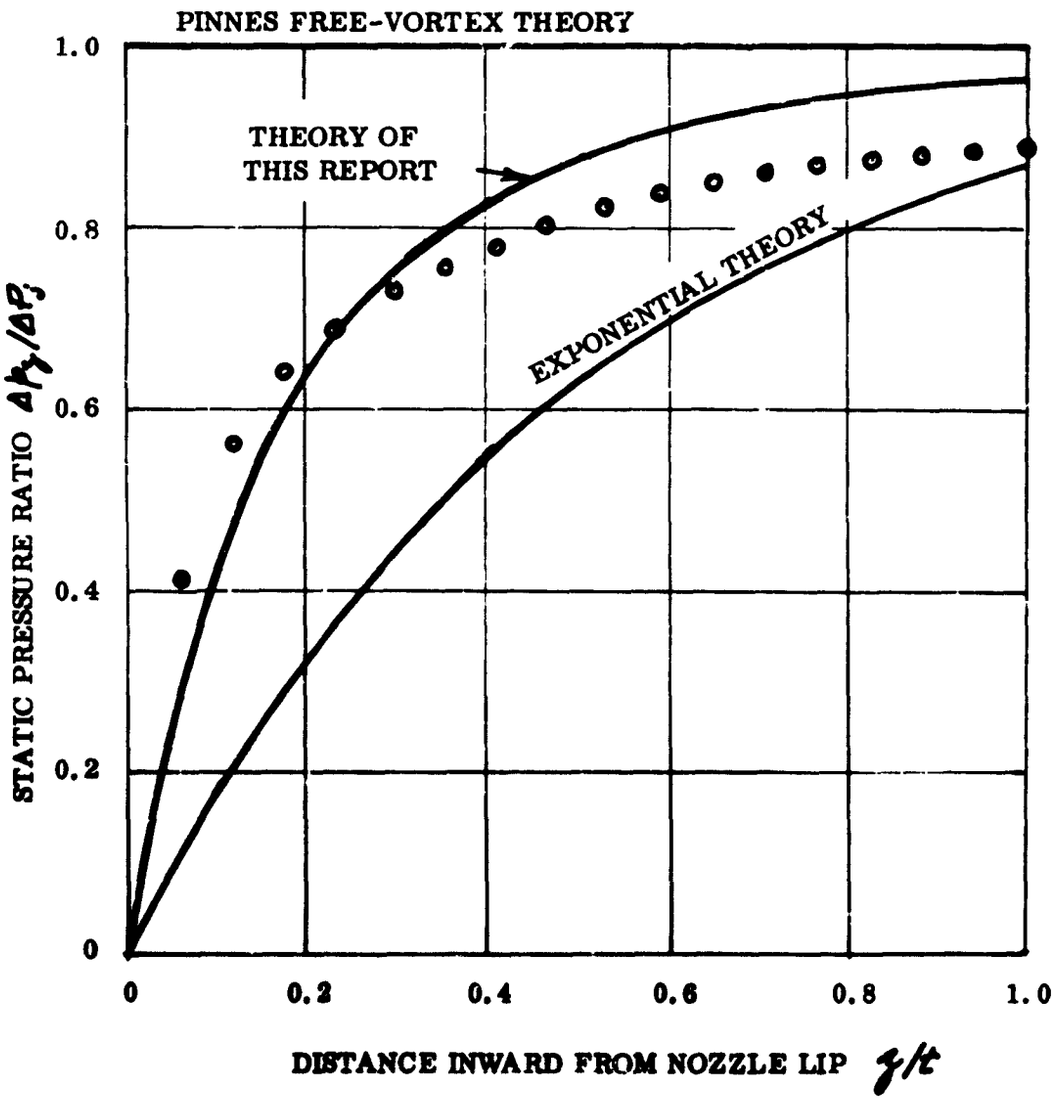

Figure 60. Static Pressure Variation Across a Jet - Comparison of Theoretical and Experimental Values.

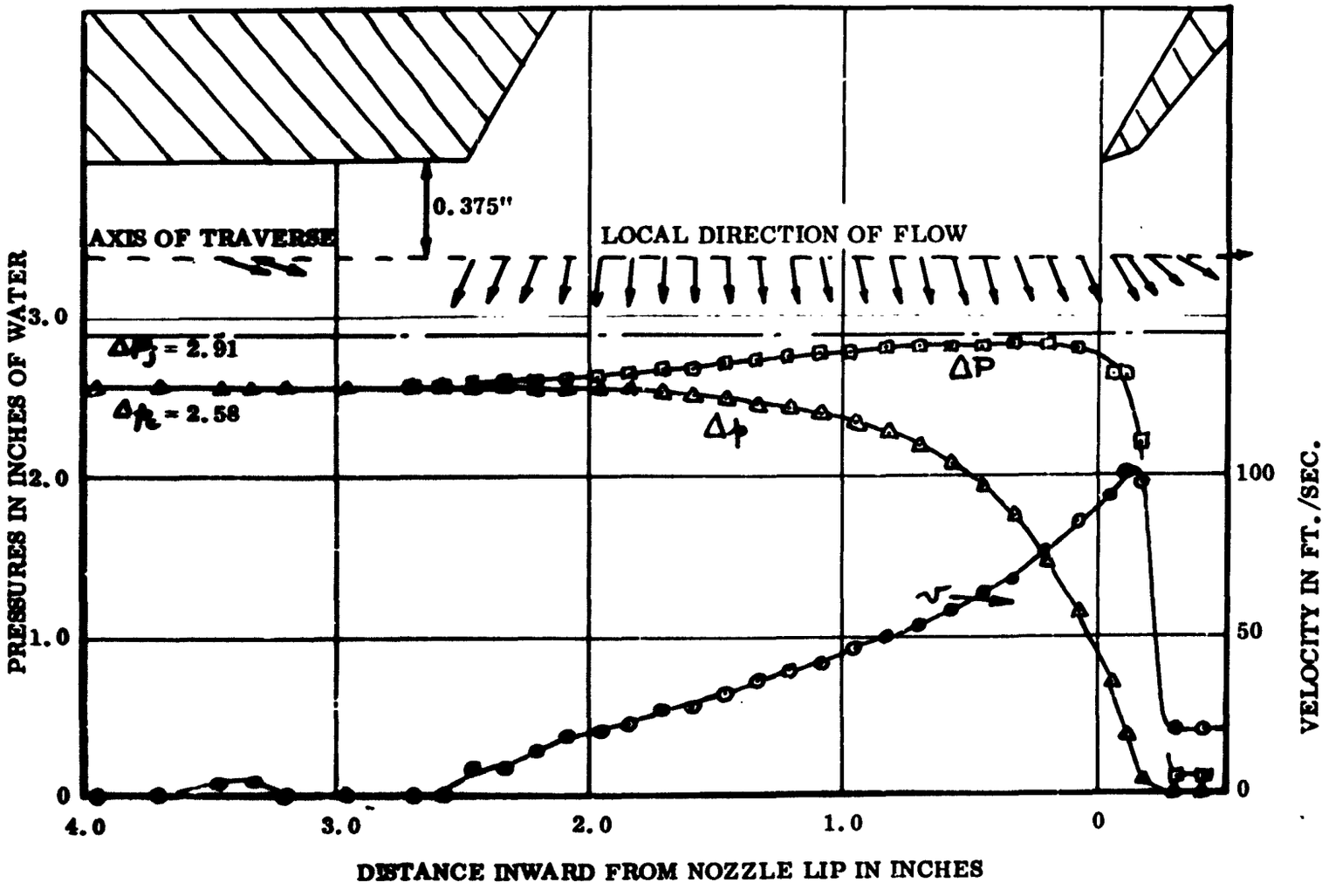

Figure 61. Pressures and Velocity in Annular Jet and Cushion. (Flat Cushion Board t/h = 1.0 θ = 30°).

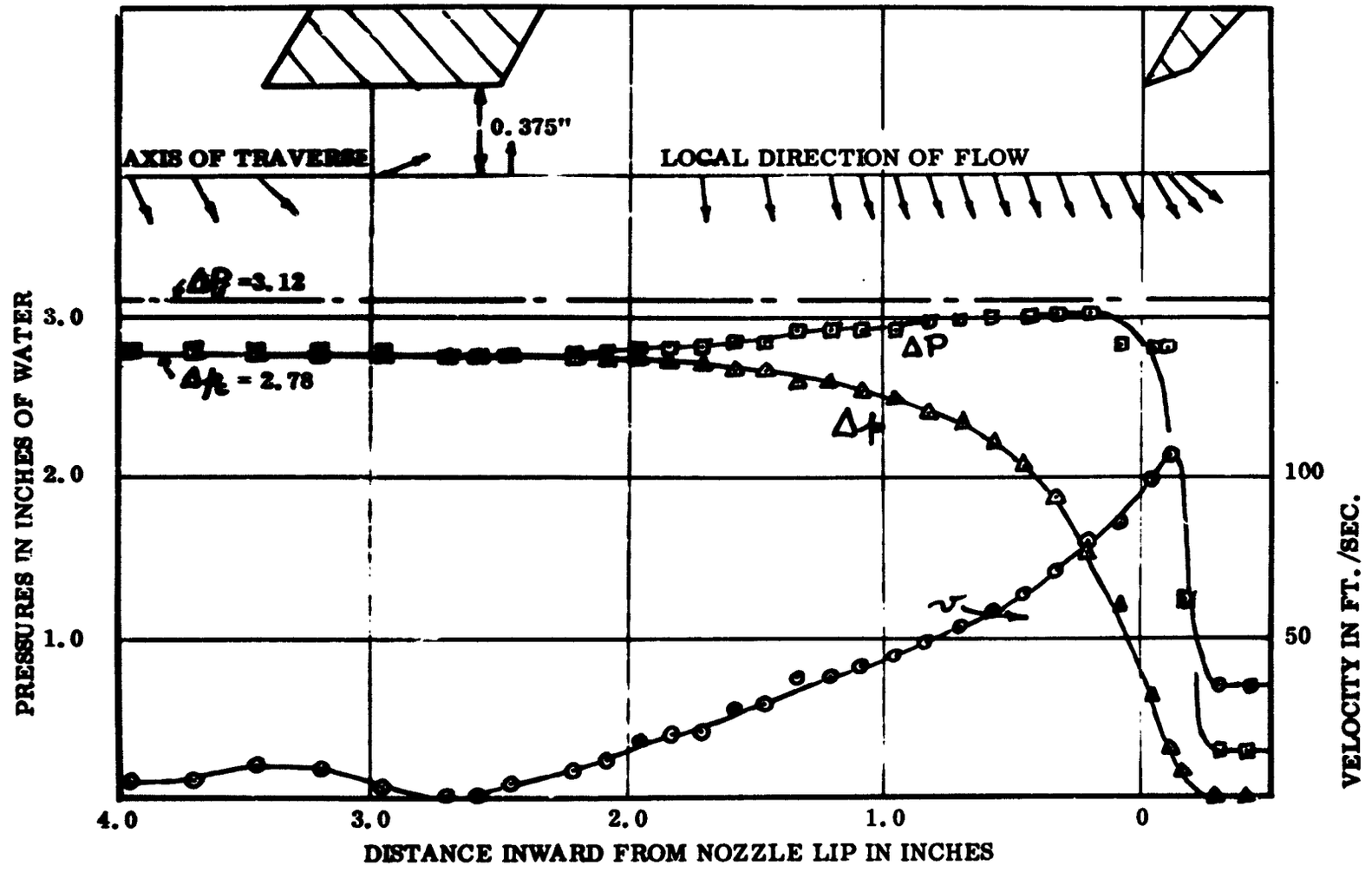

Figure 62. Pressures and Velocity in the Annular Jet and Cushion. (High Cushion Board t/h = 1.0 θ = 30°).

As in the preceding measurements, the values here plotted are computed from the new data without smoothing or selection.

The results show that there is a slight improvement in cushion pressure with the large cavity. The blower was able to pull the outlet depression down to 3.12 inches of water, as against 2.91 inches, with the small cavity (low cushion board). The preceding test (Figure 58) gave slightly higher values: $\Delta\phi_c = 2.61$, $\Delta P_j = 2.94$, $\Delta\phi_c/\Delta P_j = 0.892$. This difference, when expressed in terms of positive supply pressure, appears as a higher supply pressure and higher cushion pressure. This is presumably due to long-term supply voltage variations to the rig motor rather than a change in the total rig loss coefficient. The cushion pressure ratio for both tests $\left(\Delta\phi_c/\Delta P_j\right)$ remains practically the same at

$$\Delta\phi_c/\Delta P_j = \frac{2.78}{3.12} = 0.890 \qquad \text{(large cavity)}$$

$$\Delta\phi_c/\Delta P_j = \frac{2.58}{2.91} = 0.887 \qquad \text{(small cavity).}$$

Thus, there is no difference between the two configurations, within the experimental accuracy of the tests.

Some movement of air, downward in the large cavity and upward in proximity to the jet, was detected. The velocities were in the range of 0 - 10 feet per second and were presumably evidence of a primary cushion vortex driven by the jet. With the low cushion board, practically no air movement was detected; there were traces of flow at 5 feet per second or so toward the jet along the underside of the cushion board but the reality of these is somewhat questionable.

In all other respects the traverses are almost identical and consistent with the measurements closer to the jet (Figure 58). This consistency, incidentally, increases confidence in the accuracy of the instrumentation used in these experiments.

Chapter Five

THE EFFECT OF TOTAL PRESSURE VARIATION ACROSS AN ANNULAR JET

The general solution for an annular jet (Equation 94) contains the local jet total pressure (ΔP_3) as a variable of ζ . So far, the equation has been solved only for the case ΔP_3 = constant.

In a practical application ΔP_3 is rarely constant, because of the losses incurred upstream of the nozzle. Thus it is of interest to discover the effect of varying ΔP_3 across the jet.

From a more academic point of view, there is no reason to suppose that constant total pressure gives the maximum lift per unit jet power expended, and it would be instructive to discover the true optimum distribution. In practical cases where some adjustment of the ΔP_3 distribution is possible (an annular jet driven as an eductor, for example) it may then be possible to bias the distribution in the direction of this theoretical optimum.

There is also another practical aspect. It is usual to reduce experimental measurements of cushion pressure by dividing by the mean jet total pressure. If this parameter is not independent of the total pressure distribution shape -- as we shall see that it is not -- then this method of presenting results is unsatisfactory.

THE SPECIAL CASE OF CONSTANT JET VELOCITY

In this section the annular jet equations will be solved for the special case of an annular jet whose total head distribution is such that the jet velocity is constant across the duct.

Since

$$\Delta P_3 = \Delta p_3 + \tfrac{1}{2}\rho v_j^2 , \qquad (174)$$

Equation (174) can be substituted for ΔP_3 in the basic equation of motion. From Equation (97), the equation for curved flow becomes

$$\frac{d\Delta p}{d\zeta_3} + \frac{2}{r_0 + \eta_3}\Delta p_3 = \frac{2}{r_0 + \eta_3}\left(\Delta p_3 + \tfrac{1}{2}\rho v_j^2\right) \qquad (175)$$

or

$$\frac{d\rho}{dz_3} = \frac{\rho v_j^2}{z_0 + \eta z_3} ;$$

$$\therefore \quad \Delta p_{z_3} = \int_0^{z_3} \frac{\rho v_j^2}{z_0 + \eta z_3} \, dz_3 \tag{176}$$

$$= \rho v_j^2 z_3 / z_0 \quad \text{for } \eta = 0 \tag{177}$$

$$= \frac{\rho v_j^2}{\eta} \log \left| 1 + \eta z_3 / z_0 \right| \quad \text{for } \eta \neq 0 . \tag{178}$$

Substituting in (174) for Δp_{z_3},

$$\Delta P_{z_3} = \tfrac{1}{2} \rho v_j^2 \left(1 + z_3 / z_0 \right) \quad \text{for } \eta = 0 \tag{179}$$

$$= \tfrac{1}{2} \rho v_j^2 \left(1 + \frac{2}{\eta} \log \left| 1 + \eta z_3 / z_0 \right| \right) \text{ for } \eta \neq 0 . \tag{180}$$

The cushion pressure is obviously

$$\Delta p_c = \rho v_j^2 z_0 / z_0 \qquad \eta = 0 \tag{181}$$

$$= \frac{\rho v_j^2}{\eta} \log \left| 1 + \eta z_0 / z_0 \right| \qquad \eta \neq 0 . \tag{182}$$

The jet power is

$$\frac{P_j}{C t (z_0)^{1/2}} = \frac{1}{t} \int_0^t \Delta P_{z_3} \left(\Delta P_{z_3} - \Delta p_{z_3} \right)^{1/2} dz_3$$

$$= \frac{\left(\tfrac{1}{2} \rho v_j^2 \right)^{1/2}}{t} \int_0^t \Delta P_{z_3} \, dz_3 . \tag{183}$$

Thus, by substituting (177) or (178) in (183), and by using equation (181) or (182) for the cushion pressure, we can determine the parameter $\Delta\bar{p}_c$.

Determination of the Jet Curvature Parameter η

The nozzle mass flow is obviously

$$\dot{m} = \rho C_t v_j . \tag{184}$$

At ambient pressure, the local velocity will be given by

$$\dot{m} = \rho C \int_0^{z'} \left(\frac{2}{\rho}\Delta p_z\right)^{1/2} dz'$$

$$= \rho C_t v_j \int_0^{t/r_0} \left(1 + \frac{2}{\eta}\log\left|1 + \eta z/r_0\right|\right)^{1/2} d(z/r_0) . \tag{185}$$

Combining (184) and (185) gives the integral relationship

$$\frac{t}{r_0} = \int_0^{t/r_0} \left(1 + \frac{2}{\eta}\log\left|1 + \eta z/r_0\right|\right)^{1/2} d(z/r_0) . \tag{186}$$

But, from Equation (107)

$$\eta = \frac{t/r_0 + \sin\theta}{1 + \sin\theta} .$$

These two equations enable us to determine η .

Calculation of $\Delta\bar{p}_c$ for Free-Vortex Flow

For η = 1.0 Equations (180) and (183) give

$$p_j = C_t \cdot \tfrac{1}{2}\rho v_j^2 \cdot \int_0^t \left(1 + 2\log\left|1 + z/r_0\right|\right) dz$$

$$= C_t \cdot \tfrac{1}{2}\rho v_j^2 \left[-1 + \frac{2r_0}{t}(1 + t/r_0)\log\left|1 + t/r_0\right|\right] . \tag{187}$$

Thus, from Equation (145),

$$\frac{t}{h}\Delta\bar{p}_c = \frac{\left[2\log\left|1 + t/r_0\right|\right]^{3/2}}{\frac{1 + t/r_0}{t/r_0}\log\left|1 + t/r_0\right| - 1/2} . \tag{188}$$

Since $r_0 = R - t$,

$$r_0/t = R/t - 1 \quad \text{and} \quad t/r_0 = \frac{t/R}{1 - t/R}$$

$$\frac{t}{h}\Delta\bar{p}_c = \frac{t/R \cdot \left[2\log\left|1/(1 - t/R)\right|\right]^{3/2}}{2.\log 1/(1 - t/R) - t/R} . \tag{189}$$

Calculation of $\Delta\bar{p}_c$ for Constant Radius Flow

For $\eta = 0$, Equations (179) and (183) give

$$p_j = C \cdot \tfrac{1}{2}\rho v_j^2 \int_0^t (1 + 2z/r_0)\, dz$$

$$= C r_0 \cdot \tfrac{1}{2}\rho v_j^2 \cdot \frac{t}{r_0}(1 + t/r_0). \tag{190}$$

Thus, from Equation (145),

$$\frac{t}{h}\Delta\bar{p}_c = \frac{(2t/r_0)^{3/2}}{1 + t/r_0} \tag{191}$$

where $r_0 = R$ in this case.

Discussion of Results

The total head variations necessary to give constant jet velocity are given in Figure 63 expressed as the ratio $\Delta p_c/\Delta p_a$. This ratio uniquely defines Δp_j for the constant radius of curvature case, since the variation is linear across the jet (Equation 179), but not the free-vortex solution.

Values of $\frac{t}{h}\Delta\bar{p}_c$ plotted in Figure 64 show a substantial difference between the two curvature assumptions, but little difference in each case for constant

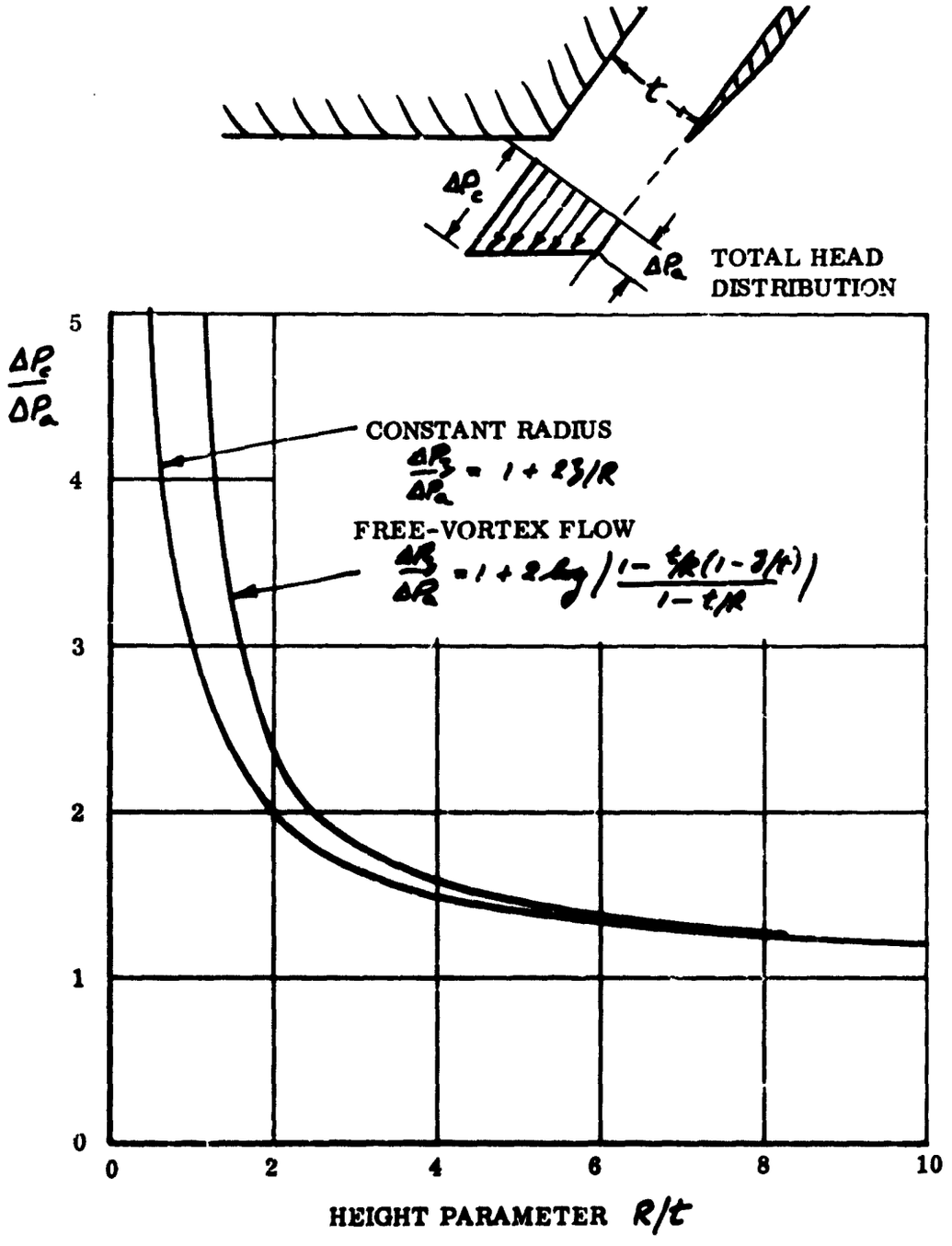

Figure 63. Jet Total Head Distribution Needed To Give Constant Jet Velocity.

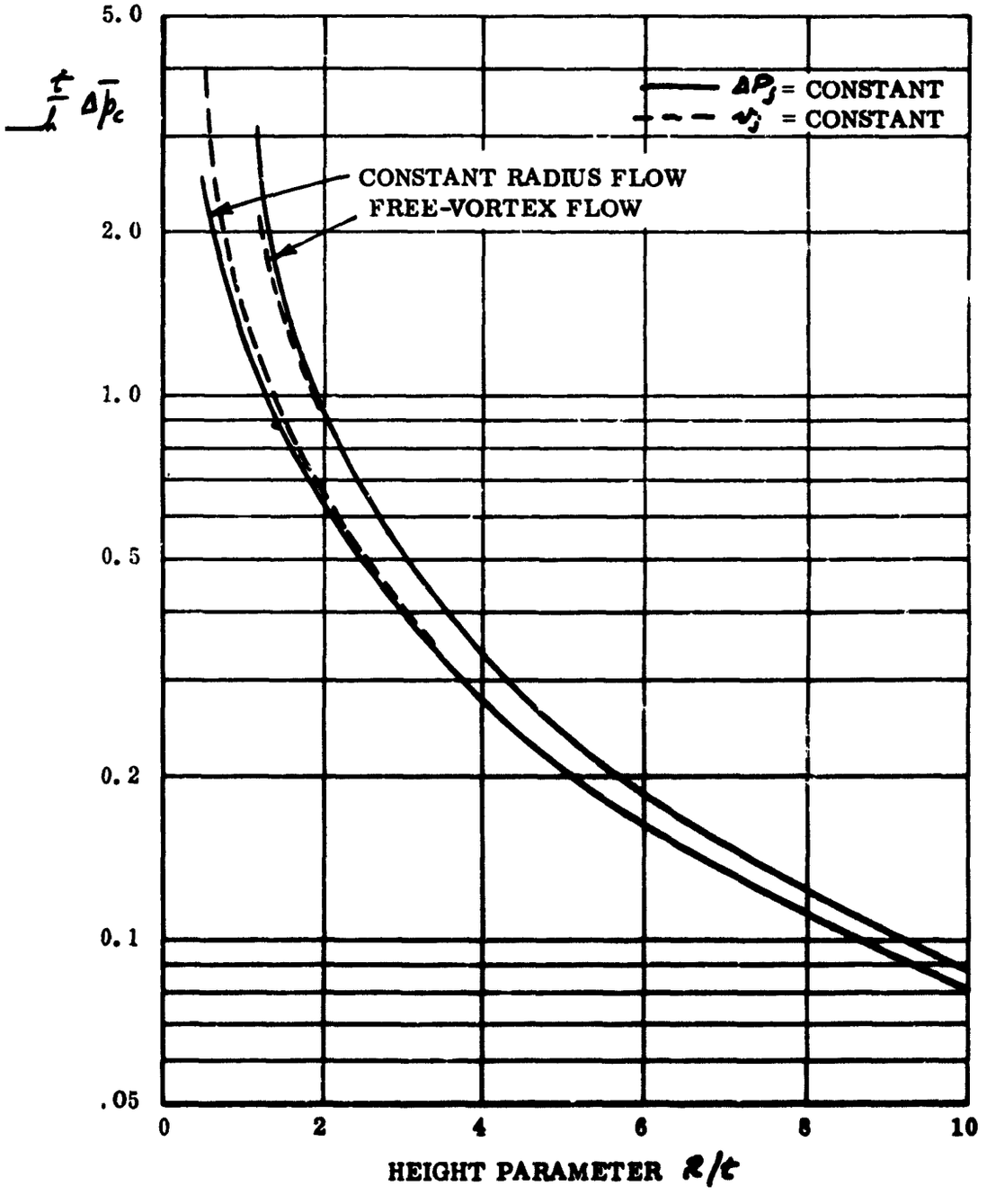

Figure 64. The Cushion Pressure Parameter $\Delta\bar{p}_c$ as a Function of the Height Parameter R/t.

jet velocity as against constant total head, except at very low values of R/h. Figure 65 emphasizes this point, and it is interesting to note that, whereas constant jet velocity increases the lift per unit power for constant radius theory, it decreases it in free-vortex flow. Only the constant radius solution is significant for $R/h < 1.0$, of course.

THE INFLUENCE OF THE TOTAL PRESSURE DISTRIBUTION ON CUSHION PRESSURE IN TERMS OF MEAN TOTAL PRESSURE, FOR FREE-VORTEX FLOW

It is normal to express cushion pressure as the ratio $\Delta p_c/\Delta p_j$. For example, exponential theory gives

$$\frac{\Delta p_c}{\Delta p_j} = 1 - e^{-2h/R}$$

for a constant total head in the jet.

We have seen that in reducing experimental data, when Δp_j is not constant across the jet, it is usual to find the mean value Δp_m and hence the ratio $\Delta p_c/\Delta p_m$. It will be shown below that this is acceptable when the total pressure profile is symmetrical about the midpoint, but not when the distribution is skewed, for the case of free-vortex flow.

For the case $n = 1$, Equation (95) gives the cushion pressure as

$$\Delta p_c = \frac{2}{(r_0+h)^2}\int_0^h (r_0+z)\,\Delta p_j\,dz$$

$$= 2(r_0/R)^2\left[r_0/R\int_0^h \Delta p_j\,dz + 1/R\int_0^h \Delta p_j\,dz\right].$$

That is, $$\Delta p_c = 2(r_0/R)^2\left[\frac{1-h/R}{r_0/R}\int_0^1 \Delta p_j\,d(z/h) + \int_0^1 (z/h)\,\Delta p_j\,d(z/h)\right]. \quad (192)$$

Thus the determination of the cushion pressure depends upon the evaluation of the two integrals

$$\int_0^1 \Delta p_j\,d(z/h) = \Delta p_m \quad \text{(the mean total pressure)}$$

and $$\int_0^1 (z/h)\,\Delta p_j\,d(z/h) \quad \text{(a weighted mean).} \quad (193)$$

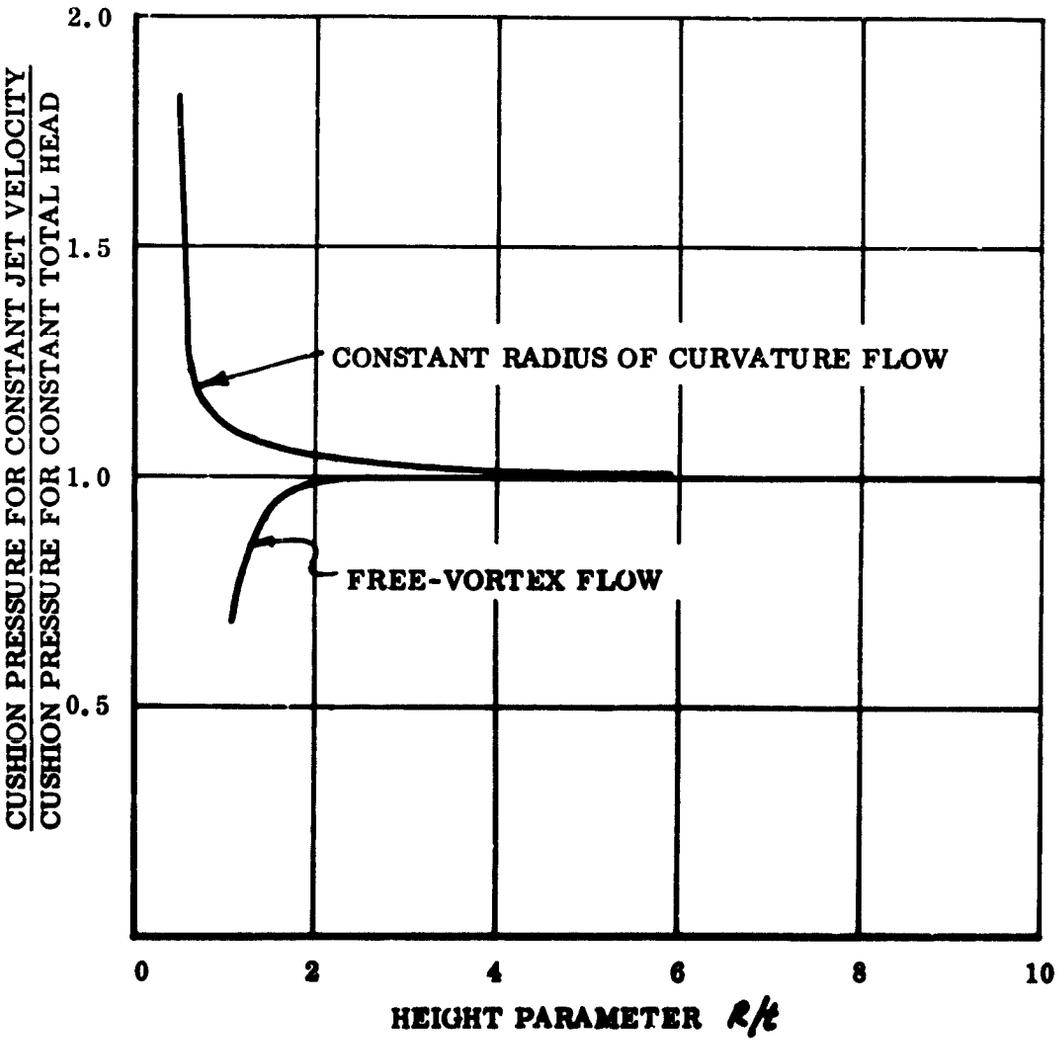

Figure 65. Comparative Effect of Constant Jet Velocity and Constant Total Head on Cushion Pressure Per Unit Air Power.

Equation (192) can be rewritten as

$$\frac{\Delta p_c}{\Delta P_m} = 2(t/R) - 2(t/R)^2 + 2(t/R)^2 \frac{\int_0^{3/t} \Delta P_3 \alpha(3/t)}{\int_0^1 \Delta P_3 \alpha(3/t)} \cdot \qquad (194)$$

If a shape integral is defined as

$$\lambda = \frac{\int_0^{3/t} \Delta P_3 \alpha(3/t)}{\int_0^1 \Delta P_3 \alpha(3/t)} - \frac{1}{2}, \qquad (195)$$

Equation (194) becomes

$$\frac{\Delta p_c}{\Delta P_m} = \left[2 t/R - (t/R)^2\right] + 2(t/R)^2 \lambda \qquad (196)$$

= (value for a constant total pressure distribution) + (increment due to the shape factor)

In the case of profiles which are symmetric about $3 = t/2$, it can be shown that $\lambda = 0$ always. This is proved as follows:

$$\int_0^{3/t} (3/t) \Delta P_3 \alpha(3/t) = \int_0^{\frac{1}{2}} (3/t) \Delta P_3 \alpha(3/t) - \int_{\frac{1}{2}}^{3/t} (3/t) \Delta P_3 \alpha(3/t)$$

If $t - 3 = \psi$, $3 = t - \psi$, $\frac{d3}{d\psi} = -1$;

$$\therefore \int_{\frac{1}{2}}^{3/t} (3/t) \Delta P_3 \alpha(3/t) = -\int_{\frac{1}{2}}^{0} (1 - \psi/t) \Delta P_\psi \alpha(\psi/t)$$

$$= \int_0^{\frac{1}{2}} \Delta P_\psi \alpha(\psi/t) - \int_0^{\frac{1}{2}} (\psi/t) \Delta P_\psi \alpha(\psi/t);$$

$$\therefore \int_0^{\frac{1}{2}} (3/t) \Delta P_3 \alpha(3/t) = \int_0^{\frac{1}{2}} \Delta P_\psi \alpha(\psi/t);$$

$$\therefore \lambda = \frac{\int_0^{\frac{1}{2}} \Delta P_\psi \alpha(\psi/t)}{2\int_0^{\frac{1}{2}} \Delta P_3 \alpha(3/t)} - \frac{1}{2} = 0.$$